# POLITECNICO
## MILANO 1863

**SCUOLA DI INGEGNERIA INDUSTRIALE E DELL'INFORMAZIONE**

Plant Design and Optimization of Hydrogen Production from Non-Condensable Gas of Plastic Pyrolysis

TESI DI LAUREA MAGISTRALE IN

ENERGY ENGINEERING

INGEGNERIA ENERGETICA

Author: **Mehran Akbarzadeh**

Student ID: 10709426
Advisors: Prof. Matteo Carmelo Romano & Prof. De Chen
Co-advisors: Dr. Kumar Ranjan Rout & Abdelrahman Mostafa
Academic Year: 2021-22

# Abstract

This thesis work aims to find the optimal configuration for a plant able to operate flexibly, performing pyrolysis of the municipal plastic waste and producing hydrogen. The plant would utilize newborn technology to produce hydrogen, namely sorption-enhanced steam reforming process (SESR) coupled with a plastic pyrolysis and carbon capture and storage units. The process would operate by burning a part of pyrolysis gas produced in the pyrolysis unit. The advantage of this technology is the ability to perform a pre-combustion separation of the $CO_2$ produced by the reformer. The plant would produce the hydrogen for hydrogenation of the pyrolysis oil, either exporting hydrogen depending on the different prices for the two products to always keep the chemical island in function.

The modeled configuration was first simulated in Aspen Plus, validating the obtained results with data from the literature; then, the integrated cycle was also simulated in Aspen Plus. Different configurations were simulated at different calcination pressures and temperatures.

As a result, in terms of hydrogen production, it is better to have a moderate vacuum integrated with a temperature swing and use as little as possible steam to control the partial pressure of $CO_2$ in the calcination step to avoid very high vacuum requirements.


**Keywords:** Hydrogen, reforming, calcination, Aspen Plus, SESR.

# Sommario

Questo lavoro di tesi mira a trovare la configurazione ottimale per un impianto in grado di operare in modo flessibile, effettuando la pirolisi dei rifiuti plastici urbani e producendo idrogeno. L'impianto utilizzerebbe una tecnologia appena nata per produrre idrogeno, vale a dire il processo di reforming del vapore potenziato dall'assorbimento (SESR) accoppiato con una pirolisi plastica e unità di cattura e stoccaggio del carbonio. Il processo opererebbe bruciando una parte del gas di pirolisi prodotto nell'unità di pirolisi. Il vantaggio di questa tecnologia è la possibilità di effettuare una separazione pre-combustione della $CO_2$ prodotta dal reformer. L'impianto produrrebbe l'idrogeno per l'idrogenazione dell'olio di pirolisi, sia esportando idrogeno a seconda dei diversi prezzi per i due prodotti per mantenere sempre in funzione l'isola chimica.

La configurazione modellata è stata prima simulata in Aspen Plus, convalidando i risultati ottenuti con i dati della letteratura; poi il ciclo integrato è stato simulato anche in Aspen Plus. Diverse configurazioni sono state simulate a diverse pressioni e temperature di calcinazione.

Di conseguenza, in termini di produzione di idrogeno, è meglio avere un vuoto moderato integrato con uno sbalzo di temperatura e utilizzare meno vapore possibile per controllare la pressione parziale di $CO_2$ nella fase di calcinazione per evitare requisiti di vuoto molto elevati

**Parole chiave:** Idrogeno, reforming, calcinazione, Aspen Plus, SESR.

# Contents

# 1 Introduction

The problem with fossil fuels

Nowadays, half of the global electric production comes from fossil fuels (primarily coal and natural gas). Fossil fuels discharge pollutants (namely particulate matter, CO, NOx, unburned hydrocarbons…) and greenhouse gases (GHG). Greenhouse gases are already present in the atmosphere, but the growth of their concentration, due to anthropogenic activities can change the climate contributing to global warming and weather extremization. The most known greenhouse gas is $CO_2$, mainly produced during the oxidation of fossil fuels for power generation, followed by $CH_4$ derived by the agricultural sector (1); alongside many other gases and hydrocarbons, they are responsible for the Greenhouse effect. The radiation from Sun, after being partially reflected, reaches the ground, piercing through the atmosphere, then it heats the soil that emits back part of this energy in the infrared wavelength (IR); if GHG is abundant, they can absorb and reradiate this radiation trapping it under the atmospheric layer and heating back the Earth's surface. A cyclic variation in $CO_2$ concentration in the atmosphere repeats in millennia associated with temperature shifts; for this basis, Global warming is not without any doubt recognized because of this GHG increase, but there's an increasing agreement in relating the two of them. During the past century, the temperature increased by about 0.5°C (associated with an increase from 280 to 370 ppmv of $CO_2$,'s concentration) (2). This steep increase was not followed in previous centuries. Figure 1-1 shows the trends for $CO_2$ and temperature in the past geological eras, while Figure 1-2 highlights the possible scenarios modeled by the Intergovernmental Panel on Climate Change (IPCC). The projections foresee an increase in temperature, as a matter of fact, if emissions are not abated. Even the most optimistic scenario predicts at least 1.5 °C of mean temperature increase worldwide with respect to the average in the period 1986-2005.
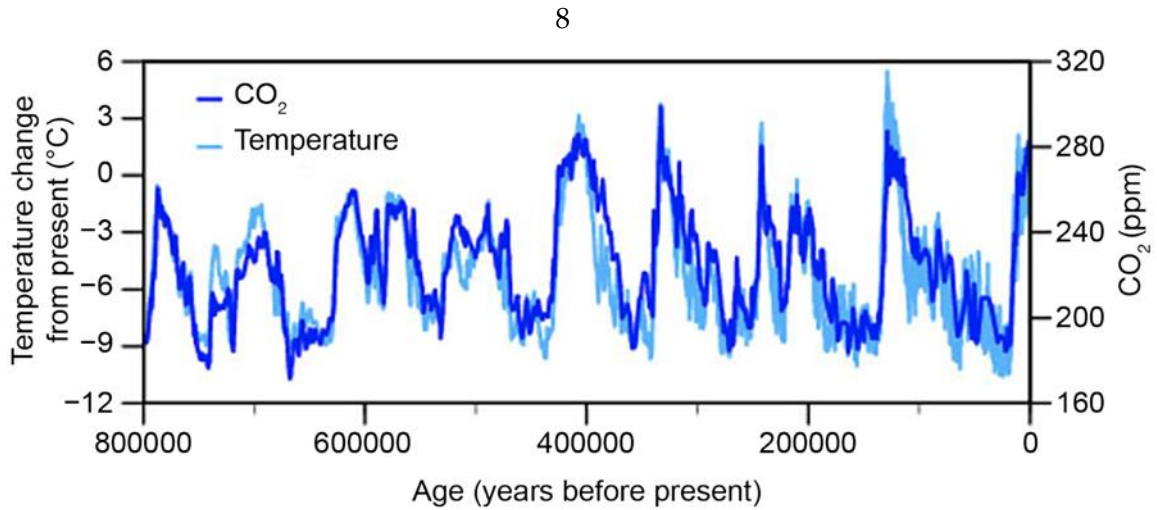
Figure 1-1 Temperature change (light blue) and carbon dioxide change (dark blue) measured from the EPICA Dome C ice core in Antarctica.
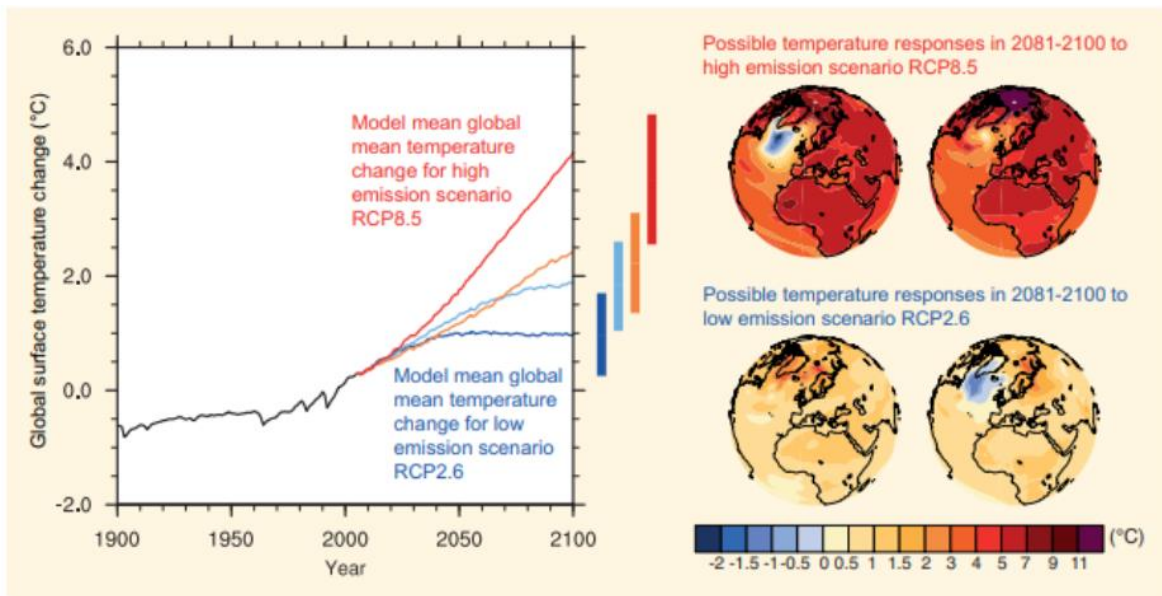


Figure 1-2 Scenarios from IPCC (3).

Renewable sources may represent part of the solution to this problem alongside with construction of new nuclear plants. In the last years, the electric market started undergoing some significant changes. Renewable sources are increasing in installed capacity worldwide at a rapid pace. Hydropower is the first renewable source, and it is pretty stable, while the addition of wind and solar technologies accounted for 90% of all the new capacity established in 2019 (4). As it is possible to see in Figure 1-3, Asia is responsible for 44% of all the capacity in the world and is continuing to invest in that path. The direction for investments in renewable sources is rising year by year, and it seems that investments in non-renewable

sources are broadly lowering (Figure 1-3). Transformation of the electric market is happening with the phasing out of coal plants; it's likely to see a future market dominated by renewables and nuclear.
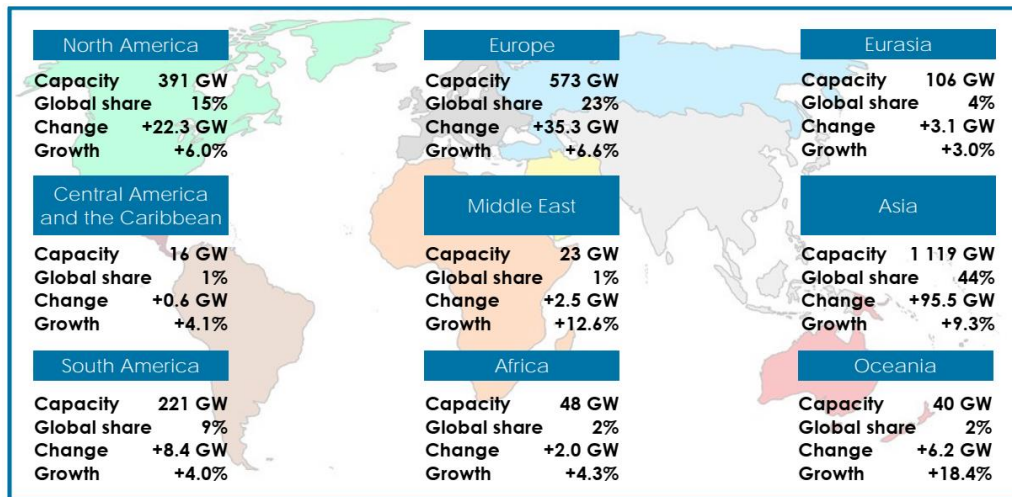


Figure 1-3 Renewable generation capacity by region (4).
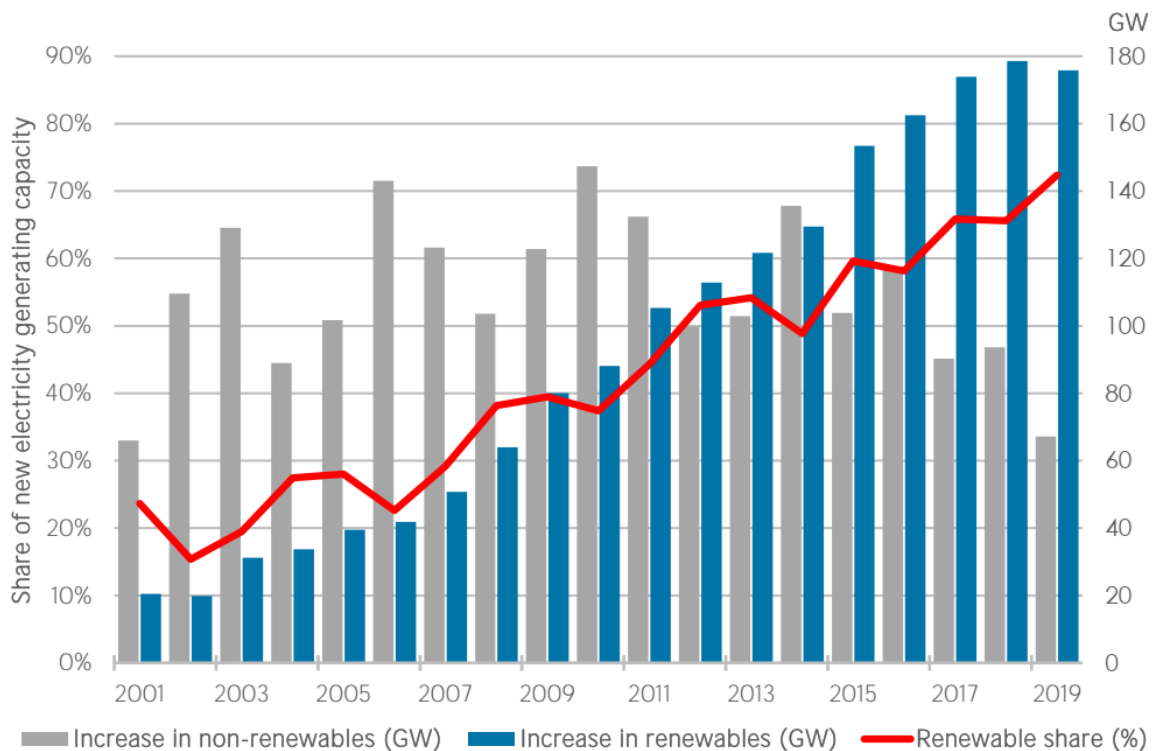


Figure 1-4 Renewable share of annual power capacity expansion (4).

The decoupling of electricity and emissions in advanced economies is due in large part to the growth in renewables. In 2019, almost 70% of the new global generation

was from renewables compared to only 25% in 2001, as shown in Figure 1-4. In 2017, 20% of global power capacity was renewables; in 2019, it was one-third!

Wind and solar PV are not-programmable sources; this means that their production is not connected to the electricity demand and cannot be planned without multiple uncertainties. Intense penetration of variable renewable electricity (VRE) would require higher flexibility for the electric system; in particular, variable renewables can peak their production at periods of low demand; hence they would require strong support from ancillary assistance to obtain a reliable and smooth operation (5). The ancillary market could acquire priority and offer more and more differentiated services thanks to a strong presence of electricity storage systems (ESS).

One of the ways for decarbonization is the production and utilization of hydrogen from fossil fuels and then couple this system with a carbon capture and storage unit. $H_2$ as an energy carrier can become an effective way of storing energy utilizing directly in reciprocating combustion engines (6) and in fuel cells to produce electricity. Moreover, the production of green hydrogen can push further the renewables penetration in the electricity market. The International Renewable Energy Agency (IRENA) assessed in its roadmap how it is possible to obtain a value of 6% (7) of hydrogen share in total energy consumption in 2050, while for the Hydrogen Council, 18% of penetration can be obtained with Carbon Capture and Storage (8).

Carbon Capture and Storage

Nowadays, most of the $H_2$ is produced starting from fossil fuels with significant emissions of $CO_2$. Indeed, as of today, costs for producing hydrogen from renewables are too high compared to the ones from fossil fuels. The introduction of Carbon Capture and Storage can help reduce this emission, helping the hydrogen economy develop. Indeed "Blue Hydrogen" can be produced with proven processes and is characterized by lower costs (3-4 €/kg) compared to electrolysis (9). The CCS technology has the capacity of sequestrating the $CO_2$ produced to store it permanently inapposite sites so that it is not emitted into the atmosphere. $CO_2$ is separated at high purity in fitting pipes and then sent to the injection site. This is not unusual since carbon dioxide naturally accumulates under the ground and is commonly found when extracting fossil fuels. In the United States alone, more than 70 projects inject circa 30 Mtonn/year of $CO_2$ [20B]. It is estimated that in the world, there's the possibility to store more than 1000 Gtonn (10)

CO₂ can be stocked in many ways:

- Oil or Natural gas fields: this can be done for depleted fields or to extract oil further or natural gas by injecting compressed $CO_2$ in the so-called Enhanced Oil Recovery (EOR) practice; this is the leading method since it guarantees an economic return.
- Oceanic depths: a substantial percentage of the emitted $CO_2$ is already absorbed by the Oceans; in this case, $CO_2$ is injected at more than 1000 m depth; this could contribute to water acidification, and it does not guarantee that $CO_2$ will remain at that depth due to diffusion.
- Non-exploitable carboniferous veins (ECBM): in this case, $CO_2$ can free methane and other gases with lower affinity trapped in the porous carboniferous rocks again, and an economic return is predicted.
- Mineral seizure: $CO_2$ reacts with silicates to form a solid phase.
- Saline aquifers: $CO_2$ is trapped at 800-1000 m under the ground in a porous rock saturated with water bordered by layers of non-permeable rock (caprock); it remains in place due to residual trapping, and after long permanence, it can dissolve in water (dissolution trapping) or form carbonates (mineral trapping).

Figure 1-5 gives a visual representation of some possible choices for storing CO₂.
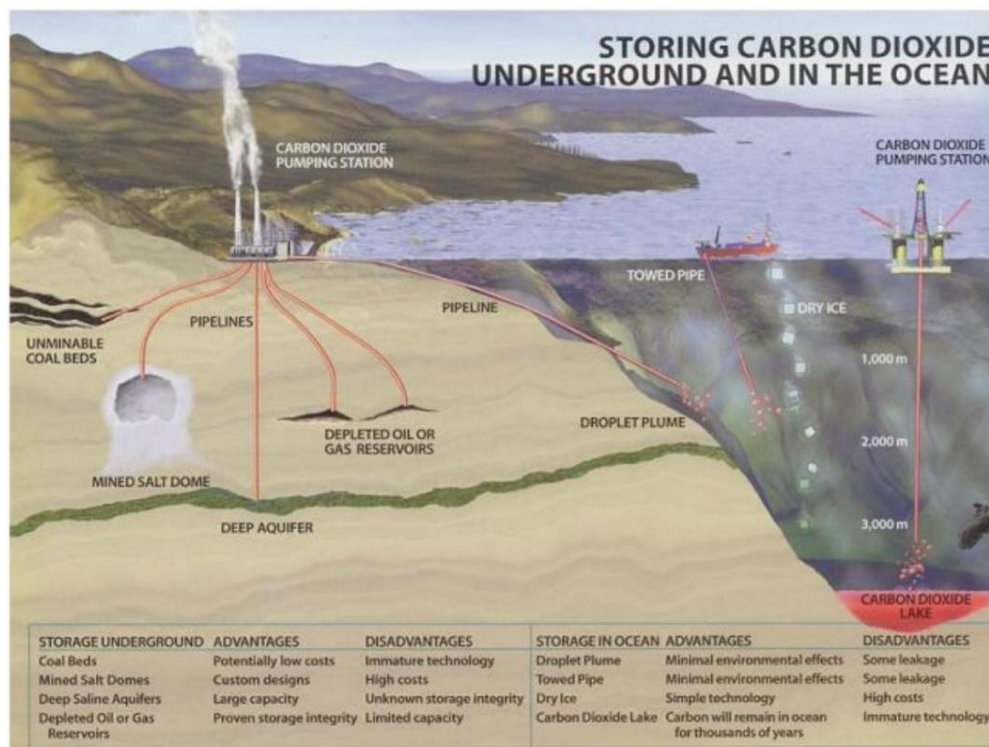


Figure 1-5 visual representation of some possible choices for storing

# 2 State of the art in H₂ production

The various pathways for H₂ production are shown in Figure 2-1
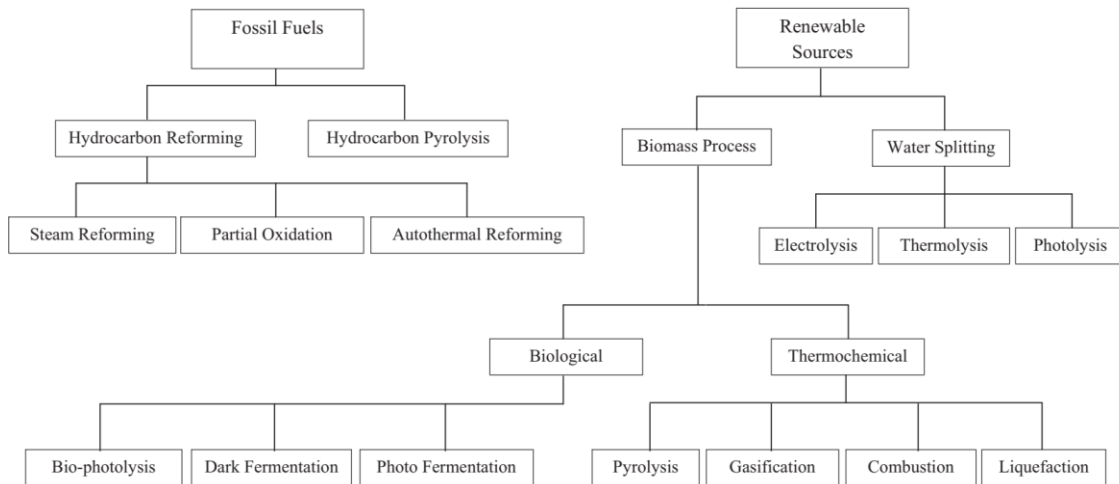


Figure 2-1 H₂ production methods (11).

## 2.1. H₂ production from fossil fuels

There are two main technologies for producing H₂ from fossil fuels, which are hydrocarbon reforming and pyrolysis. These techniques are the most progressive and normally used, meeting almost all H₂ markets. Mainly, up to date, H₂ was produced 48% from natural gas, 30% from heavy oils and naphtha, and 18% from coal (12). Nowadays, fossil fuels retain their dominant role in the world's H₂ supply as the production costs are highly correlated to fuel prices that are still kept to acceptable levels.

Several technologies produce H₂ from fossil fuels. Currently, the leading technologies are:

- Steam methane reforming (SMR)
- Auto thermal reforming (ATR)
- Partial oxidation (POX)
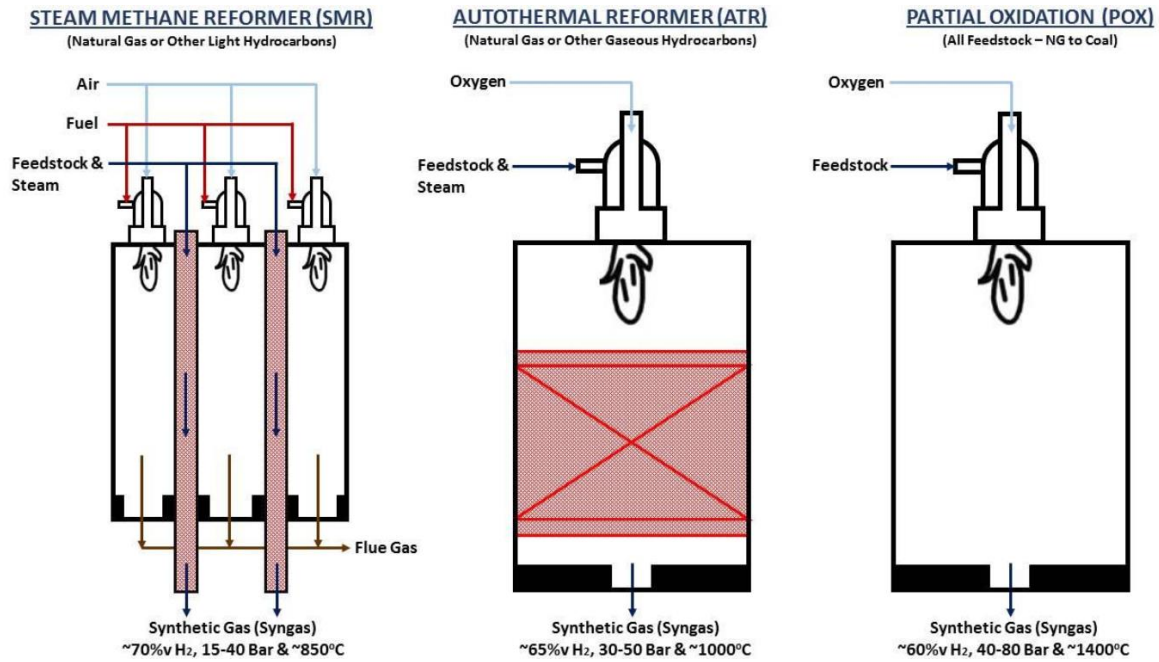
Figure 2-2 Main H₂ production processes (13).

## 2.1.1. Hydrocarbon reforming

Hydrocarbon reforming is how the hydrocarbon fuel is turned into H₂ through some reforming techniques. In addition to the hydrocarbon, the other reactant for the reforming process can be either steam or oxygen. The reaction with steam which is endothermic is known as steam reforming, and the reaction with oxygen, which is exothermic, is known as partial oxidation. When these two reactions are integrated, it is termed the autothermal reaction (14) A typical reforming plant consists of the desulphurization unit, the reforming and clean-up sections, and the auxiliary units such as pumps, compressors, expanders, heat exchangers, coolers, combustors, etc., (15).

Adiabatic Pre-Reformer

After removing all the detrimental species, the feed stream is mixed with steam from the regenerative section of the plant at about 300 °C in order to reach adequate steam to carbon ratio (S/C). In the case of large plants (more than 60000 Nm3/h (13), it is required to insert a pre-reforming section in which heavier hydrocarbons are converted into methane, H₂, and carbon oxides upon entering the main reforming section.

Heavier hydrocarbons (C2+) perform steam reforming at a temperature lower than the ones for methane, as it can be clear considering the higher standard enthalpy of reaction (highly endothermic reaction) visible in Table 2-1. This could allow the

formation of non-saturated compounds and carbon deposits if the inlet temperature is too high, which is a problem for the downstream catalysts of the main reforming reactor; moreover, fouling of heat exchangers can happen. The reactor is a vessel with catalysts based on Nickel (16) that operates at a temperature between 600-700°C, and under this condition, it can be assumed that all the heavy hydrocarbons are converted. The main advantages consist in:

- reducing the heat required for the main reformer
- preventing carbon deposits on nickel catalysts or fouling of heat exchangers
- reducing the necessary S/C ratio for the main reformer (steam is formed in the adiabatic reformer)
- allowing higher inlet temperatures for the reformer

Table 2-1 Steam Reforming Reactions (16).

| Reaction | Std. enthalpy of reaction $(-\Delta H^o_{298}$, kJ/mol) | Equilibrium constant $\ln K_p = A + B/T^a$ | |
|---|---|---|---|
| | | A | B |
| 1. $CH_4 + H_2O \rightleftarrows CO + 3H_2$ | −206 | 30.420 | −27,106 |
| 2. $CH_4 + CO_2 \rightleftarrows 2CO + 2H_2$ | −247 | 34.218 | −31,266 |
| 3. $CO + H_2O \rightleftarrows CO_2 + H_2$ | 41 | −3.798 | 4160 |
| 4. $C_nH_m + nH_2O \rightarrow nCO + (n + \frac{m}{2})H_2$ | −1175[b] | 21,053[b] | −141,717[b] |

[a] Standard state: 298 K and 1 bar.
[b] For $n$-$C_7H_{16}$.

$$C_n + nH_2O \leftrightarrow nCO + \left(n + \frac{m}{2}\right)H_2 \qquad \text{2-1}$$

$$CO + 3H_2 \leftrightarrow CH_4 + H_2O \qquad \text{2-2}$$
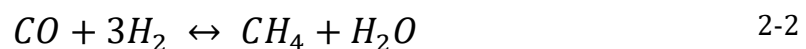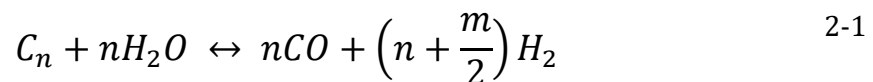
Whether one reaction prevails over the other, the global balance could be exothermic or endothermic. For what concerns natural gas, the global reaction is endothermic, so the outlet temperature will be reduced, while for diesel or kerosene, it is exothermic. Before entering the main reforming section, the outlet stream must be preheated.

Steam reforming

The feed from the adiabatic pre-reformer enters the primary reforming section. At this point is important to point out the main distinctions among all the different technologies and solutions for performing Steam Methane Reforming.

The steam reforming (SR) method concerns a catalytic conversion of the hydrocarbon and steam to $H_2$ and carbon oxides and consists of the main steps of reforming or synthesis gas (syngas) generation, water-gas shift (WGS), and gas purification. Raw materials range from methane to natural gas and other methane-containing gases through light hydrocarbons, including ethane, propane, butane, pentane, and light and heavy naphtha. To produce the desired purified $H_2$ product and prevent coking formation on the catalyst surface, the operation parameters of the reforming reaction are selected at high temperatures, pressures up to 3.5 MPa, and steam-to-carbon ratios of 3.5 (15). After the reformer, the gas mixture passes through a heat recovery step and is fed into a WGS reactor where the CO reacts with steam to produce additional $H_2$, and then, the mixture passes either through a $CO_2$-removal and methanation or through a pressure swing adsorption (PSA), leaving $H_2$ with a purity of near 100% (17) The $CO_2$ emissions can be strongly reduced by $CO_2$ capture and storage (CCS), through which $CO_2$ is captured and injected into geological reservoirs or the ocean (18). The main chemical reactions that take place in SR are shown in Eqs. 2-3 to 2-4

*Reformer*
$$C_nH_m + nH_2O \leftrightarrow nCO + \left(n + \frac{m}{2}\right)H_2 \qquad \text{2-3}$$

*WGS reactor*
$$CO + H_2O \leftrightarrow CO_2 + H_2 \qquad \text{2-4}$$
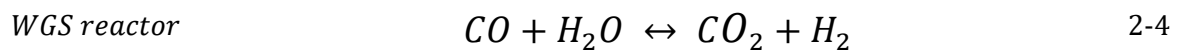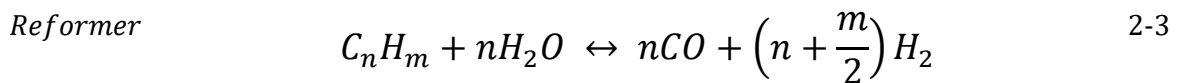
SR of methane can be defined by applying n=1 and m=4 to the Eq. 2-3, and the heat of the reaction will be -206 Kj/mol. Steam methane reforming (SMR) is the most typical and developed technique used for large-scale $H_2$ production, with 74–85% conversion efficiency. Figure 2-3 shows a simplified flow diagram of $H_2$ production from methane. Steam and natural gas are reacted over a nickel-based catalyst to produce syngas at temperatures of about 850–900 °C, and higher quality $H_2$ (99,999%) is acquired by applying PSA to separate $H_2$ from the other components (14). The fuel required for reforming to obtain of 63.3 kJ/mol $H_2$ can be provided by 30–35% of the total amount of natural gas as a process fuel-producing other stack gases with $CO_2$ concentration, resulting in total emissions of up to 0.3–0.4 m3 $CO_2$ per m3 of $H_2$ delivered (19).
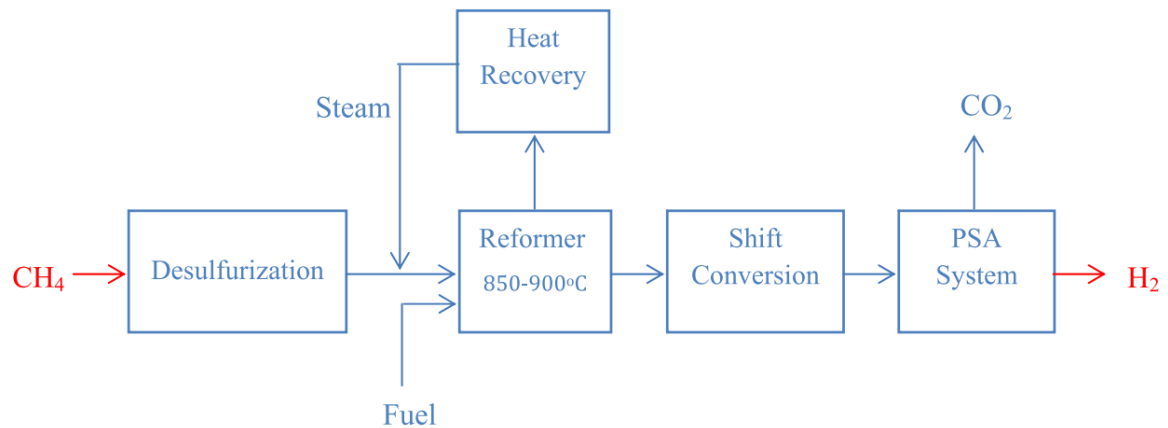
Figure 2-3  Flow diagram of the steam methane reforming process.

Here, we are going to explain about different configurations of reactors:

Fired tubular reactors

It consists of a furnace in which many catalysts-filled tubes are placed. In the furnace, natural gas from the feed (or recycled $H_2$) is burned with a specific excess of air to give heat to the reactor. The tubes placed in the radiant part of the heater are heated thanks to radiation and convection and transfer heat by conduction to the catalysts that fill the tubes. Many different configurations can be adopted for the geometry of the reactor, as shown in Figure 2-4. (20).



Bottom Fired          Top Fired          Terrace Wall          Side Fired
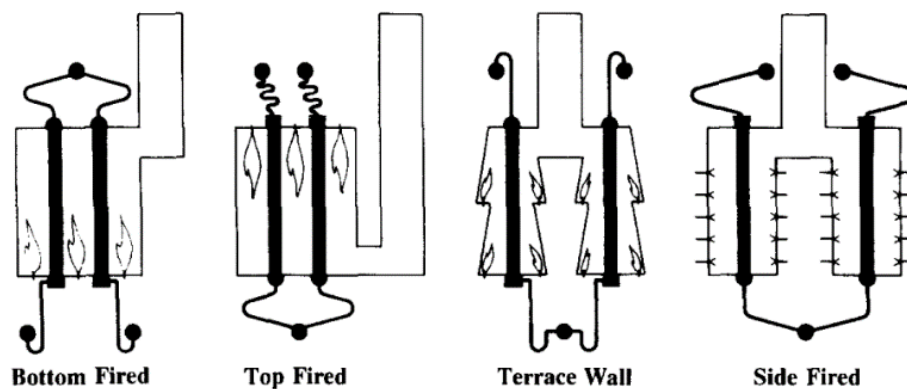
Figure 2-4 Different configurations for Fired tubular reactors (20).

The tubes are produced in high alloy metals such as HP 25/35 Ni-Cr alloy that is able to withstand high temperatures (around 1000°C) and considerably high pressure (30 bar) (21). Typically, the length of each tube is approximately 10-14 m and with a diameter in between 100- 180 mm with a thickness of around 8-20 mm (22).

An important relationship can be drawn for the maximum of the tube stress value (in N/m2).

$$\sigma = P \cdot \frac{D}{2s} \; [\frac{N}{m^2}] \qquad\qquad \text{2-5}$$

Where P is the pressure [bar], D is the diameter of each tube, and s is the thickness of the pipes. For a better choice of the materials that can withstand creep, the Larson-Miller parameter can be used:

$$P_{LM} = T \cdot (a + ln_{10} t) \qquad\qquad \text{2-6}$$

Where $P_{LM}$ is univocally linked to the stress-level $\sigma$ that the considered metal can sustain, it is thus kept constant so that a correlation between time of rupture t and temperature T is found; a is a parameter, and it is equal to 20. So that considering a certain number of hours, 100000, for example, (22) , it is possible to calculate a maximum temperature of around 1050 °C that must not be overcome. For what concerns, the operating pressure is clearly related to the considered metal, and it is around 25-35 bar. The temperature range is between 870-920°C (23).

For what concerns the steam to carbon ratio, it is between 2.7-4 for this technology, and it will vary considering auto-thermal reformers. As it has been already discussed, increasing this value has some positive outcomes, particularly in increasing the amount of $H_2$ produced. On the other side, by considering a high value, more heat would be required to heat all the needed steam, which behaves as inert, so the amount of natural gas to be burned in the furnace would increase; thus, $H_2$ efficiency would decrease. The minimum value is 2.7, and not less since by reducing the amount of steam in the tubes, the thermal resistance of the design changes, so the temperature of the wall (consequently the temperature gradient of the wall) can increase, resulting in higher thermo-mechanical stresses. Moreover, the reaction slows down due to the lower steam molar fraction in the reactants, which can also lead to carbon deposits on the walls that cause an increase in the wall's resistance and, more importantly, catalyst deactivation. A visual representation of an FTR scheme is presented in Figure 2-5. (13)
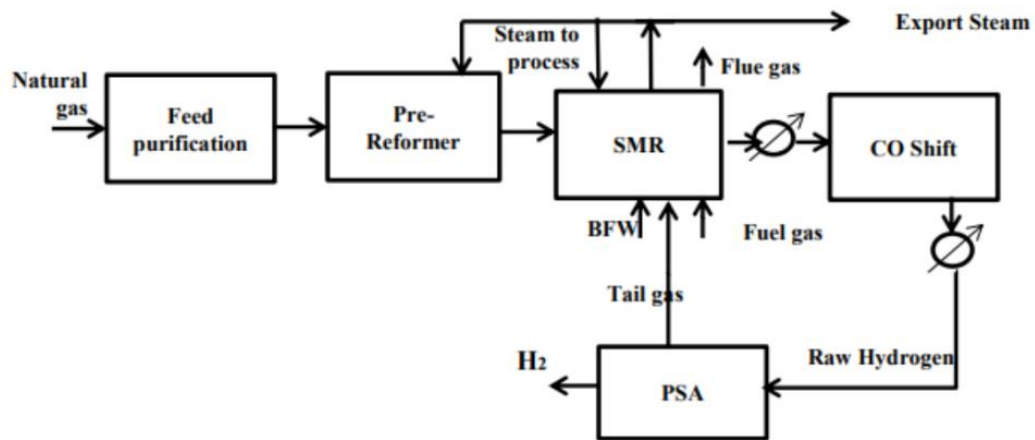
Figure 2-5 Block Flow Diagram of an FTR-SMR (13)

Heat Exchanger Reformer

This reactor is like an FTR in which the necessary heat is exchanged thanks to convective heaters (Figure 2-6) and not by radiative heat as for a fired tubular reactor. Process gases give all the heat or part of it. It can be utilized as a single-stage reformer for applications in small plants that feed fuel cells; those applications require compactness and high efficiencies. For these reasons, the typical size is around 50-4000 Nm3/h (fuel cell operating conditions (20)), while for high-pressure applications, the "convection reformer" can be considered. The convection reformer consists of bayonet tubes in which flue gases and reformer gases both flow upwards and heat the reformer. The geometry as described in (20) allows optimizing the heat exchange so that the reformer exhibits lower maximum temperature for walls and insensitivity to variations of operating conditions. Both flows leave the reactor at around 600°C (20).
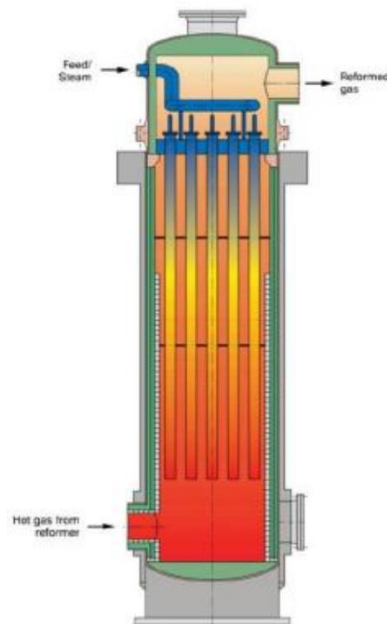
Figure 2-6 Heat exchanger reactor

Typically, this reactor is used in a two-step configuration. An FTR or an Auto-Thermal reactor feeds it, and it behaves as an adiabatic pre-reformer fed by the convective heat released by reformer gases. Two possible configurations are shown in Figure 2-7, in which the reformer is referred to as Gas Heated Reformer (GHR). In this case, most of the heat for the reaction is given in the main reactor (60-80%) while the reaction is completed in the second step.
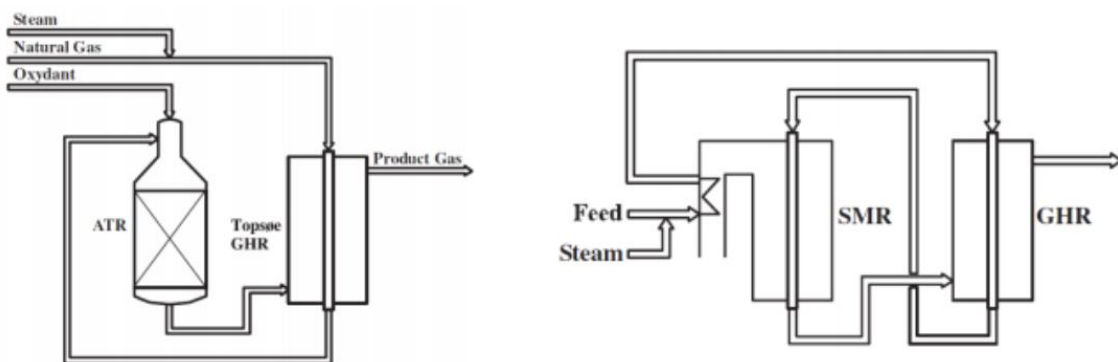


Figure 2-7 Heat exchanger reformer in two-step configuration

One of the problems related to this configuration that takes place when gases rich in carbon monoxide are in contact with the metal walls of the tubes is metal dusting corrosion. If the gas has a temperature lower than the Boudouard temperature, the Boudouard reaction, which is highly exothermic, can occur,

leading to the formation of carbon deposits on the walls. Carbon atoms can form carbides diffusing in the metal and end up corroding the walls of the heat transfer surfaces. Metals on the walls decompose in dust formed by metal oxides, carbides, and carbon atoms. The Boudouard temperature highly depends on the molar fraction of CO in the gases. Typically, during operation in the range of temperature 400- 800°C (16), metals that are contacted with gas at high CO content can be damaged and incur failures. To avoid this phenomenon high steam to carbon ratio is used (24).

Autothermal reforming
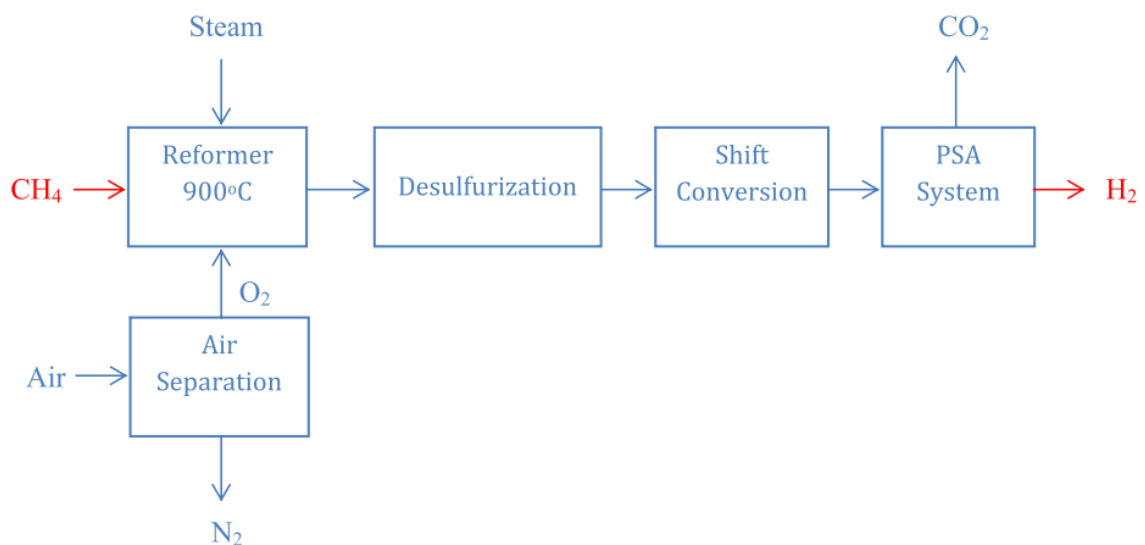


Figure 2-8 Flow diagram of the autothermal reforming of methane process.

Autothermal reforming, as presented in Figure 2-8, combines a catalytic combustion reaction with a catalytic reaction in an adiabatic vessel. The heat necessary to sustain the reforming reactions is delivered due to partial oxidation in a sub-stoichiometric environment of part of the natural gas inserted as a feed, as illustrated in Figure 2-9 (25).
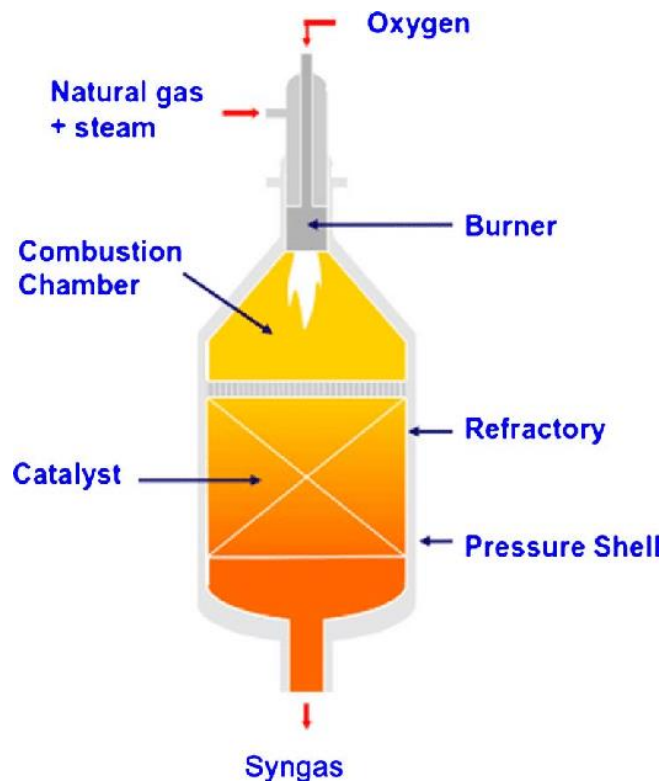
Figure 2-9 Auto-thermal reactor (25)

The ATR reactor is made up of a burner, a combustion chamber in which a flame is generated, and a catalyst bed, isolated by ceramic plates to protect it from the radiating heat of the flame; all of the components are held in a refractory lined pressure shell. The global reactor is adiabatic.

The partial oxidation reactions occur in the homogeneous phase in the combustion chamber, while in the catalytic zone, reactions become heterogeneous.

The combustion chamber temperature is about 1100 1300°C next to the catalyst bed, while it can reach more than 2500°C in the core of the flame. Steam methane reforming and water gas shift happens in the catalytic zone and the combustion zone without the need for catalysts due to the high temperatures. In order not to consume all the feed, combustion is sub-stoichiometric with overall oxygen to hydrocarbon ratio of 0.55-0.6 (16).

$$CH_4 + \frac{3}{2}O_2 \rightarrow CO + 2H_2O \ \ (\Delta h\degree_f(298\ K) = -519\ \frac{Kj}{mol}) \qquad \text{2-7}$$
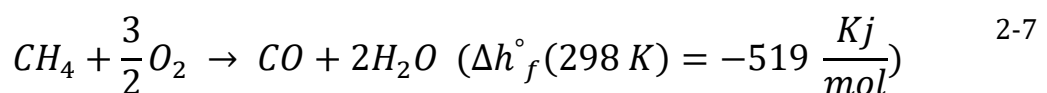
Due to the presence of water as a product of the reactions, reducing the steam to carbon ratio by a significant amount with respect to an FTR is possible. Values of steam to the carbon of around 1.5 are accepted due to the continuous production of water that moves the products of the SMR and WGS reactions.

Due to the ceramic refractory layers, lower temperatures are reached on the walls, allowing designers to use less creep-resistant materials such as carbon steels. For these reasons, pressure conditions are less strict and can reach up to 80 bar (22). The outlet temperatures are in the range of about 800-1100°C.

ATR can be fed with air or pure oxygen depending on the typical use; for example, the air is the standard if the plant is employed to produce ammonia. It is necessary to insert nitrogen for these applications to obtain an $H_2$ to nitrogen ratio ($H_2/N_2$) of around 3.

$$\frac{3}{2}H_2 + \frac{1}{2}N_2 \rightarrow NH_3 \ (\Delta H°r = -92 \ \frac{Kj}{mol}) \tag{2-8}$$
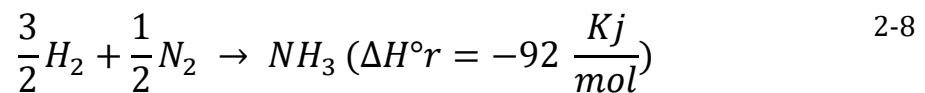
For regular operation in $H_2$ production, O2 is inserted with natural gas. To deliver the necessary amount of oxygen it must be used an Air Separation Unit (ASU) (Figure 2-10). This component produces a feed of pure (95%) oxygen alongside Ar and $N_2$. Due to the presence of this component which costs and energy requirements are elevated, the ATR is preferred to FTR for large plants producing more than 300000 Nm3/h (9).
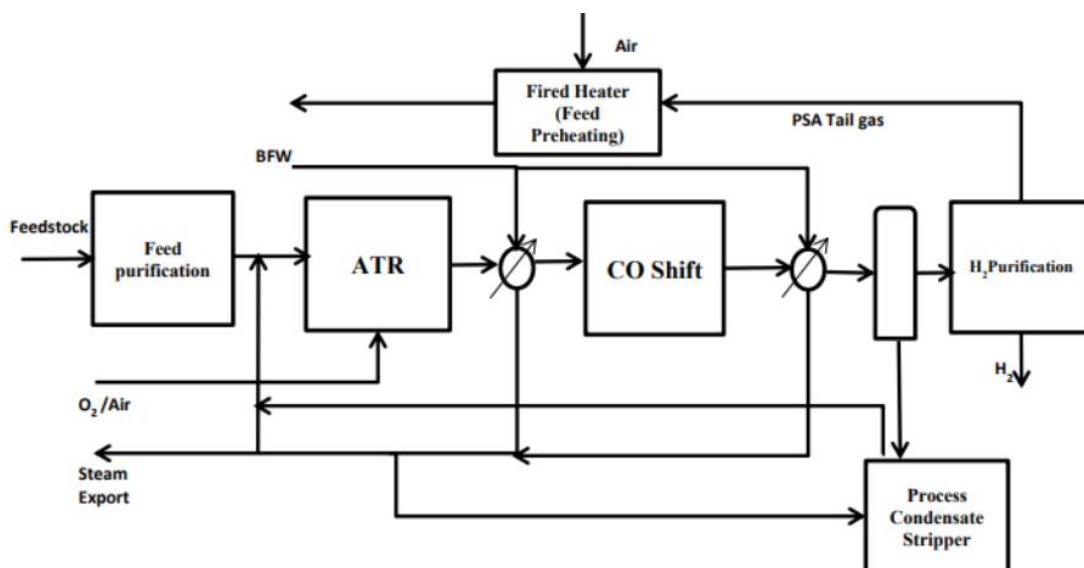


Figure 2-10 BFD of an ATR

Sorption-enhanced steam methane reforming (SE-SMR)

Sorption-enhanced steam methane reforming (SE-SMR) represents a novel, energy-efficient hydrogen production route with in situ $CO_2$ capture, shifting the reforming and water gas shift reactions beyond their conventional thermodynamic limits. A chapter is dedicated to this subject further.

The equipment's costs as a percentage of the overall $H_2$ production cost for SMR are as follows: 60.7% feedstock, 29.1% capital investment, and 10.2% O&M (17). It is estimated that the $H_2$ production cost, corresponding to plants with a design capacity of 379,387 kg/day, at a 90% capacity factor and a natural gas cost of 10.00 $/MMBtu, is 2.27 $/kg and 2.08 $/kg with and without carbon capture and sequestration, respectively (26).

## 2.1.2. Partial oxidation

The partial oxidation (POX) method involves the transformation of steam, oxygen, and hydrocarbons into $H_2$ and carbon oxides. The catalytic process, which happens at about 950 °C, works with feedstock ranging from methane to naphtha. In contrast, the non-catalytic process, which occurs at 1150–1315 °C, can operate with hydrocarbons, including methane, heavy oil, and coal (27). After sulfur removal, pure O2 is used to partially oxidize hydrocarbon feedstock, and the syngas produced is treated in the same way as the product gas of the SR process. The cost of the oxygen plant and the further costs of desulphurization steps make such a plant overly capital intensive (28). In the catalytic process, the heat is delivered by controlled combustion, and from methane, the thermal efficiency is 60–75% (29).

A typical flow sheet for $H_2$ production via the partial oxidation (POX) method is illustrated in Figure 2-11
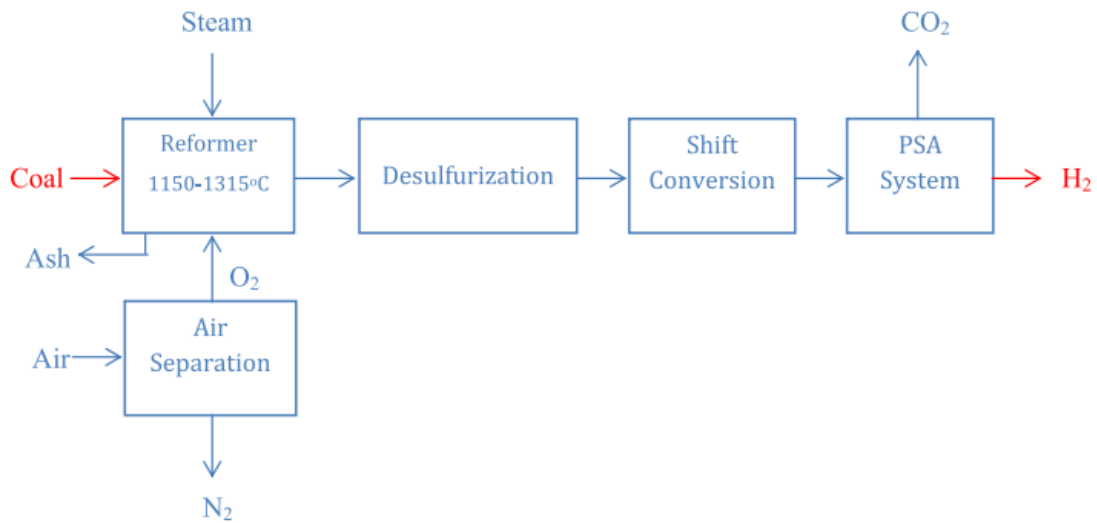
Figure 2-11 Flow diagram of the partial oxidation process.

## 2.2. Green H2 production by electrolysis

Although hydrocarbons are nowadays the primary feedstock used for H2 production, the need to increase the integration of renewable technologies will become inevitable. As fossil fuels are decreasing, and the Greenhouse effect is attracting greater attention, the percentage of renewable technologies will increase shortly. It is expected to dominate conventional technologies (30) in the long term. Although there are many processes for H2 production from renewable resources, a brief description of Electrolysis water splitting is included here.

Water is one of the most plentiful on Earth and can be utilized for H2 production through water-splitting processes such as Electrolysis (31). If the needed energy input is provided from renewable energy sources, the H2 produced will be the cleanest energy carrier that could be used by mankind.

Electrolysis is an established and well-known process, constituting the most effective technique for water splitting (32). The reaction, however, is very endothermic; thus, the required energy input is provided by electricity (33). A standard electrolysis unit or electrolyzer consists of a cathode, and an anode dipped in an electrolyte. Generally, when an electrical current is applied, water splits, and H2 is produced at the cathode while oxygen is evolved on the anode side via reaction 2-9 (34):

$$H_2O \rightarrow H_2 + \frac{1}{2}O_2 \ (\Delta H°r \ = \ +237\frac{MJ}{kmol})$$
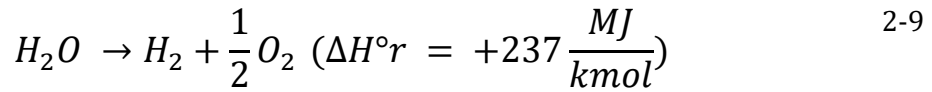
Although extremely pure hydrogen could be simply produced from water by electrolysis, the high consumption of electricity by electrolyzers prevents the production cost from competing with other large-scale technologies contributing with a share of about 5% to the total generation (35). However, if the electrical energy is provided by RES, such as hydro, wind, and solar, the H2 produced is the cleanest energy carrier, which can be used to store the excess electricity and improve the plant-load factor and efficiency on small scales (30).

Hydrogen offers a flexible energy storage solution for accommodating load variability of long duration, as is shown in Figure 2-12:
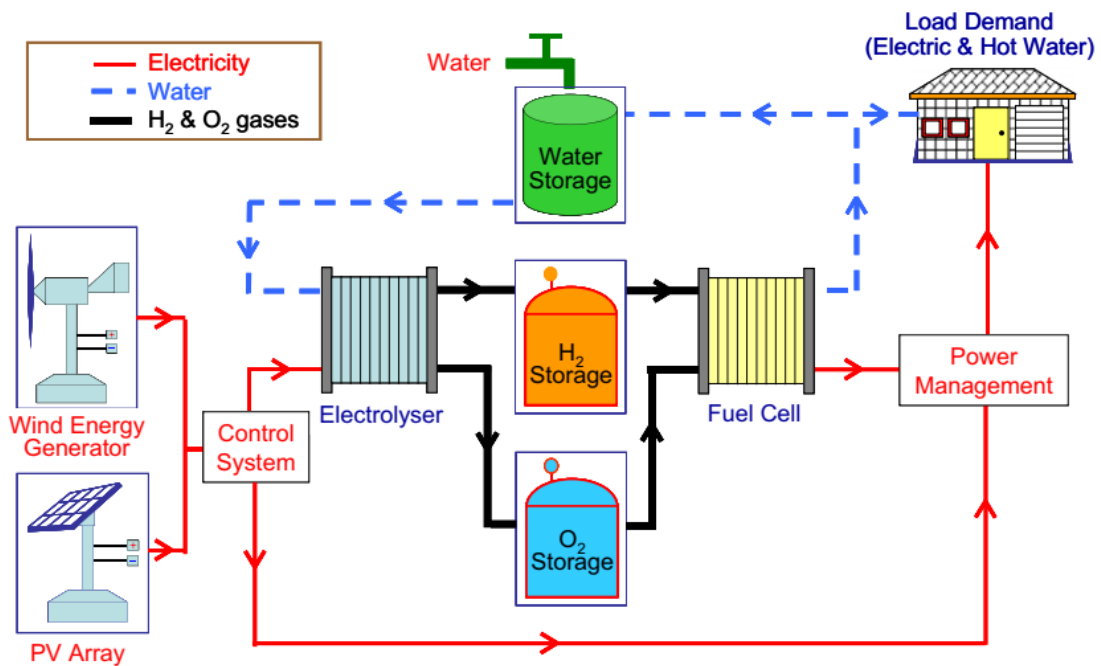


Figure 2-12 Renewable energy and hydrogen storage solution (36).

## 2.3. Coal and Biomass Gasification

Coal gasification is the second leading technology for hydrogen production, so a brief overview will be given. Due to the lower cost for the feedstock, it would probably remain a valid alternative to SMR in the future years even if it would necessarily require a CCS section; carbon content is indeed much greater with respect to Natural gas.

Chemically speaking, the gasification process is a non-catalytic process in which oxygen from an ASU and steam (as temperature moderator) is fed and mixed with the hydrocarbons from coal that are partly oxidized (auto-thermal) and partly react, forming syngas (mainly hydrogen and carbon monoxide).

Biomass gasification is the thermochemical conversion of biomass into a gaseous fuel (syngas) in a gasification medium such as air, oxygen, and/or steam. It occurs at temperatures between 500 °C and 1400 °C, with working pressures from atmospheric to 33 bar depending on the plant scale velocity of the gasifying agent (37) , respectively.

## 2.4.   Heat recovery section

To improve the global performance of the plant, making it more profitable, a heat recovery section is currently able to recover heat from the synthesis gas, producing valuable steam necessary for the plant itself and producing electricity and steam as valuable by-products. This increases the overall energy efficiency of the plant.

The gas leaving the reforming section has a high carbon monoxide content (13) and can therefore be shifted to improve the plant's hydrogen production and convert all the components that contain carbon into carbon dioxide. WGS is a slightly exothermic reaction, so it is favored at lower temperatures, so it is required to decrease the temperature of the synthesis gas. The equilibrium constant is given (38):

$$\ln K_p : \frac{4577.8}{T} - 4.33 \qquad\qquad \text{2-10}$$

Where T is in Kelvin, visual representation is given in Figure 2-13.
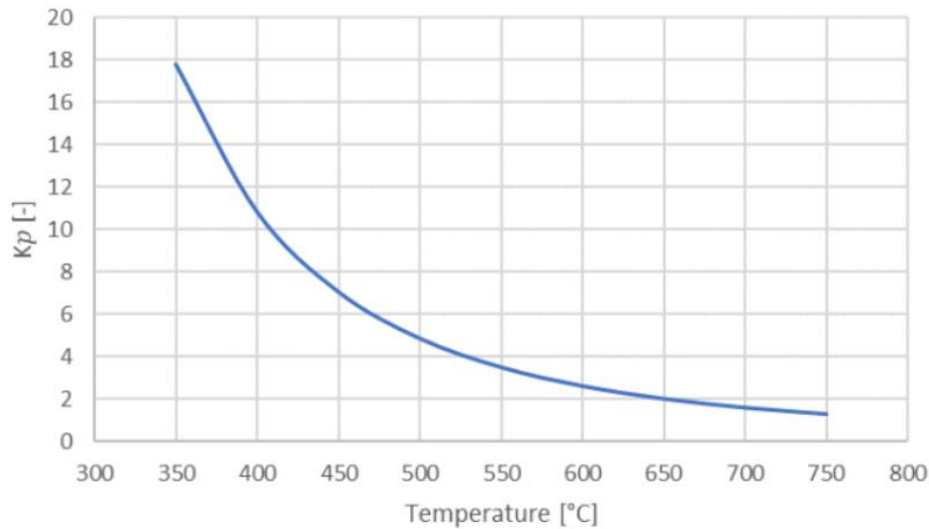
Figure 2-13 Equilibrium constant for WGS reaction as a function of temperature.

This can be done by introducing the heat recovery system that consists of economizers, evaporators, and superheaters thermally linked with the reformer. Generally, the reformed gas is cooled down to 350°C upon entering the High-Temperature Shift (HTS) reactor that uses an iron-based catalyst if sulfur is not anymore present and works in the range of 320-360°C (39) and 10-60 bar (wide range since it does not influence equilibrium composition). Further, a second reactor, Low-Temperature Shift (LTS), can be present that works with a copper catalyst around temperatures of 190-250°C (39); this reactor allows a high conversion. The WGS reaction can always be considered at equilibrium for these temperature ranges. The shifted gases are cooled down in the last part, delivering heat to the recovery section until around 35-40°C (13), and are flashed to remove water.

## 2.5.  CO2 separation

After the heat recovery section, Syngas gives a molar composition consisting primarily of $H_2$ and $CO_2$. Generally, in an SMR plant producing hydrogen, up to 60% of the $CO_2$ produced is present in the shifted gas and ends up in the off-gas recirculated to the reformer as additional fuel for the furnace. The typical pre-combustion technology is expressed in the following. It is possible to introduce another section to remove carbon dioxide with the proper purity for transport and storage (around 95%) (40).

One of the possible configurations adopted for $CO_2$ removal is presented in Figure 2-14, where two sections are present, one mandatory for capturing $CO_2$ from the Syngas after the recovery section and the other for purifying the exhaust gases that leave the furnace. Obviously, the typical position and technology for performing the separation strongly depends on the conditions of the stream and thus on the situation in the plant; an overview of the possible places is well described in Figure 2-15.
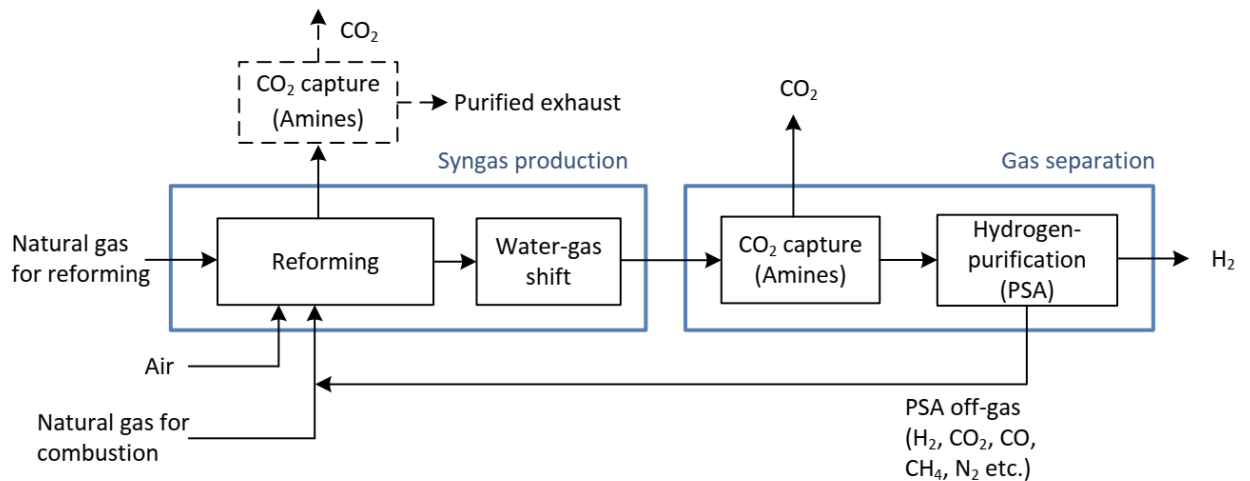


Figure 2-14 Modern reforming plant with CCS (40)
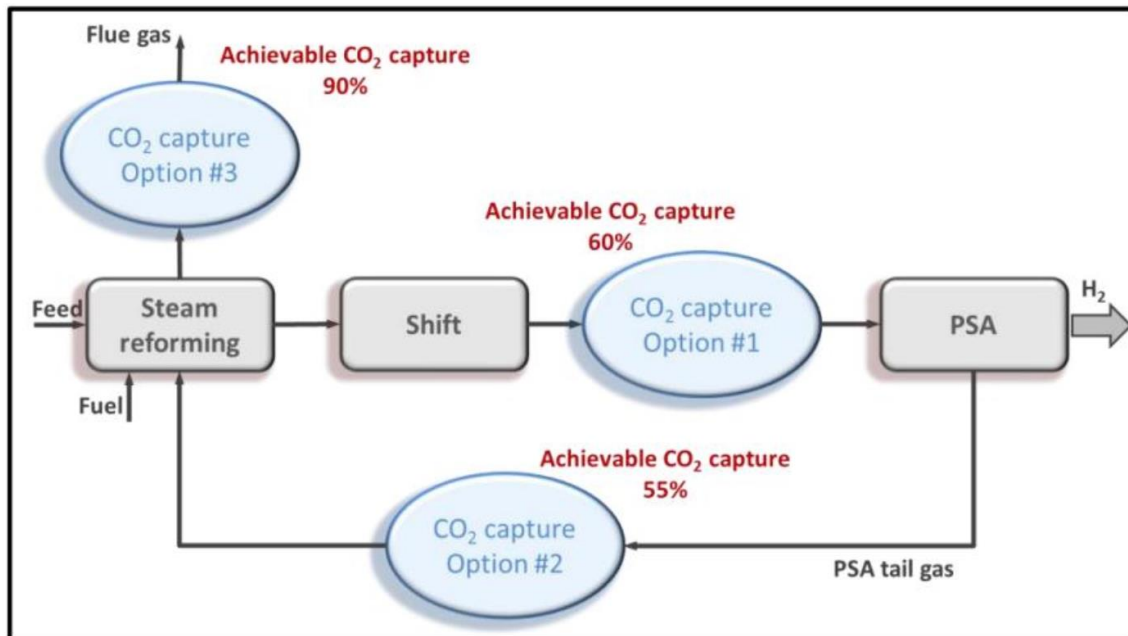


Figure 2-15 Different possibilities for placing the carbon removal section.

The resulting technique is decided considering the performances expressed in Table 2-2, where $\eta CO_2$ is the percentage difference between the emitted $CO_2$ and the emission without the CCS section.

Table 2-2 Comparison of the different choices for carbon removal.

| $CO_2$ removed from: | $CO_2$ removed from each stream (%) | Overall $\eta CO_2$ (%) |
|---|---|---|
| 1.PSA inlet (syngas) | 100 | 60 |
| 2.PSA tail gas | 90 | 55 |
| 3.SMR flue gas | 90 | 90 |

It's now essential to consider the purification technologies for both $H_2$ and $CO_2$ separation.

- Adsorption: a physical process in which gaseous substances are fixed to solid phases (called adsorber) based on the different affinities of each specie in the gaseous phase with the adsorber itself. Pressure Swing Adsorption (PSA), Temperature Swing Adsorption (TSA), and Vacuum Swing Adsorption (VSA) operate on this principle and are typically used for removal of both $CO_2$ and $H_2$ but also air separation when the production of O2 does not exceed 2000 Nm3/h (41).
- Absorption: performed by contacting two streams in a scrubber column: the syngas to be purified with the countercurrent liquid solvent as presented in Figure 2-16. The solvent is selective to the component that must be separated, and once it exits from the lower part of the column as a rich solvent, it is reheated or/and depressurized to allow the regeneration in a stripper column.
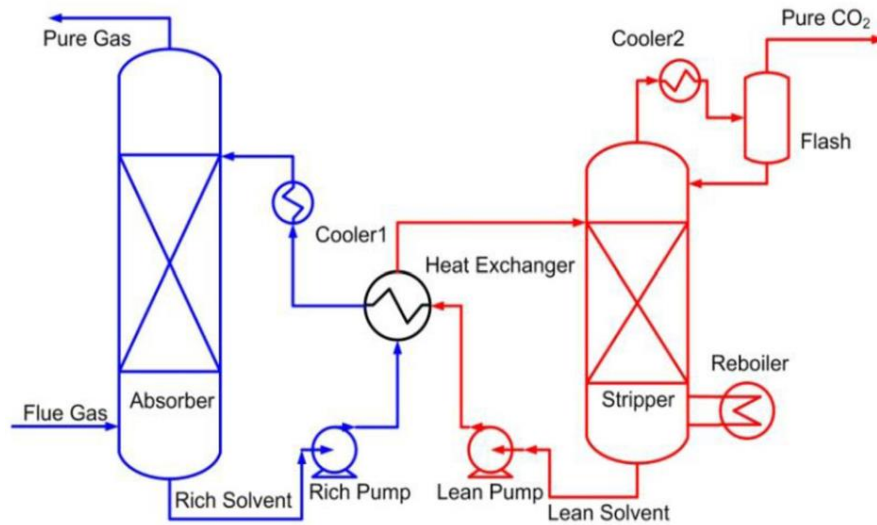
Figure 2-16 Process for CO₂ purification.

- Other technologies: the other leading technologies are membranes and cryogenic separation. Membranes allow the separation of acid gases from the feed due to the selective permeation of these species based on a difference in partial pressure among the two sides of the membrane. Cryogenic technologies separate carbon dioxide at quite low temperatures (after water removal) to liquefy up to a certain purity.

Among the different technologies, the most mature and adopted for carbon capture is absorption with solvents (39). Other advanced technologies for hydrogen production with chemical looping and low-temperature separation are under analysis, but those will not be considered in this thesis work.

## 2.6. Pressure swing adsorption

Hydrogen must be separated from the off-gas; Equilibrium based PSA offers the possibility to obtain hydrogen with a purity of 99.9999% (39). PSA works using the principle of adsorption, a physical process in which gaseous substances are fixed to solid phases (called adsorber). The schematic is presented in Figure 2-17; the syngas enters at high pressure and due to different selectivity of the adsorber with respect to all the species, except hydrogen that is practically not adsorbed (42). Indeed, hydrogen exists as pure hydrogen from the bed. To regenerate the bed, its pressure is lowered, and a certain part of the produced hydrogen is recirculated back. To reduce the self-consumption of hydrogen, a more complex configuration can be utilized; efficiency is then improved with a proper organization of the operation/regeneration cycles for each bed that is shifted in times and is made

such that the hydrogen for removal of impurities can be taken from a bed that is under depressurization step.
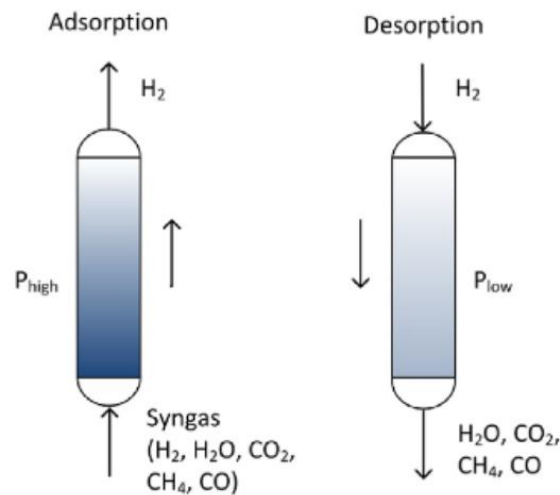


Figure 2-17 PSA beds in operation and regeneration modes.

Typical adsorbents are highly porous materials with a greater surface-on-volume ratio, such as silica gel, alumina, activated carbon, and zeolite, and typically different adsorbers are placed as individual layers in each bed to adsorb all the impurities (42).

PSA works at ambient temperature (adsorption is promoted at low temperature and higher partial pressure of the considered species). The feed pressure is between 20-60 atm while hydrogen leaves with a small pressure drop (<1 bar), and the off-gas is delivered at pressures around 1.1 to 1.7 atm (43).

# 3   Pyrolysis

Pyrolysis is a thermal process where the organic material is degraded in the absence of oxygen and air in a temperature range of 300 - 1110 $\circ$C. The cracking of the organic matter will result in three products, including liquids, gases, and solids. The product's ratio depends on the velocity or the residence time of the reaction, which separates pyrolysis into three groups: Slow pyrolysis, fast pyrolysis, and flash pyrolysis (44), Where the different conditions and the main products are shown in Table 3-1.

Table 3-1 Categorization of the different pyrolysis methods (45)

| Method | Temperature [°C] | Residence time | Major products |
|---|---|---|---|
| Slow pyrolysis | Med-high | Long | Gases |
| | 400-500 | 5-30 min | Char |
| | | | Liquid |
| Fast pyrolysis | Med-high | Short | Liquid |
| | 400-650 | 0.5-2 s | Gases |
| | | | Char |
| Flash pyrolysis | High | Very short | Gases |
| | 700-1000 | < 0.5 s | Liquid |

## 3.1.  Biomass Pyrolysis

Thermochemical processes constitute the technique of transforming biomass into hydrogen and hydrogen-rich gases (46) (47). Hydrogen-rich gas production from synthesis gas obtained from such methods is a practical step forward for a climate with zero emission of greenhouse gases necessary for sustainable development (48). Thermochemical technology mainly involves pyrolysis and gasification. Both conversion processes produce, among other gaseous products, $CH_4$ and CO, which can be further processed for more hydrogen production through steam reforming and WGS reaction. They offer low hydrogen production, with the first

emitting polluting byproducts and the second requiring challenging to be achieved operation conditions of 5–20 MPa in the absence of air (49).

Biomass pyrolysis is the thermochemical process of generating liquid oils, solid charcoal, and gaseous compounds by heating the biomass at 650–800 K at 0.1–0.5 MPa (50). It takes place in the total absence of oxygen, excluding when partial combustion is allowed to provide the thermal energy needed for the process [52n]. Methane and other hydrocarbon gases produced can be steam reformed, and for even more hydrogen production WGS reaction is applied. After CO is converted into $CO_2$ and $H_2$, the desired purified $H_2$ is obtained by PSA (51). The individual steps of the biomass pyrolysis process, shown in Figure 3-1, are represented by the following Eqs.:

$$Pyrolysis\ of\ biomass \rightarrow CO + H_2 + CO_2 + \text{hydrocarbons} \qquad \text{3-1}$$

$$C_nH_m + nH_2O \rightarrow nCO + \left(n + \frac{m}{2}\right)H_2 \qquad \text{3-2}$$

$$CO + H_2O \rightarrow CO_2 + H_2 \qquad \text{3-3}$$
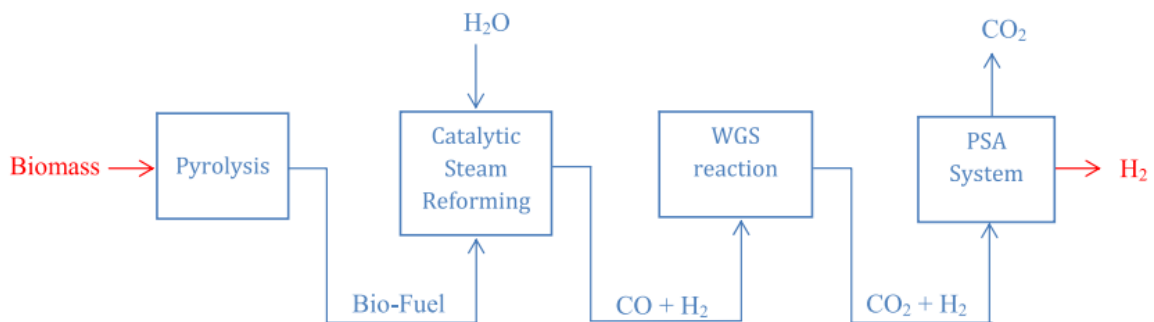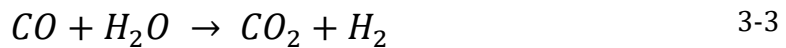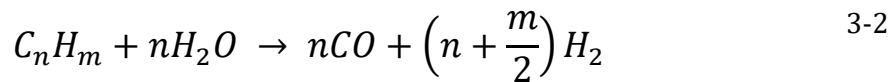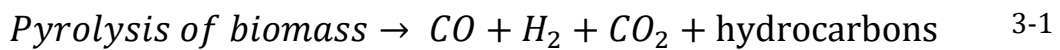


Figure 3-1 Flow diagram of the biomass pyrolysis process.

## 3.2. Plastic pyrolysis

### 3.2.1. Reactor

Multiple different reactors are designed to convert plastic into gaseous, liquid, and solid products (52). The design of the reactor and the operational conditions affect

the different yields of the three products (53). The sticky nature and the low thermal conductivity of plastic must be considered when choosing a reactor for thermal pyrolysis (54). In the literature, several cases of plastic pyrolysis have been documented using a fluidized bed reactor (55) (56) (57) (58). The reactor's ability to reach high heat and mass transfer rates enables it to work under isothermal conditions (54). A different reactor that has been studied for the cracking of plastic is the conical spouted bed reactor (CSBR) (54) (59) (60) (61) (62). Before the pyrolysis, the plastic is melted, making it able to coat the solid particles (sand or catalyst) contained in the CSBR (54).

Along with the cyclic movement of the coated solid particles, the CSBR can avoid agglomeration problems that may be caused due to the melted plastic (63). The CSBR has a wide range of gas residence times, which minimizes the potential secondary reactions like the condensing of light olefins to produce polyaromatics (54). The CSBR contributes to a high selectivity of waxes (C21+), which may be used downstream for catalytic upgrading to obtain valuable products or as feedstocks for refinery units in the petrochemical industry (63). However, the CSBR is quite expensive as it needs high gas velocities to fluidize the bed (64). It has a rather complex design based on a conical geometry and has some scale-up limitations (64). Nevertheless, FernandezAkarregi et al. designed a conical spouted bed reactor pilot plant for biomass pyrolysis of 25 kg/h (65).

## 3.2.2.  Catalytic Pyrolysis

As mentioned earlier, thermal pyrolysis of plastic results mainly in waxes. Catalytic pyrolysis is an excellent option to increase selectivity toward valuable products from plastic pyrolysis. Studies comparing the thermal and catalytic pyrolysis of plastic have shown that catalytic pyrolysis with zeolite ZSM-5 produces mainly gaseous species and a smaller liquid fraction than thermal pyrolysis, as seen in Table 3-2 (65).

Table 3-2 comprising of yields pyrolysis of HDPE with ZSM-5 (65)

| Yield [Wt%] | | Thermal pyrolysis | Catalytic pyrolysis (ZSM-5) |
|---|---|---|---|
| **Gas** | | 13.00 | 63.50 |
| **Liquid** | Total | 84.00 | 35.00 |
| | $C_6$-$C_{12}$ | 56.55 | 99.92 |
| | $C_{13}$-$C_{23}$ | 37.79 | 0.08 |
| | >$C_{23}$ | 5.66 | 0 |
| **Solid** | | 3.05 | 2.50 |

Catalytic fast pyrolysis (CFP) can either be performed as an in-situ or an ex-situ process, as shown in Figure 3-2. In the in-situ pyrolysis, the catalyst is mixed with the plastic and fed together to be pyrolyzed in the reactor (66). On the other hand, ex-situ catalytic pyrolysis is a two-step process involving a thermal pyrolysis reactor where the plastic is pyrolyzed, followed by a catalytic reactor downstream to upgrade pyrolysis vapors produced in the first reactor (54).
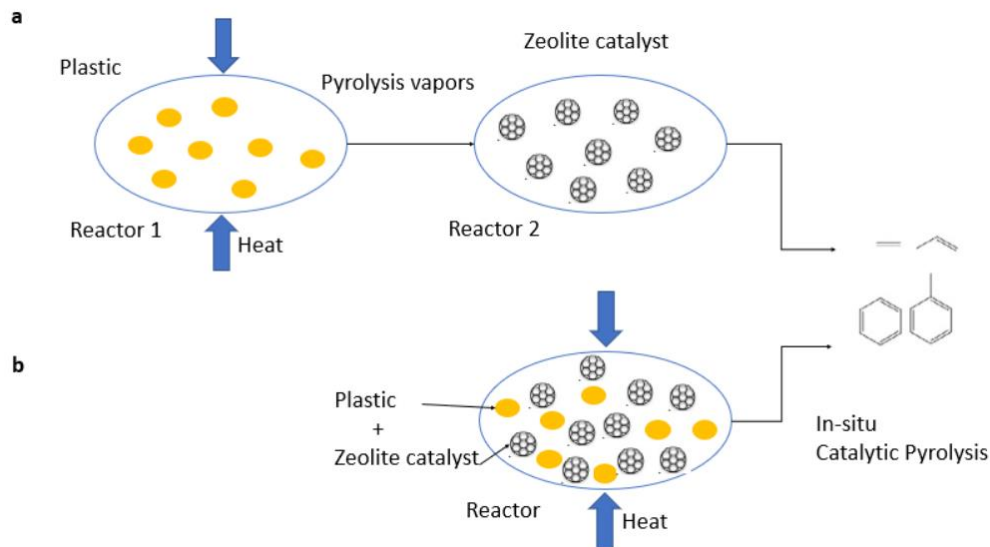


Figure 3-2 The schematic process of ex-situ catalytic pyrolysis (a) and in-situ catalytic pyrolysis (b) (66)

As the in-situ CFP is conducted in one reactor, a high catalyst/plastic ratio is required to ensure a high-quality upgrading product. Also, the temperature in the reactor must be regulated according to the thermal pyrolysis, which may not be the optimal temperature for the catalyst (67). This can also lead to a higher coke formation on the catalyst, which must be regenerated frequently. Compared to the in-situ CFP, the two-step system in ex-situ CFP makes it possible to use different temperatures and contact times in each reactor (68). The upgrading can be run with the optimal conditions for the catalytic performance resulting in the highest yield of the desired product, in this case, olefins (54). Another advantage of the ex-situ configuration is the possibility of removing char and solids after the first reactor, creating a milder environment for the catalyst performance (69). As the in-situ CFP only consists of one reactor, the process will result in a lower investment capital than the ex-situ process but a higher operating cost due to the high coke formation.

Regarding olefins production, Wang et al. reported that an ex-situ catalytic pyrolysis of biomass gave a higher yield of olefins than an in-situ catalytic pyrolysis process (66). This can also be seen in various articles regarding the

pyrolysis of plastic. The highest olefins yields are usually through ex-situ pyrolysis or catalytic upgrading of the pyrolysis vapors (70).

The most common reactors used for catalytic upgrading are the fluidized or fixed bed reactors. The fluidized bed reactors have a remarkable ability for heat and mass transferring (54). Nevertheless, the fixed bed reactor's catalyst flexibility provides greater control over the chemistry and the product distribution (71). Comparing the cost of the two reactors, the fixed bed reactor has a higher capital cost but a lower catalyst cost than the fluidized bed systems, which makes the overall costs comparable. There are many ways to heat a fixed bed reactor, one of which is using a multitubular reactor (72). The catalyst is arranged in straight parallel tubes surrounded by a heat carrier circulating, providing the heat needed for the reaction. For reaction temperatures above 500 ∘C, hot flue gas is the most common heat transfer medium.

### 3.2.3. Industrial scale

Today, there are many large-scale pyrolysis plants for the degradation of waste plastic worldwide (73). The largest Waste-plastics-to-oil recovery plant in Japan is called Sapporo Plastic Recycling (SPR). Through thermal pyrolysis, they recover light oil for chemical feedstock

for new plastics, a medium fuel oil like diesel, and a heavier oil used to generate energy. As feedstock, they use waste polypropylene (PP), polystyrene (PS), polyethylene terephthalate (PET), and polyvinyl chloride (PVC), recycling an amount of 15 000 tones/year of waste plastic.

# 4   SE-SMR

## 4.1.  Introduction

Hydrogen can be acquired from renewable energy resources, such as bioethanol, glycerol, bio-oil, and biomass, although nowadays, hydrogen is mostly produced from fossil fuels. More than 50% of the global hydrogen production is provided by methane steam reforming, while 30% is obtained from oil/naphtha reforming and 18% from coal gasification. (74)

Sorption Enhanced-Steam Methane Reforming (SE-SMR) is an advantageous process that allows $H_2$-rich stream production in a single reactor from natural gas while capturing the $CO_2$ by reaction with a solid sorbent.

The capture of $CO_2$ in different plants can be accomplished by employing various strategies.

Pre-combustion separation technologies usually imply a three-stage fuel processing series where:

1.  the primary feedstock is first converted at high temperature into a synthesis gas stream where carbon is mainly in the form of carbon monoxide (CO).
2.  Most of the heating value of the syngas is reallocated from CO to $H_2$ through an intermediate temperature, catalytically activated water gas shift reaction, which at the same time converts CO to $CO_2$.
3.  Removing $CO_2$ from syngas is accomplished at ambient temperature through appropriate selective solvents. (75)

This arrangement suffers from two significant disadvantages: (i) plant complexity due to the presence of different sections, each designated to execute one single processing stage; (ii) different temperature levels for each stage, indicating syngas cooling, which in turn requires extensive heat transfer surfaces and brings about a significant conversion efficiency decay.

Instead, a substantial improvement would be achieved if all these stages could be compacted into a single step. This can be obtained, for instance, by subtracting $CO_2$ from the gaseous phase during the syngas generation process, which in turn significantly improves the conversion of CO to $CO_2$ due to the removal of the reaction product. This thesis investigates how this concept can find practical application when plastic pyrolysis NCG is used as primary feedstock, and $CO_2$

removal is carried out by reaction with calcium oxide through a Sorption Enhanced-Steam Reforming (SER) process. (75)

## 4.2. Thermodynamic principles

The following steam methane reforming (SMR) reactions:

$$CH_4 + H_2O \leftrightarrow CO + 3H_2 \ (\Delta H°r \ (298 \ K) = +205.9\frac{MJ}{kmol}) \qquad \text{4-1}$$

$$CH_4 + 2H_2O \leftrightarrow CO_2 + 4H_2 \ (\Delta H°r \ (298 \ K) = +165\frac{MJ}{kmol}) \qquad \text{4-2}$$
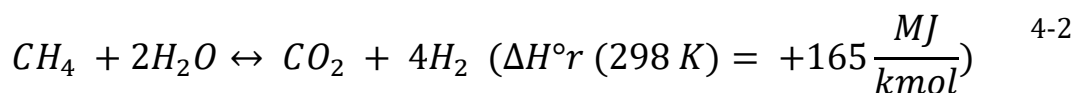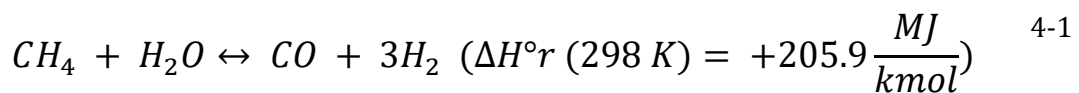
are the reference for $H_2$ production from natural gas in mid and large-scale plants. Since reforming reaction is endothermic and the moles of products are more than reactants, high temperatures and lower pressures favor high conversion extents.

When a carbon-free synthesis gas is required, for example, in low $CO_2$ emission power plants, carbon monoxide generated by the reforming reaction is converted into $H_2$ and $CO_2$ according to the water gas shift (WGS)4-3:

$$CO + H_2O \leftrightarrow CO_2 + H_2 \ (\Delta H°r \ (298 \ K) = -41.2\frac{kJ}{mol}) \qquad \text{4-3}$$
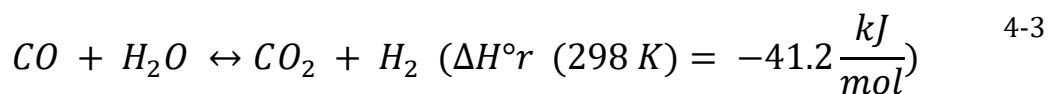
Usually, two WGS reactors with intermediate cooling are operated in order to: (i) combine high CO conversion in the colder reactor with faster kinetics in the hotter one and (ii) retrieve with a higher efficiency the heat of reaction after the first WGS reactor, which is available at high temperature (400-500°C) (75).

An option to obtain high methane to $H_2$ conversions in a single step is removing one of the reaction products from the gaseous phase. In Sorption Enhanced-Steam Methane Reforming (SE-SMR) processes, $CO_2$ is adsorbed over a solid sorbent while SMR and WGS reactions occur. Therefore, the progression of the gaseous phase reactions 4-1 and 4-3 is not limited to the equilibrium set by $CO_2$ formation and proceeds almost to a complete depletion of reactants. A promising sorbent for

SE-SMR applications seems to be calcium oxide, which can react with $CO_2$ generating $CaCO_3$ according to the following carbonation reaction 4-4:

$$CaO_s + CO_2 \leftrightarrow CaCO_{3s} \ (\Delta H°r \ (298 \ K) = -179.2 \frac{kJ}{mol}) \qquad \text{4-4}$$
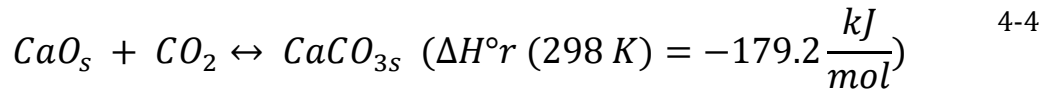
Being 4-4 a gas-solid reaction, a definite $CO_2$ partial pressure, a function of temperature, is established in the gas phase at chemical equilibrium. Equation (4), reported in (76) and obtained from thermochemical data in (77), is an example of an equation expressing the increase of equilibrium $CO_2$ partial pressure with temperature:

$$P_{CO2,eq}[Pa] = 4.137 * 10^{12} * e^{(\frac{-2047}{T})} \qquad \text{4-5}$$

The overall calcium-based SE-SMR reaction, which results from the single reactions 4-1, 4-3, and 4-4, is reported in 4-6:

$$CH_4 + 2H_2O + CaO_s \leftrightarrow 4H_2 + CaCO3_s \ (\Delta H°r \ (298 \ K) = -14.5 \frac{kJ}{mol}) \qquad \text{4-6}$$
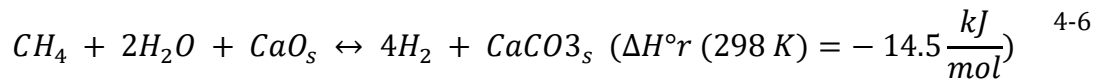
The enthalpy balance of the overall eq. 4-6 is only 14.5 MJ/kmol, meaning that it is slightly endothermic, and therefore not only the carbonation reaction facilitates $H_2$ production by removing $CO_2$ from the gaseous phase but also provides the heat required for the steam reforming reaction, allowing for the use of adiabatic reactors, or at least with limited heat duties. So, SE-SMR makes it possible to affirm that high $H_2$ yields and $CO_2$ separation can be carried out in a single step at temperatures much lower than required by conventional reformers (75).

## 4.3. Reactor

SE-SMR is usually carried out in a one-stage multifunctional reactor of a particular type, called the adsorptive reactor (78), in which chemical reactions and in situ sorption of produced $CO_2$ are merged. The process principle is shown in Figure 4-1 where the active reactor packing consists of the catalyst and sorbent particles.
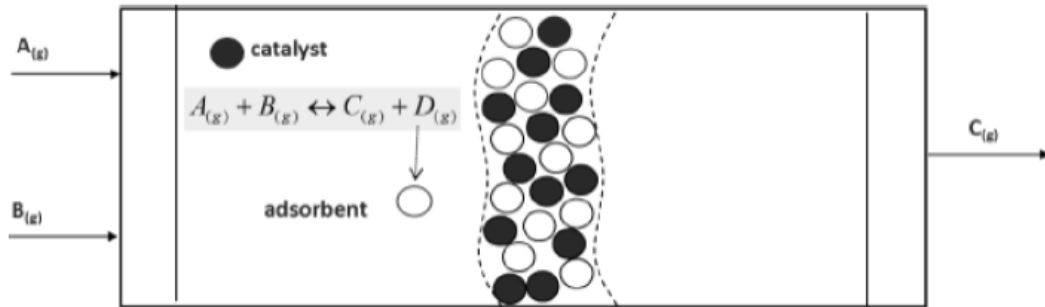


Figure 4-1 The principle of operation of the adsorptive reactor.

However, in some practical solutions, the use of bi-functional (or generally called multifunctional) packing grains is proposed, in which structured grains play simultaneously the catalyst as well as the $CO_2$ sorbent roles (79). sometimes, a more complex configuration of the reactor bed is employed, including the number of subsections, each with a different adsorbent to catalyst mass ratio (80). In this approach, also called the subsection controlling strategy (81), three subsections in the adsorptive reactor column can be distinguished, each with a different adsorbent to catalyst ratio and a different reactor wall temperature within the chosen section(s) can be applied. Also, the tandem bed configuration was proposed (82), where different sorbents are placed in an upstream and a downstream section of the bed, respectively.

The adsorptive reactor shown in Figure 4-1 is founded on the fixed packed bed concept (83), while in numerous papers, binary fluidized bed reactors are also described in which cyclic operation of the reforming process and the sorbent calcination are investigated (84).

As each $CO_2$ sorbent employed in the SE-SMR process has a limited capacity, in the entire installation for hydrogen production, two steps can be characterized; in the first one, methane is converted and produced $CO_2$ simultaneously adsorbed, while in the second one, the sorbent is regenerated, and $CO_2$ released (desorbed) (85)

In packed bed reactors, a cyclic operation is carried out. I.e., just before a complete sorbent saturation with $CO_2$, the feed of $CH_4/H_2O$ is switched off, then the bed is heated up and the sorbent regenerated, so the sequential working mode is used. Therefore, a battery of reactors working in parallel can be employed, and the most straightforward configuration consisting of two reactor columns is shown in Figure 4-2. Notice that the regeneration temperature–$T_R$ (usually 800–1000°C) is significantly higher than the SE-SMR process temperature – $T_P$ (480–580 °C). (85)
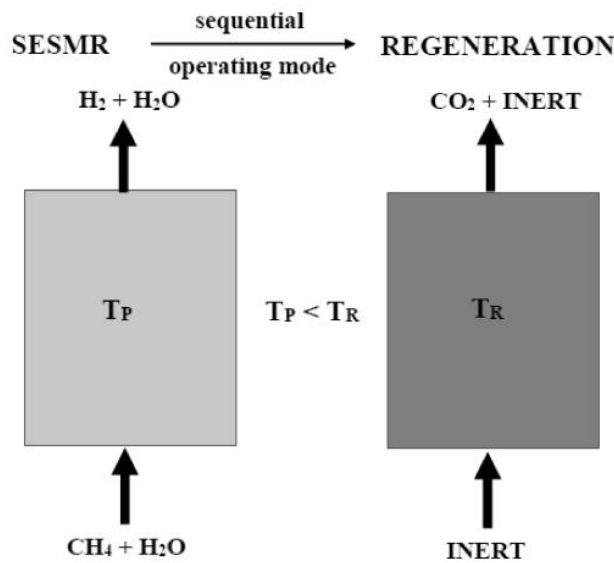


Figure 4-2 Configuration of cyclic process carried out in the fixed packed bed reactor (SE-SMR process) and operating

In circulating fluidized bed reactors, a design of two fluidization columns (reactor-regenerator system) operating simultaneously is used. Figure 4-3. The solid phase consisting of the catalyst and sorbent fine particles is circulated between the reactor and the sorbent regenerator unit. The reactor operates in the bubbling fluidization state, while the regenerator is in the fast fluidization state (86). Also, in this case, the temperature–$T_R$ is higher than $T_P$. $G_S$ is the flux of solids circulating between reactor and regenerator, $C^P_S$, $CO_2$, and $C^R_S$, $CO_2$ are $CO_2$ concentration in sorbent solids leaving the reactor and the regenerator, respectively (85).
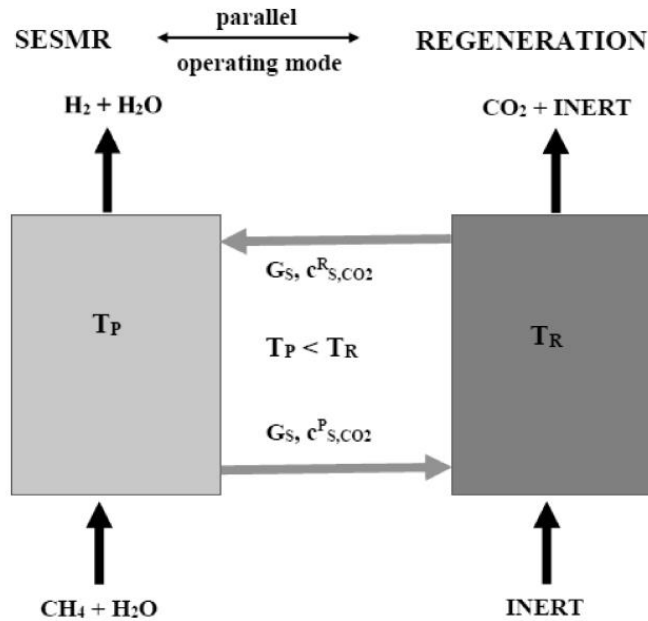
Figure 4-3 Configuration of the continuous steady-state process carried out in fluidized bed reactor (SE-SMR process) and operating in parallel with the sorbent regenerator.

Recently, an application of gas-solid-solid trickle flow reactor (GSSTFR) was applied to carry out a continuous SE-SMR process with simultaneous sequestration of $CO_2$ on fly ashes (87). In such an approach, the catalyst active sites can be immobilized on the fixed carrier of large pore size while fine particles of sorbent (fly ashes) flow downwards through the voids. Gas can flow downwards (co-currently to the fly ashes stream) or upwards (counter-currently). The idea of the gas-solid-solid trickle flow reactor (GSSTFR) was firstly suggested by Westerterp and Kuczynski (88) (89) to carry out the integrated sorption enhanced process with equilibrium reaction – namely the methanol synthesis. This idea was later extended and demonstrated in more recent contributions to be applied in methane oxidation to methanol (90) and industrial size reactors for methanol synthesis (91). The obtained results indicate the feasibility of the proposed approach and increased process productivity compared to conventional solutions. Therefore, it seems that an application of GSSTFR to carry out the considered SE-SMR process with simultaneous sequestration of $CO_2$ could be quite effectively executed on an industrial scale, as currently, numerous commercial solutions for open-cell metallic and ceramic foams with "tailored" structures (void size and their tortuosity) can be found (92).

## 4.4.  Catalyst and the reaction kinetics

The catalysts used for SMR and SE-SMR processes are very well established. Primarily commercial nickel-based catalysts on $Al_2O_3$ support are employed [69w], but different active metals, additives, and supports are also assessed. A novel, highly active Rh/CeaZr1−aO2 catalyst was characterized and used to carry out the SE-SMR process [34]. Also, many studies have been carried out with nickel catalysts on different supports to increase their thermal stability and/or activity (93) ,where $ZrO_2$, and Ce-$ZrO_2$ supports are investigated on paper (94) , where the addition of Zr to the Ni/$SiO_2$ catalyst for improvement of steam resistance is reported.

The most common kinetics of the steam methane reforming (SMR) process represented by a set of reversible reactions shown in Eqs. 4-1, 4-2 and 4-3 has been described by Xu and Froment (95), who, for a nickel catalyst supported on MgO/$Al_2O_3$, proposed expressions enabling estimation of appropriate reaction rates. For each reaction listed in Eqs. 4-1, 4-2 and 4-3 and  the appropriate rate expressions read as follows:

$$r_I = \frac{1}{M^2} * \frac{k_I}{p_3^{2.5}} * \left(p_1 * p_2 - \frac{p_3^3 * p_5}{k_I}\right) \qquad \text{4-7}$$

$$r_{II} = \frac{1}{M^2} * \frac{k_{II}}{p_3^{2.5}} * \left(p_1 * p_2 - \frac{p_3^4 * p_4}{k_{II}}\right) \qquad \text{4-8}$$

$$r_{III} = \frac{1}{M^2} * \frac{k_{III}}{p_3^{2.5}} * \left(p_5 * p_2 - \frac{p_3 * p_4}{k_{III}}\right) \qquad \text{4-9}$$

In which $r_i$  is reaction rate, $k_i$ is the reaction rate constant, $p_i$ the partial pressure of i-th compound, $K_i$ Constant.

Where the value M appearing in denominators of these equations is equal to:

$$M = 1 + K_5 * p_5 + K_3 * p_3 + K_1 * p_1 + \frac{K_2 * p_2}{p_3} \qquad \text{4-10}$$

## 4.5. Sorbent

### 4.5.1. Sorbents and sorption kinetics

Intensive research on sorbents, which can be appropriate to carry out SE-SMR processes effectively, is still in progress. In general, under the operating conditions of the SE-SMR process, the sorbent must be highly selective towards $CO_2$, and the sorption rate should be compatible with the reaction rate – i.e., the rate of $CO_2$ production. Further, these sorbents should have a sufficiently high sorption capacity and mechanical, thermal, and chemical durability due to their multiple cyclic regenerations. A lot of contributions dealing with investigations of $CO_2$ sorbents can be found in the literature, and some fundamental conclusions can be grouped as follows:

- CaO and alkali-modified hydrotalcite are mainly used as efficient sorbents for $CO_2$ capture during the SE-SMR process (79). Ca-based sorbents are especially advantageous due to their low cost, availability, high $CO_2$ capacity, and good sorption kinetics. Nevertheless, they are unstable in long-term sorption-desorption operations due to sintering (96). Therefore, many investigations are still carried out to improve their durability in the cyclic process by adding various precursors and different treatments. However, the results obtained are sometimes contradictory (96).

- Lithium oxides and lithium-containing materials (mainly $Li_2ZrO_3$; K-doped $Li_2ZrO_3$, and $Li_4SiO_4$) are also considered an effective alternative due to their stability and good sorption kinetics, although they suffer from a relatively small $CO_2$ capacity (97).

- Hybrid catalyst-sorbent structured systems are proposed and investigated to eliminate mass transfer resistances. However, most proposals are just conceptual, and a more practical approach and results are still expected (96).

The main problem in the practical application of the integrated SE-SMR process is the limited sorption capacity of used sorbents. After their saturation with $CO_2$, the process must be stopped, and regeneration of sorbent accomplished. Such a cyclic operation of adsorptive reactors makes the process complex, increases exploitation costs, and generates special sorbent requirements. It should be pointed out that desorption of $CO_2$ from a saturated CaO-based sorbent ($CaCO_3$) and regeneration of this sorbent is usually carried out at a temperature as high as 900–1000 ◦C.

Taking the above into account, an application of fly ashes (FA) originating from power plants seems to be a promising concept. Because fly ashes - abundantly available industrial wastes - are very cheap, practical aspects of their use in the SE-SMR process are related to the fact that after full or partial saturation with $CO_2$, they do not have to be regenerated and can be even further utilized in building industry or directly in road construction and mines (85). So, through the use of fly ashes as $CO_2$ acceptors, the economic efficiency of hydrogen production can be significantly improved. Additionally, all $CO_2$ emitted during the hydrogen production process is sequestrated. So, an application of fly ashes in the SE-SMR process helps reduce the emission of $CO_2$ and, in consequence, improves ecological factors of hydrogen production.

For CaO-based sorbents, the unreacted core model can predict sorption (chemisorption) rates (98). The representative results for this kind of sorbent are summarized with the following carbonation rate equation (99):

$$r_{s,CaO} = \frac{1}{M_{CaO}} * \frac{k_c}{(b+t)^2} * e^{\left(\frac{-28882}{R*T}\right)} \qquad \text{4-11}$$

In which $r_s$ is adsorption rate, M is the molar mass, and b and t are the constants.

Then, neglecting the short initial period, the $CO_2$ sorption rate can be estimated with the expression:

$$r_{s,4} = 2.41 * e^{\left(\frac{-12171}{T}\right)} \qquad \text{4-12}$$

## 4.5.2.  Sorbent materials

### 4.5.2.1.  CaO based sorbents

The advantages of low-cost sorbents for hydrogen production are very apparent. To date, CaO-based sorbents have been one of the most promising candidates for their $CO_2$ sorption capacities under the conditions for steam reforming, and it is thermodynamically the best candidate among metal oxides for $CO_2$ capture in zero-emission power generation systems. CaO is capable of scavenging $CO_2$ to very low concentrations at moderate temperatures (450–750°C) and at atmospheric pressure (100).

Figure 4-4 illustrates the $CaCO_3$ product formation during the carbonation reaction of CaO involved with steam. During the initial stage, a certain amount of $CaCO_3$ is produced. It grows as the morphology of the island, meaning a part of the CaO particle surface is covered by these $CaCO_3$ islands, whereas the other part of the CaO surface remains in contact with $CO_2$ (101). In the product layer diffusion-controlled stage, the produced $CaCO_3$ (higher molar volume of 36.9 cm3/g) covers almost all the CaO (16.7 cm3/g) particle surface to hinder the direct contact of CaO with $CO_2$. In this case, the carbonation process is controlled by ion diffusion through the $CaCO_3$ product layer (100). As proposed (102), the counter-current and co-current diffusion processes occur on the particle's surface. $CO_3^{2-}$ diffuses inward from the $CaCO_3$-gas interface to the $CaCO_3$–CaO interface, whereas $O^{2-}$ diffuses in the opposite directions. The involved $H_2O$ molecule dissociates to $H^+$ and $OH^-$. With a very small radius, $H^+$ easily diffuses through the $CaCO_3$ product layer to the $CaCO_3$–CaO interface and interacts with $O^{2-}$ to form $OH^-$. Then, $OH^-$ diffuses outwardly to the $CaCO_3$–gas interface to react with $CO_2$, as shown in Figure 4-4.
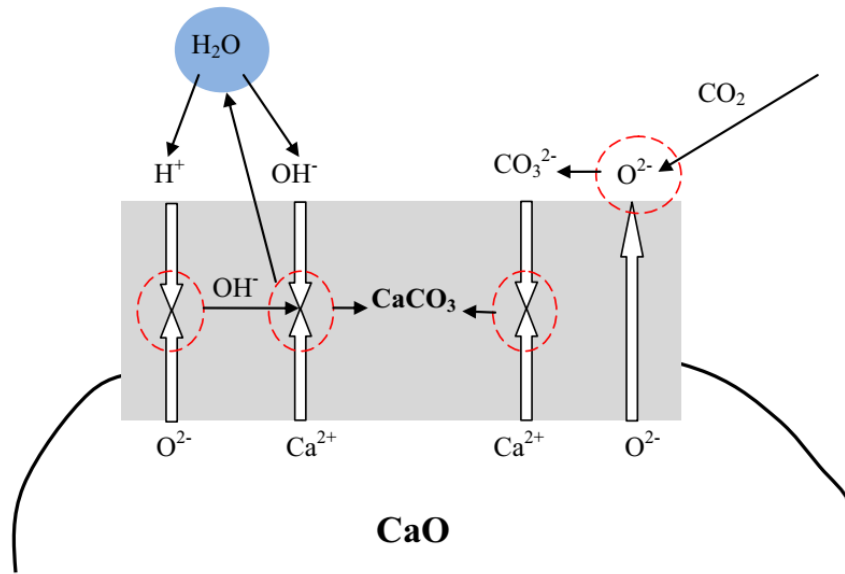
Figure 4-4 Mechanism of CaO carbonation (CaCO₃ formation, growth, and ion diffusion) by CO₂ in the presence of water vapor.

### 4.5.2.2. MgO based sorbents

Magnesium oxides are plausible $CO_2$ sorbent candidates for their moderate $CO_2$ sorption capacity. They perform well under wide operating temperatures from room temperature to around 500 °C and also under water vapor concentrations of 8–17 vol% (103). Also, their benefits are the wide availability of natural minerals and low cost. Based on $MgO$–$CO_2$ carbonation/decomposition equilibrium diagram (Figure 4-5), it is theoretically possible to carry out a regenerative MgO-based process for $CO_2$ sorption. To make this process economically viable, highly stable, reactive, and mechanically strong, those MgO-sorbent candidates must minimize attrition losses and the fresh sorbent makeup rate. Modified MgO-based sorbents are usually promoted with elements of K, Na, Al, Ti, etc., by co-precipitation or impregnation methods. Mesoporous magnesia synthesized with mesoporous silica SBA-15 (treated with sucrose and sulfuric acid to obtain mesoporous carbon, CMK-3) through the nano-casting process exhibit superior $CO_2$ adsorption capacity (103). The $CO_2$ sorption capacities over MgO-based sorbents were studied at temperatures lower than Ca-based sorbents (both carbonation and regeneration temperatures).
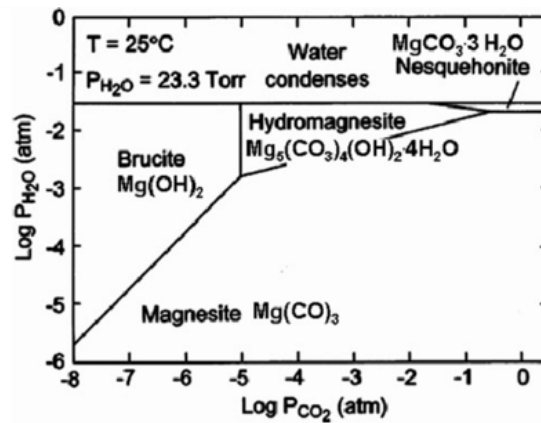
Figure 4-5 Phase diagram for the MgO-CO 2-H 2 O system in the solid vapor region. (104)

With the presence of steam in the gas mixture, MgO-based sorbents in the carbonation reaction could significantly increase the reactivity and capacity (105). $MgCO_3$ can be formed in the presence of $H_2O$ due to the reactions of 4-13 and 4-14, And the used sorbent can be regenerated into $Mg(OH)_2$ (shown as 4-15) at relatively low temperatures:

$$MgO_s + H_2O \ \rightarrow \ Mg(OH)_2 \text{s} \qquad\qquad 4\text{-}13$$

$$Mg(OH)_2 \text{g} + CO_2 \ \rightarrow \ MgCO_{3s} \qquad\qquad 4\text{-}14$$

$$MgCO_{3s} + H_2O \ \rightarrow Mg(OH)_2 \text{s} + CO_2 \qquad\qquad 4\text{-}15$$
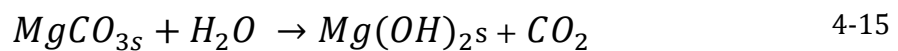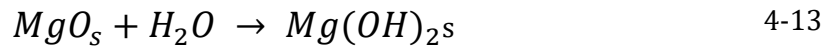
### 4.5.2.3. Hydrotalcite based sorbents

Hydrotalcite (HTlc), known for its layered double hydroxides (LDH) (structure belongs to the anionic and basic clays) (106). And it has been developed as a $CO_2$ sorbent candidate for its desirable properties such as lower energy consumption for regeneration, retention of sorption capacity after multiple cycles, and suitable kinetics of $CO_2$ sorption (107). Hydrotalcite materials have been found to have an adequate $CO_2$ sorption capacity of 0.45–1.0 mol/kg at a high temperature of 400–450 °C, and steam has been determined to enhance the sorption capacity and stability (106). Ding and Alpay studied $CO_2$ adsorption on hydrotalcite, and sorption saturation capacity of around 0.58 mol/kg was measured at 450 °C in the

presence of water vapor (108). However, the adsorption capacity is very low, which may restrict its potential for an industrial scale. The reported reaction rate for this kind of sorbents is too slow to compete with calcium-based ones. Hufton et al. reported on $H_2$ production through SE-SMR using a $K_2CO_3$-treated hydrotalcite sorbent, the low $CO_2$ capacity (109). Some studies also presented an experimental study for a newly modified $K_2CO_3$-promoted hydrotalcite material as a novel high-capacity sorbent for $CO_2$ capture (110). A large portion of $CO_2$ is easily recovered in the first few minutes of a desorption cycle due to a fast desorption step, which is associated with a physi/chemisorption step on the monolayer surface of the fresh sorbent, and the complete recovery of $CO_2$ was then achieved in a slower desorption step associated with reversible chemisorption in a multi-layer surface of the sorbent (110). A Freundlich isotherm can adequately describe the equilibrium sorption data obtained from a column apparatus (108). Oliveira et al. studied the different HTlc samples promoted with K or Cs in the temperature range of 400–510 °C, and a biLangmuirian isotherm with physical adsorption and chemisorption is derived to describe the $CO_2$ sorption capacity over the different samples (111). Jiang carried out high-purity hydrogen production through sorption enhanced water gas shift reaction using $K_2CO_3$- promoted hydrotalcite, and the effects of various operating conditions of reaction on the process performance were studied (112). The inconsistency observed in the illustration of the $CO_2$ sorption over hydrotalcite is principally due to the large span of its nature, composition, preparation method, promoter type and impregnation degree, pressure range, and temperature range (113). The synthesis of hydrotalcite generally follows a conventional procedure of the coprecipitation method, and other processes such as microwave aging and ultrasonication of the precipitating gel methods have been known to increase the surface area of the hydrotalcite (114).

### 4.5.2.4. $Li_2ZrO_3$ based sorbents

Lithium zirconate and lithium orthosilicate have also received more attention due to their ability to retain good $CO_2$ chemisorption capacity at high temperatures,. $CO_2$ sorption occurs in two steps: $Li_2ZrO_3$ decomposes according to the following reaction:

$$Li_2ZrO_3 \rightarrow 2Li^+ + O^{2-} + ZrO_2 \qquad \text{4-16}$$
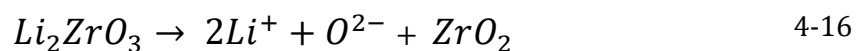
And the $CO_2$ gas dissolves as carbonate ions in $Li_2CO_3$ in the second step:

$$CO_2 + 2Li^+ + O^{2-} \rightarrow Li_2CO_3 \qquad\qquad 4\text{-}17$$
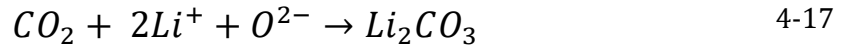
Nakagawa and Ohashi (115) (116) have firstly studied $Li_2ZrO_3$ sorbent that absorbs/desorbs $CO_2$ in the high-temperature range of 400–800 °C. $Li_2ZrO_3$ has acceptable $CO_2$ sorption characteristics, and its $CO_2$ sorption capacity was observed to be about 4.5 mol/kg compared to around 10-12 mol/kg for CaO with a small volume change during $CO_2$ sorption/desorption. Therefore, it is considered a material with potential for application in $CO_2$ capture at high temperatures. The appropriate temperature range for the solid-state reaction to prepare lithium zirconate sorbent is 850–1200 °C. Below this temperature range, the reaction to form lithium zirconate does not proceed or complete. And above this temperature range, volatilization of lithium oxide ($Li_2O$) from lithium zirconate occurs (117).

## 4.6.  Process modeling

In this section, we will discuss the process modeling, modeling parameters, and results from the analysis of a previous ASPEN modeling article. Based on (118), The Aspen Plus flowsheet of the hydrogen plant proposed is shown in Figure 4-6. The system consists of two fluidized bed reactors with solid matter recirculated across them to allow cyclic operation. Thus, two RGIBBS reactors are used for both the sorption enhanced steam reforming stage (SESR reactor) and the regeneration stage (REG reactor).
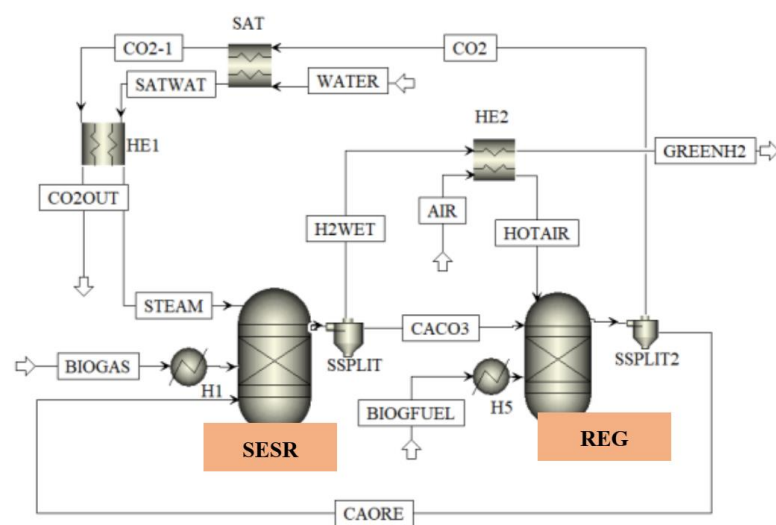


Figure 4-6 Aspen Plus flowsheet of the biogas sorption enhanced steam reforming (SESR) process with sorbent regeneration (REG) (118).

The performance of the SESR unit was assessed regarding the $H_2$ yield (4-18), $H_2$ purity (4-19), $CH_4$ conversion (4-20), and $CO_2$ capture (4-21), whereas the performance of the REG unit was evaluated with the air and biogas fuel consumption, as Air/$CaCO_3$ molar ratio and molar flow of biogas fuel, respectively. The energy analysis of the hydrogen production system with in situ $CO_2$ capture relied on the duty of the SESR reactor.

$$H2_{yield} \ (\%) = 100 * \left(\frac{F_{H2,Out}}{F_{CH4,In}}\right) \qquad \text{4-18}$$

$$H2_{purity} \ (\%) = 100 * \left(\frac{yH2}{\Sigma_i y_i}\right) \qquad \text{4-19}$$

$$CH4_{conversion} \ (\%) = 100 * \frac{\left(\frac{F_{H2,Out}}{F_{CH4,In}}\right)}{F_{CH4,In}} \qquad \text{4-20}$$

$$CO2_{capture} \ (\%) = 100 * \frac{F_{CO2\ in\ biogas} + F_{CO2\ produced\ in\ WGS}}{F_{CaCO3\ in\ produced\ in\ SESR}} \qquad \text{4-21}$$

Table 4-1 Modeling parameters. (118)

| Parameter | Value |
|---|---|
| Biogas composition ($CH_4$/$CO_2$) | [30/70]-[100/0] |
| Steam/$CH_4$ (mol/mol) | 4 |
| CaO/CaO stoichiometric (mol/mol) | 1.5 [3] |
| SESR Temperature (ºC) | 650 |
| REG Temperature (ºC) | 850 |
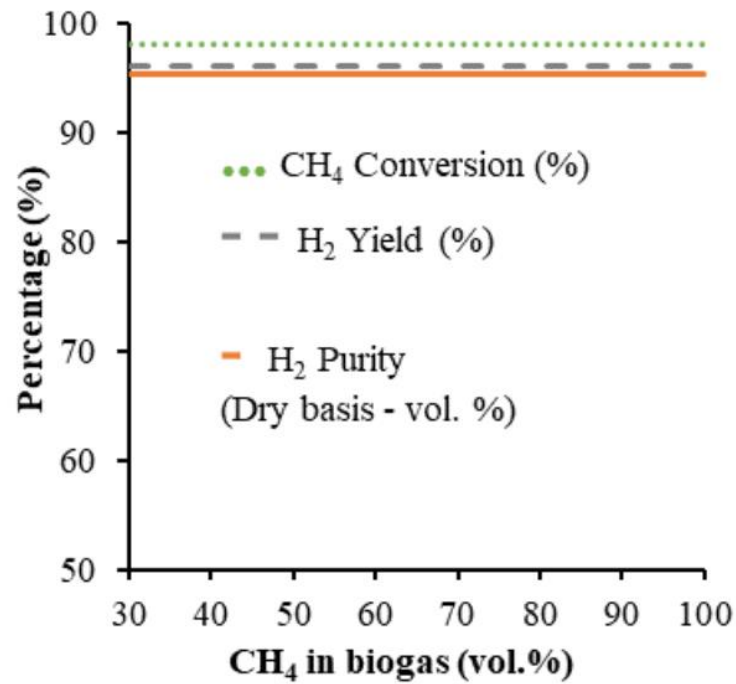
Figure 4-7 H₂ yield, H₂ purity, and CH₄ conversion for the range of biogas compositions evaluated (from 30 vol.% to 100 vol.% of CH₄, CO₂ balance).
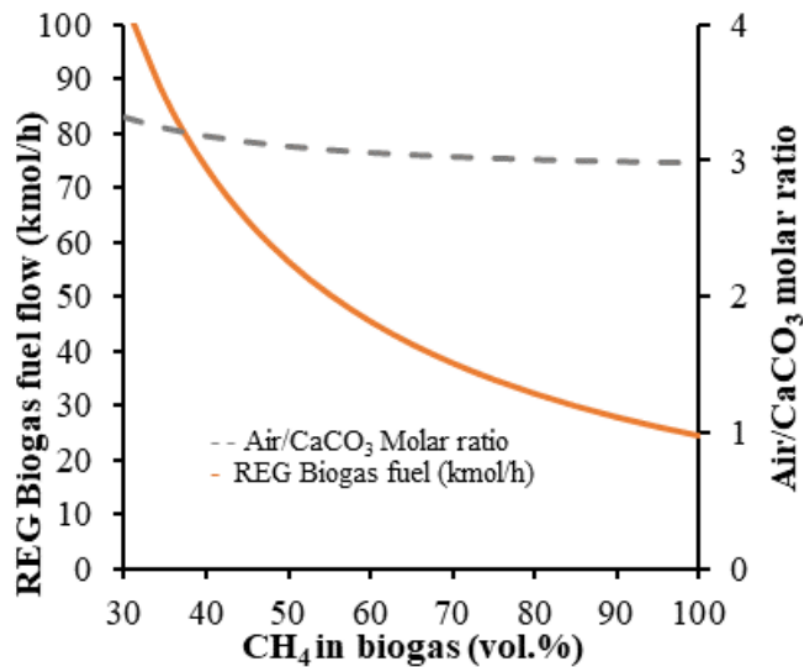


Figure 4-8 Air/CaCO₃ molar ratio and Biogas flows used as fuel in REG for the range of biogas compositions evaluated (from 30 vol.% to 100 vol.% of CH₄, CO₂ balance).
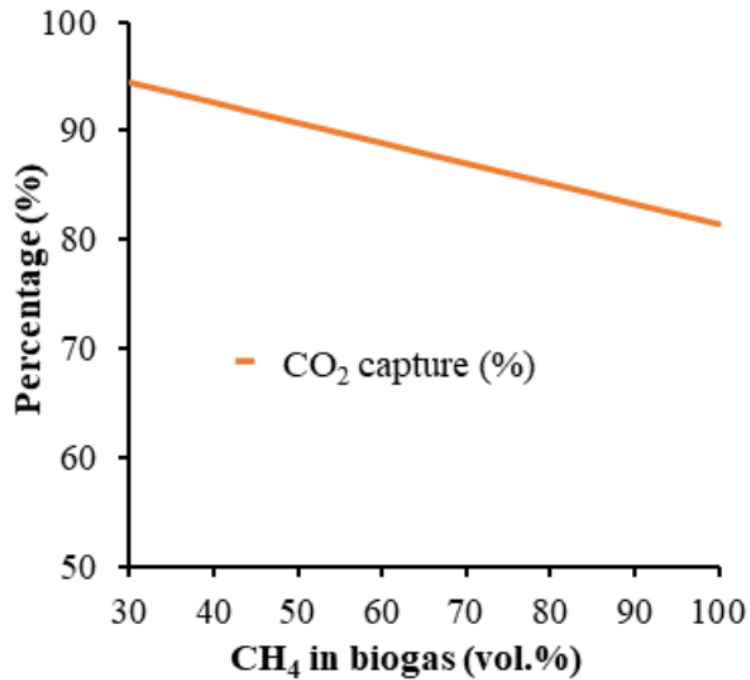
Figure 4-9 $CO_2$ captured in SESR (%) for the range of biogas compositions evaluated (from 30 vol.% to 100 vol.% of $CH_4$, $CO_2$ balance).

## 4.7. Experimental activities

Ding and Alpay (119) have demonstrated that the steady-state kinetic model of Xu and Froment (120) for SMR applies to transient reactor operation, both in the presence or absence of a sorbent. The reactor consisted of a stainless-steel tubular column with an internal diameter of 12.4 mm and a length of 220 mm, packed with a mixture of catalyst and sorbent particles. Operating conditions were fixed equal to 455 1C and 4.45 bar; S/C was 3. A commercial Ni-based catalyst (United Catalyst Inc.) containing 25–35% Ni, 2–35% NiO, 5–15% MgO and 1–25% sodium silicate was used in this work. The $CO_2$ sorbent consisted of industrially supplied potassium promoted HTC. For the reaction studies in the absence of the sorbent, approximately 7.2 g of catalyst was admixed with dense silicon carbide particles (about 1:3 mass ratio) and packed into the reactor. For the sorption-enhanced reaction studies, approximately 7.2 g of catalyst was admixed with 14.8 g of $CO_2$ adsorbent.

Results obtained from a mathematical model also developed by the authors to describe both the SMR and SE-SMR processes are in agreement with experiments.

Therefore, the rate expressions proposed by Xu and Froment are suitable for both the transient and steady-state periods of operation, even in the presence of an adsorbent. This suggests that the microkinetic dynamics of carbonation reaction are relatively fast and that the physically admixed nature of catalyst and adsorbent precludes any local effect of adsorption on reaction intermediates and hence on molecular kinetic steps.

Balasubramaniam et al. (121) have conducted experimental studies using a laboratory-scale fixed bed reactor containing a mixture of commercial reforming catalyst and CaO obtained by calcining high-purity (99.97%) $CaCO_3$ for temperatures varying from 450 °C to 750 °C. Calcination was performed using a quartz boat in a tube furnace at 750 °C and 1 atm under flowing nitrogen for four h. A range of particle sizes from 45 to 210 mm was used in the tests.

The reforming catalyst consisted of NiO (22%) supported by $Al_2O_3$. The catalyst particles were crushed and sieved with 150 mm particles used in all runs. All reaction tests were conducted at 15 atm and with an S/C equal to 4. The response from a typical reaction test is shown in Figure 4-10 shows the mol percent of $H_2$, $CH_4$, CO, and $CO_2$ in the product gas versus time.
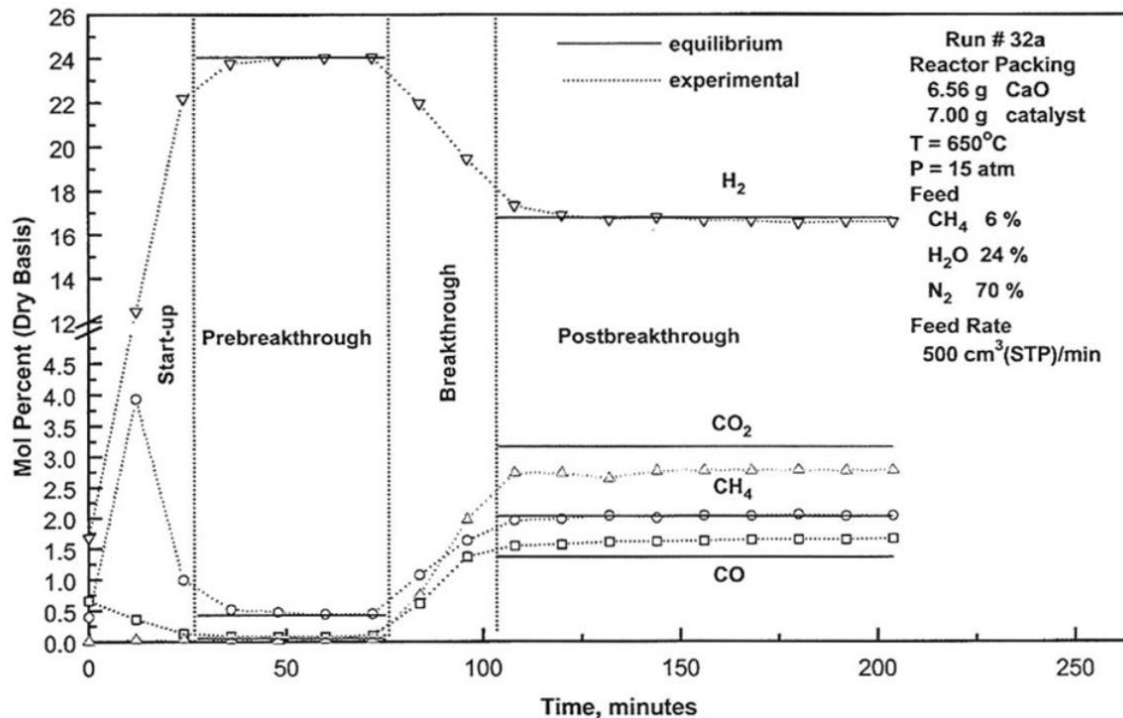


Figure 4-10 Typical reactor response curve from (121).

The trends can be divided into four regions:

- an unsteady-state start-up period, essentially due to the time needed for reduction of NiO to Ni and then for catalyst activation.
- A first period, called prebreakthrough, throughout all the reactions run at their maximum efficiency, and the molar fractions are near to the equilibrium one.
- An interval, breakthrough, during which the adsorption reaction efficiency starts decreasing.
- At last, a period called postbreakthrough, corresponds to about zero adsorption reaction rate and where only the reforming reactions occur.

The authors reported that the fractional conversion of CaO to $CaCO_3$ was 0.52 at the end of the prebreakthrough period and 0.71 at the beginning of postbreakthrough. Fractional conversion then increased slowly to 0.73 when the test was completed. Balasubramaniam et al. also reported that approximately 88% conversion of $CH_4$ is thermodynamically feasible, and the product gas contains about 95% $H_2$.

Finally, Ortiz and Harrison (122) reported experimental results tests from a laboratory-scale fixed-bed reactor using inexpensive dolomite as the sorbent precursor: the catalyst–sorbent mixture's multicycle durability was studied as a function of regenerating temperature and gas composition. A schematic diagram of the laboratory scale of the fixed-bed reactor is shown in Figure 4-11.
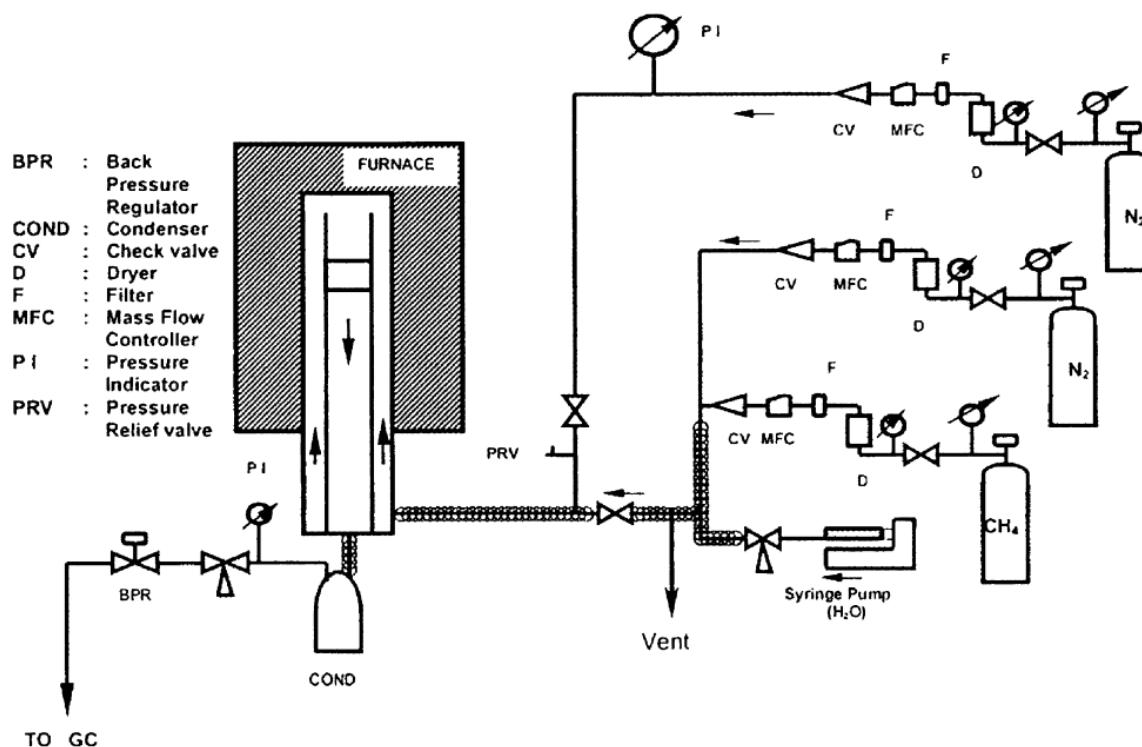
Figure 4-11 Schematic of the laboratory-scale fixed bed reactor system from (122)

Multicycle tests showed no significant decrease in the maximum $H_2$ concentration or increase in the breakthrough time (a measure of global reaction rate) except for regeneration carried out in $N_2$ at 950 °C. However, decreases in the fractional sorbent conversion at the beginning of breakthrough were detected in all multicycle tests. Some activity loss is inevitable because of the severe conditions required for the regeneration process (122).

## 4.8.   The current state of the technology

Sorption-enhanced steam methane reforming (SE-SMR) has been successfully demonstrated on a laboratory scale with natural Ca-based sorbents (calcite and dolomite) both in fixed bed reactors (123) (124) and in fluidized bed reactors (125) (126) .Moreover, comprehensive research work on the development of diverse, high-temperature synthetic $CO_2$-sorbents fitted for the SE-SMR process has been carried out by many authors. The main inspirations are the improvement of the multi-cycle capacity, absorption capacity, mechanical stability, and lower regeneration temperature of these new sorbents compared to natural Ca-based calcite or dolomite. Lithium zirconate has been proposed for its lower regeneration temperature than Ca-based sorbents (127). Nevertheless, it shows too slow

sorption kinetics for low $CO_2$ partial pressures. Sodium zirconate shows better kinetics, but the presence of sodium poisons the Ni-catalyst during the high-temperature regeneration step. Lithium silicate was seen as a promising material, but thermodynamics limits the $H_2$ yield compared to Ca-based sorbents (128). Therefore, most of the work carried out recently focuses on novel supported Ca-based materials, mainly due to the excellent availability of Ca-precursors, their lower cost, and the satisfactory kinetic properties of the carbonation reaction (129) (130).

Extensive study has also been carried out in the reactor, and process modeling adapted to the SE-SMR process for $H_2$-production shows this technology's potential (131) . However, SE-SMR in a continuous production mode still needs to be demonstrated at a level making possible a further promising up-scaling (75).

# 5   Methane SESR modeling

The scope of this thesis work is to find out which of the possible SE-SMR working conditions and configurations have the potential to be coupled with a plastic pyrolysis plant producing hydrogen. The first thing to do is to some of the related previous works and compare the results to validate the model. In this section, we used methane as a fuel to validate the model as there are many works available. comparisons are performed between the model performed by aspen plus v11 software and a study by Matteo C. Romano et al. (75) .The first thing to do is to study all the related previous works and compare the results to validate the model.

## 5.1.  Model description

The effect of the SE-SMR working conditions has been calculated by chemical equilibrium, assuming pure methane as primary fuel and over-stoichiometric amounts of CaO, so that adsorption of gaseous components is not determined by CaO availability. Hydrogen yield (defined as the moles of hydrogen generated per mole of methane, of which the maximum value is four) and carbon capture ratio (CCR, defined as the moles of C adsorbed by calcium oxide per mole of methane to the reformer).

## 5.2.  Model validation

Reforming section

In this section, validation of the reforming unit is performed by means of Hydrogen Yield (defined as the moles of hydrogen generated per mole of methane, whose maximum value is 4) comparison between the reference study and the model. Validations are presented for different S/C, equal to 3.5 and 5; Different Pressures equal to 1 bar and 25 bar, and the temperature range from 450 °C to 1000 °C. in each case, the results corresponding to the model and the reference study are shown in Figure 5-1, Figure 5-2, Figure 5-3 and Figure 5-4.
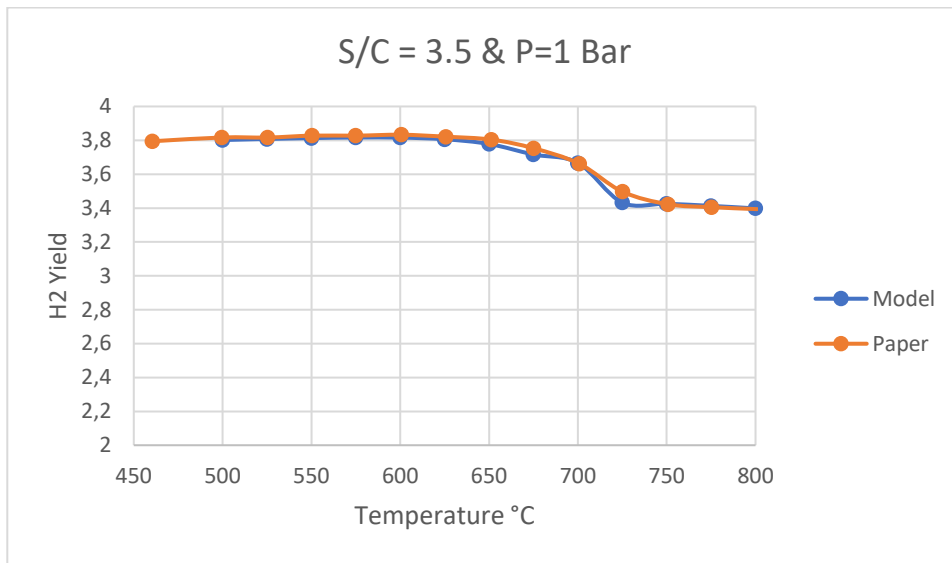
Figure 5-1 H2 yield comparison at 1 bar and S/C=3.5
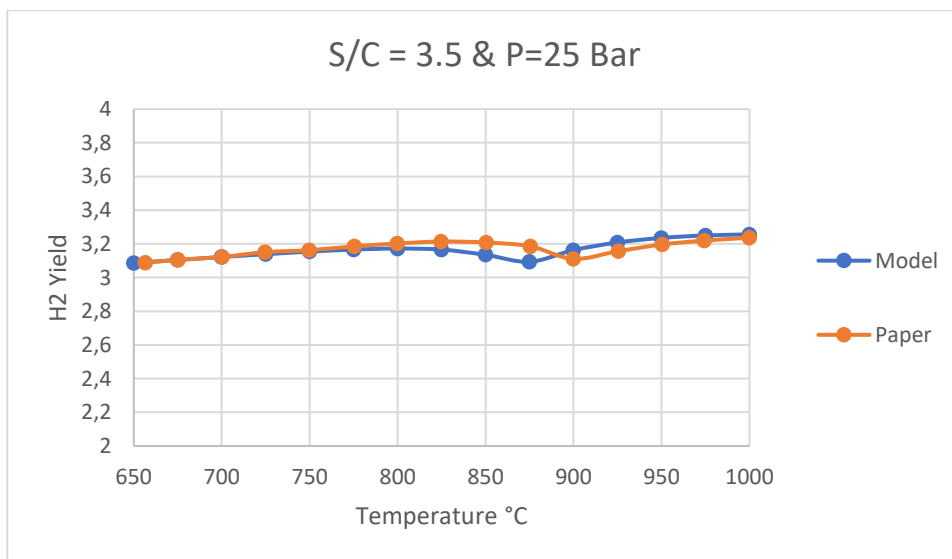


Figure 5-2 H2 yield comparison at 25 bar and S/C=3.5
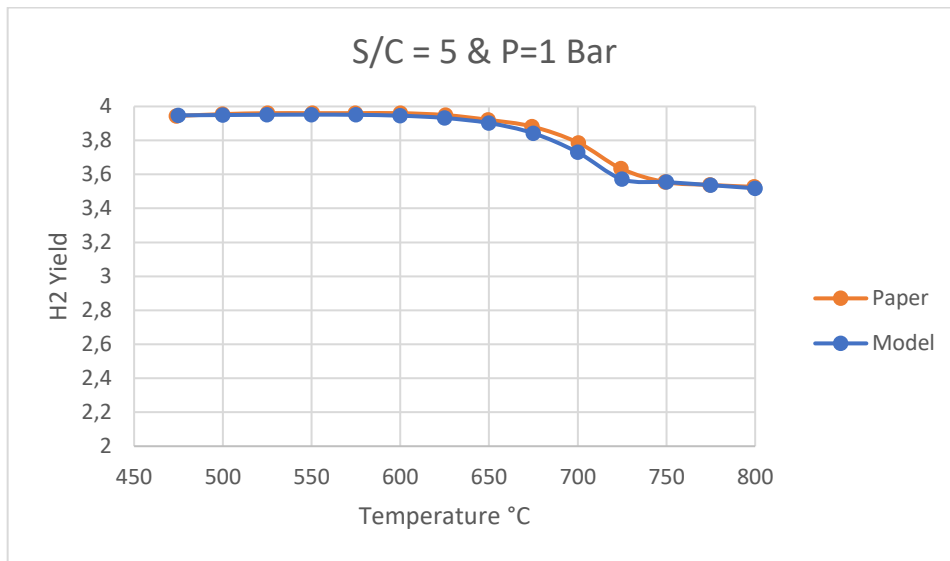
Figure 5-3 H₂ yield comparison at 1 bar and S/C=5
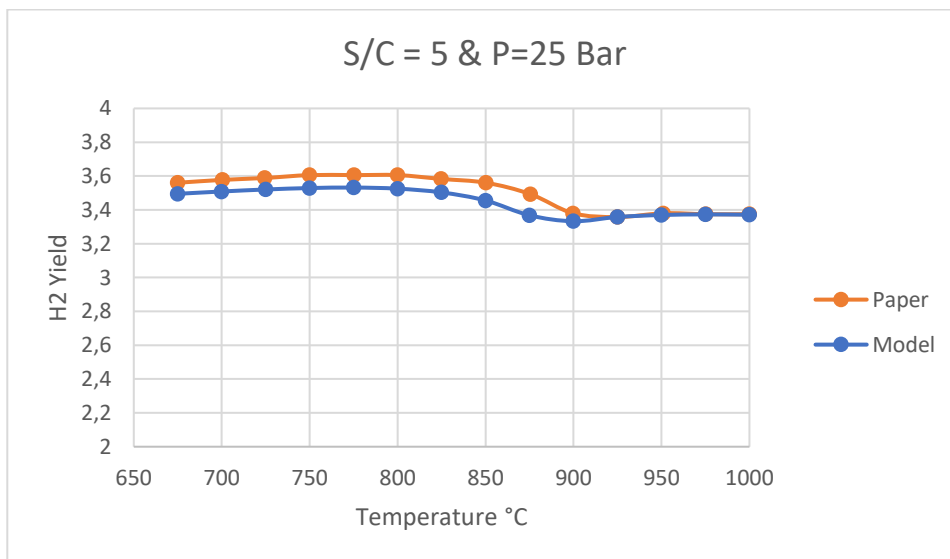


Figure 5-4 H₂ yield comparison at 25 bar and S/C=5

As we see, minor differences are recorded between the reference work and the developed ASPEN model. For the purpose of this work, the errors reported within the interesting working conditions are negligible allowing the possibility to extend the use of the developed ASPEN model for the NCG produced in plastic pyrolysis.

Using the same working conditions, the Carbon Capture Ratio (CCR), (defined as the moles of C adsorbed by calcium oxide per mole of methane to the reformer), was evaluated and compared to the plots presented in the same study (75). The results of the comparison are presented in figures in Figure 5-5, Figure 5-6, Figure 5-7 and Figure 5-8.
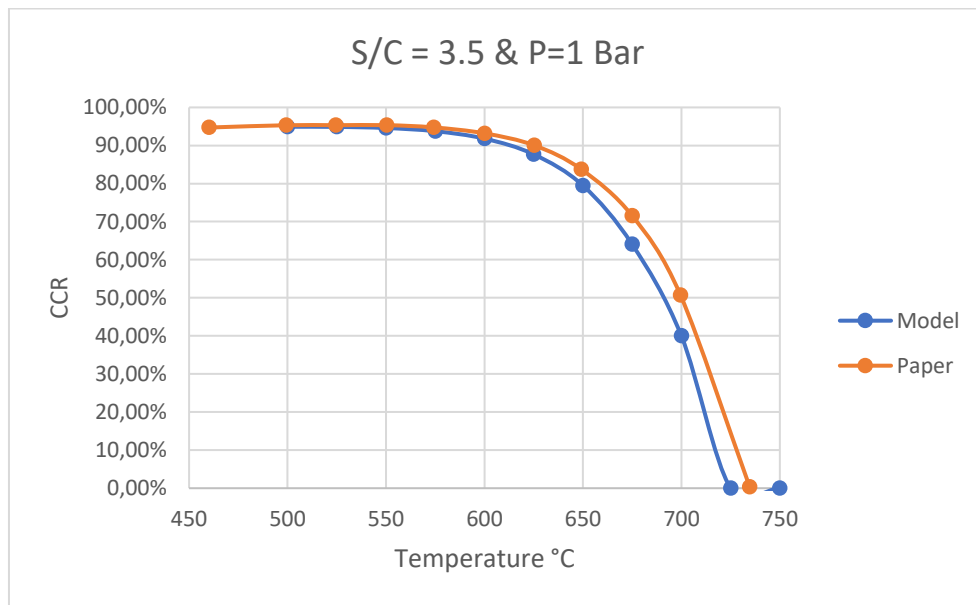


Figure 5-5 Carbon Capture comparison Ratio at 1 bar and S/C=3.5
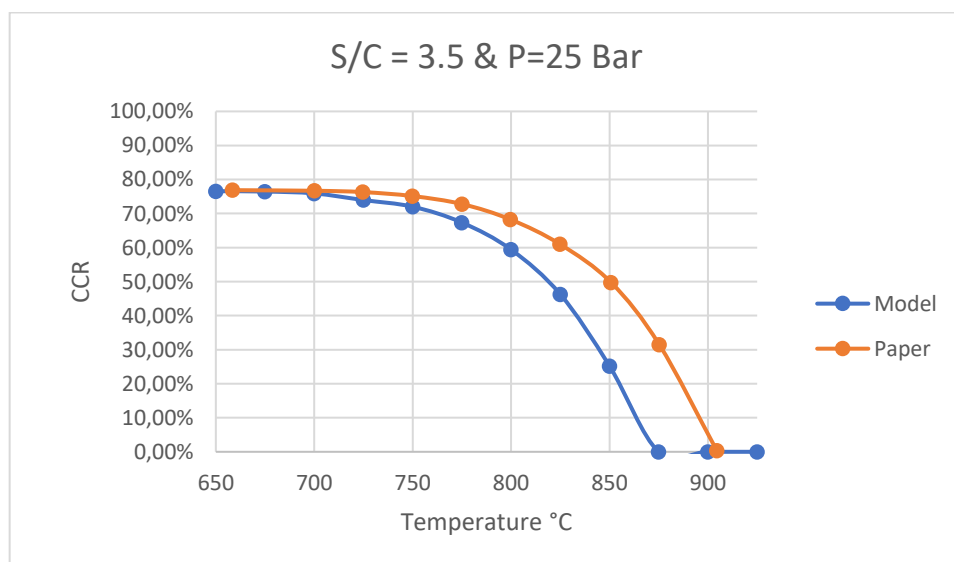


Figure 5-6 Carbon Capture Ratio comparison at 25 bar and S/C=3.5
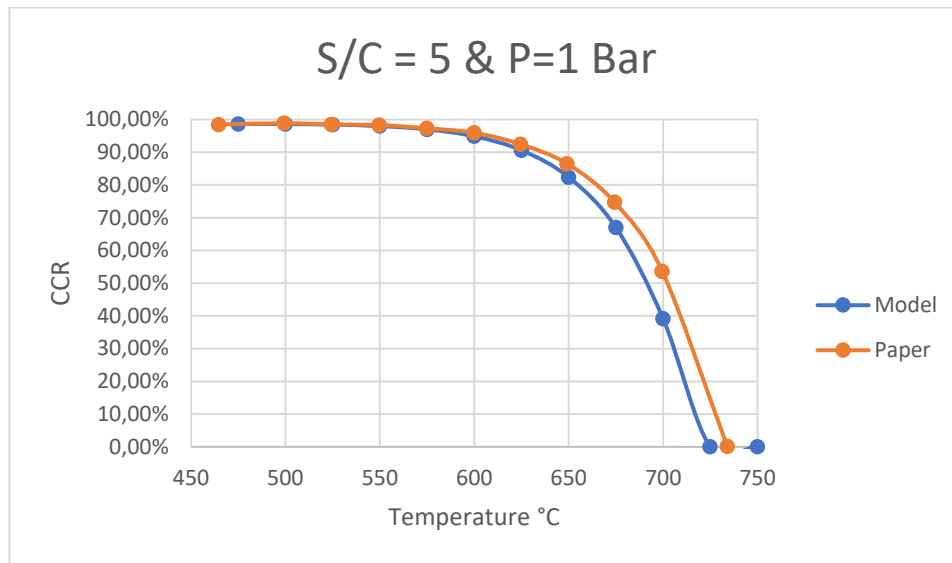
Figure 5-7 Carbon Capture Ratio comparison at 1 bar and S/C=5
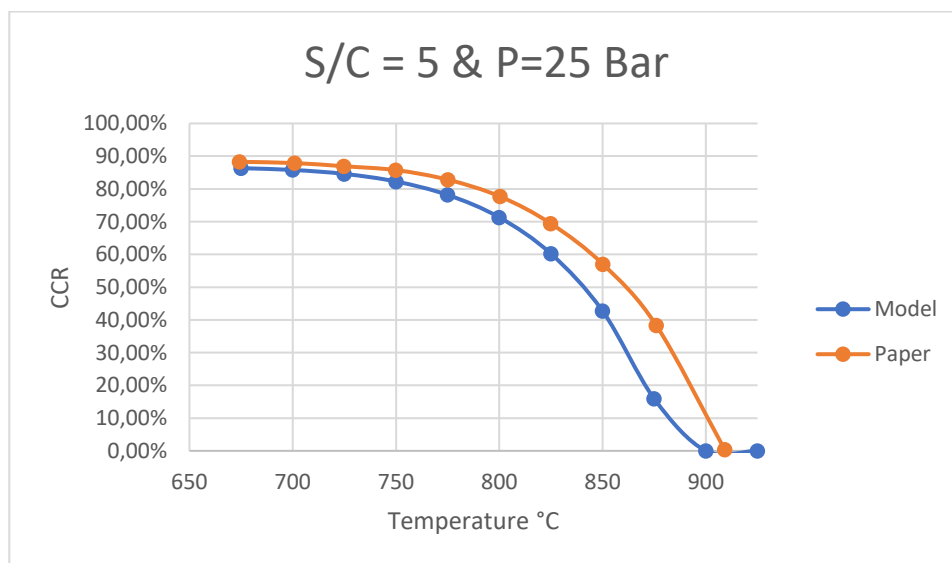


Figure 5-8 Carbon Capture Ratio comparison at 25 bar and S/C=5

As shown in the figures, deviations are predicted at high pressures and temperatures for both s/c ratios evaluated. in order to detect the origin of the deviations, it has been decided to compare the Aspen's predicted partial pressure of the $CO_2/N_2$ mixture in the carbonation reaction equilibrium with the reference study (75). After including only the carbonation reaction inside the reactor and excluding all the others, it has been confirmed that the deviations are related to the lack of accuracy of the ASPEN's modeling for the solid-gas equilibrium prediction.

However, the results fit with acceptable accuracy for the temperature range of interest of this study, 500 to 600 °C.
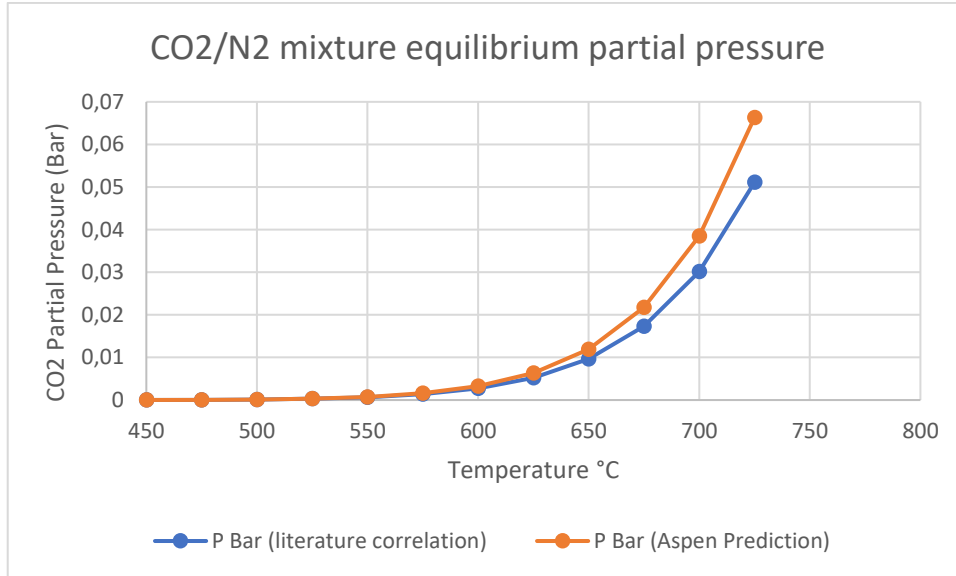


Figure 5-9 $CO_2/N_2$ mixture equilibrium partial pressure.

As we see, $H_2$ yield, as well as carbon Capture Ratio, are well predicted by the simplified model, meaning that the gas reaches the equilibrium composition, and hence the approximations made with the simplified model can be accepted.

Calcination Section

The calciner was modelled as a reactor where only the CaCO3 calcination reaction is taking place. Complete conversion of the CaCO3 is assumed and the partial pressure of the $CO_2$ in the reactor outlet is adjusted to fit the value calculated for the chemical equilibrium as a function of the calcination temperature based on eq. 5-1, reported in (132).

$$P_{CO2,eq} = 4.137 * 10^{12} * e^{(\frac{-2047}{T})}$$

5-1

To validate the heat of reaction predicted by model, the heat of the reaction at the calcination temperature using the heat of the reaction at the reference temperature and relevant coefficients for each component is calculated. The coefficient for

different species is extracted from the Coefficients for Calculating Thermodynamic and Transport Properties of Individual Species book (133).

Empirical equations for this example:

$$\textbf{\textit{Heat capacity}}: \frac{C_p^\circ(T)}{R} = a_1 + a_2 T + a_3 T^2 + a_4 T^3 + a_5 T^4 \qquad \text{5-2}$$

$$\textbf{\textit{Enthalpy}}: \frac{H_p^\circ(T)}{RT} = a_1 + a_2 \frac{T}{2} + a_3 \frac{T^2}{3} + a_4 \frac{T^3}{4} + a_5 \frac{T^4}{5} + \frac{b_1}{T} \qquad \text{5-3}$$

$$\textbf{\textit{Entropy}}: \frac{S^\circ(T)}{R} = a_1 \ln T + a_2 T + a_3 \frac{T^2}{2} + a_4 \frac{T^3}{3} + a_5 \frac{T^4}{4} + b_2 \qquad \text{5-4}$$

# 6    Pyrolysis gas SESR modeling

## 6.1.   Model description

Figure 6-1 presents the simplified plant scheme which consists of 4 main parts: Feed heating and heat recovery, sorption enhanced reforming, sorbent regeneration, and CO2 compression
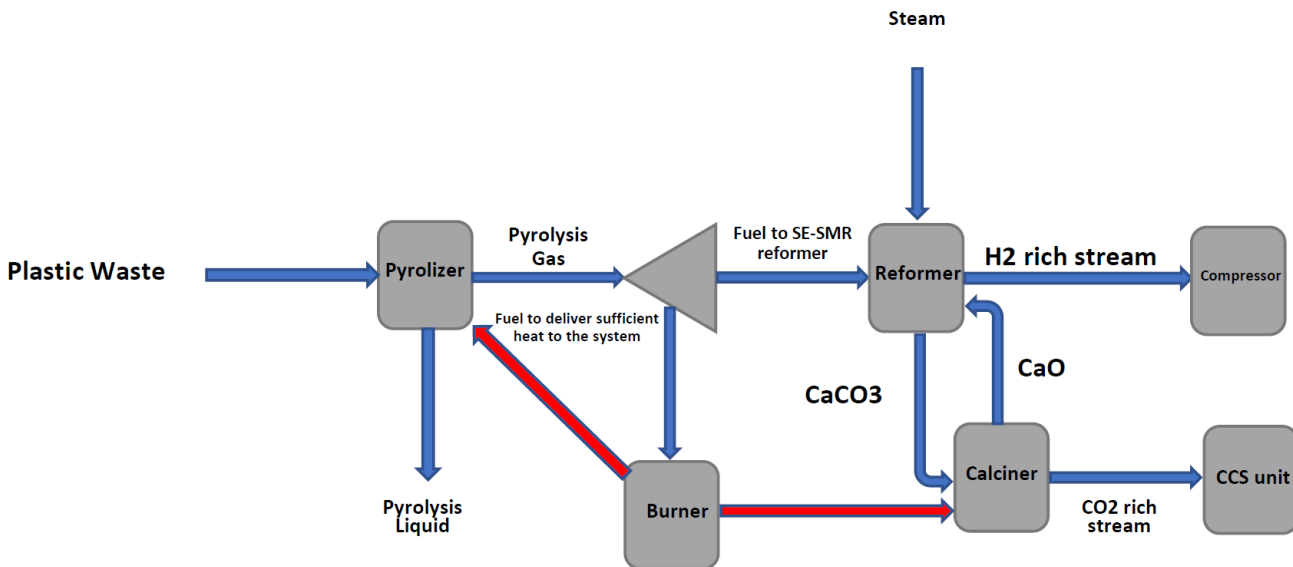


Figure 6-1 simplified plant scheme

### 6.1.1.   Plastic waste pyrolysis

The plastic is fed to the pyrolysis unit at a 625 kg/hr rate, in which the composition information is provided by experimental industry analysis. Plastic waste mixed is fed at 15 °C. other studies showed that the optimum working conditions for the pyrolizer are 500C and 1 bar, an RYIELD reactor at 500°C and 1 bar has been employed to model the energy analysis of the plastic pyrolysis unit. yields of each product are based on the average of results obtained from many experiments.

In Table 6-1, the ultimate and proximate analysis of the fed waste plastic has been presented. To consider the ash in the energy analysis, we have introduced 10% wt. The CaO enters the pyrolysis reactor at 15 °C as inert material and exits at 500°C.

Table 6-1 the ultimate and proximate analysis of the fed waste plastic.

| Plastic Waste | | Ultimate Analysis, wt. % | | | | | Proximate Analysis, wt. % | |
|---|---|---|---|---|---|---|---|---|
| | | C | H | O | N | S | Volatile | Ash |
| Mixed | | 82.67% | 14.79% | 0.97% | 0.00% | 0.00% | 90.00% | 10.00% |

For simplicity, it has been assumed zero percentage of the moisture in the plastic content, given that the average amount of the moisture in plastic is negligible.

The molar composition of the pyrolysis product based on the lab analysis is shown in Table 6-2.

Hydrocarbons having seven or more carbons are olefins.

Table 6-2 molar composition of the pyrolysis product.

| | |
|---|---|
| $N_2$ | 31.54% |
| $CO_2$ | 17.05% |
| $H_2$ | 23.14% |
| Methane | 92.57% |
| Ethane | 66.77% |
| Ethene | 75.45% |
| Propane | 54.48% |
| Propene | 54.48% |
| IButane | 0.54% |
| NButane | 9.74% |
| Butene | 16.60% |
| IPentane | 0.03% |
| NPentane | 0.28% |
| Heptane | 24.79% |
| C7 | 31.42% |
| C8 | 27.49% |
| C9 | 24.44% |
| C10 | 22.00% |
| C11 | 8.54% |
| C12 | 7.83% |
| C13 | 7.23% |
| C14 | 6.71% |
| C15 | 6.26% |
| C16 | 5.87% |
| C17 | 5.53% |
| C18 | 5.22% |
| C19 | 4.95% |
| C20 | 4.70% |
| C21 | 4.47% |
| C22 | 4.27% |
| C23 | 2.05% |
| C24 | 1.96% |
| C25 | 1.88% |
| C26 | 1.81% |
| C27 | 1.74% |
| C28 | 1.68% |
| C29 | 1.62% |
| C30 | 1.57% |
| C31 | 7.81% |
| C35 | 6.91% |

A detailed stream results is presented in Appendix A.

## 6.1.2.  SESR of non-condensable gases (NCG)

Similar to the simplified model explained in the previous chapter, in order to model, we calculate reformer and calciner at chemical equilibrium, reflecting more on what happens in a fluidized bed reactor with homogeneously mixed content and continuous flow of fresh sorbent inside, leading to the assumption of the steady flow of outlet gases, so we calculate the reactors as fluidized beds for the sake of simplicity. Still, we are assuming to change the pressures in the two phases, which is what happens in packed beds. Therefore, we assume we have a series of packed bed reactors working alternatively to maintain the steady-state assumption.

In Table 6-3, the molar composition of non-condensable gases produced in the pyrolysis unit after cooling and separation based on the lab analysis is shown.

Table 6-3 molar composition of non-condensable gases.

| | |
|---|---|
| $N_2$ | 6.75% |
| $CO_2$ | 3.65% |
| $H_2$ | 4.95% |
| Methane | 19.80% |
| Ethane | 14.28% |
| Ethene | 16.14% |
| Propane | 11.65% |
| Propene | 11.65% |
| IButane | 0.11% |
| NButane | 2.08% |
| Butene | 3.55% |
| IPentane | 0.01% |
| NPentane | 0.06% |
| Heptane | 5.30% |

For the reformer, an Rstoich reactor has been employed since we can consider equilibrium conditions with a bit of deviation, which is previously discussed.

For the calciner, an RYield reactor has been employed, and forcing the reactor to have the complete conversion of $CaCO_3$ Steam was used to reduce the partial pressure of the $CO_2$ in the calciner to the equilibrium value.

Starting with a benchmark case, the working conditions of the plant are presented in Table 6-4 Main assumptions used for the modeling of the reference case . As shown in Figure 6-1 the plant consists of 4 main sections: first, we have a pyrolizer which is modeled as a Ryield reactor working at 500 °C. the heat required comes

from the combustion of the pyrolysis gas and is assumed to be transferred in the pyrolizer through inert alumina balls. then we have reformer and calciner. the reformer and the calciner both are operating at 700 °C to prevent temperature swing but at different pressures as the calciner operate close to vacuum at 15 kPa whereas the reformer operates at 20 bars. the following section will be CCR section in which the $CO_2$ will be extracted and compressed to 100 bars. This is the first analysis that will see the main characteristics and performance indexes of the plant. Still, a more detailed study of different pressures and temperatures of the calcination step will be accomplished in the future.

The plant's performance will be carried out in different temperatures (temperature swing) and different pressures (pressure swing) using a vacuum pump plus injecting steam as an inert material to keep the partial pressure of the $CO_2$ low. the reformer/carbonator was assumed as an RGibbs reactor including in the equilibrium calculation of the species in the gas stream of the pyrolizer plus steam and CaO. Stream fed into the reformer is preheated to around 600 °C to keep the reactor thermally neutral. Hydrocarbons reforming are highly endothermic reactions, Eqs. 6-1 to 6-3 but the presence of CaO as a $CO_2$ sorbent makes the global reaction (reforming and carbonation) slightly exothermic.

$$C_2H_6 \ + \ 2H_2O \rightarrow \ 2CO \ + \ 5H_2 \ (\Delta H°r \ (298 \ K) = \ +347 \frac{MJ}{kmol}) \qquad \text{6-1}$$

$$C_3H_8 \ + \ 3H_2O \rightarrow \ 3CO \ + \ 7H_2 \ (\Delta H°r \ (298 \ K) = \ +499 \frac{MJ}{kmol}) \qquad \text{6-2}$$

$$C_4H_{10} \ + \ 4H_2O \rightarrow \ 4CO \ + \ 9H_2 \ (\Delta H°r \ (298 \ K) = \ +649 \frac{MJ}{kmol}) \qquad \text{6-3}$$
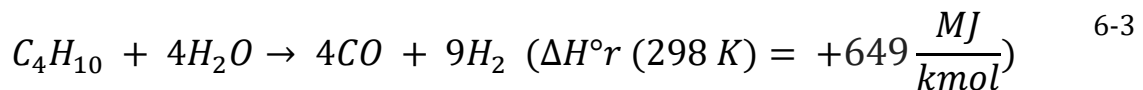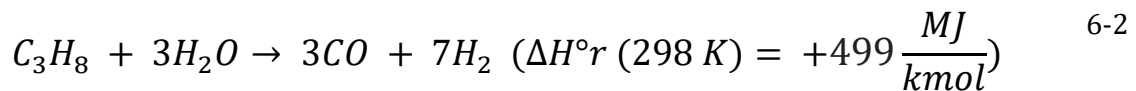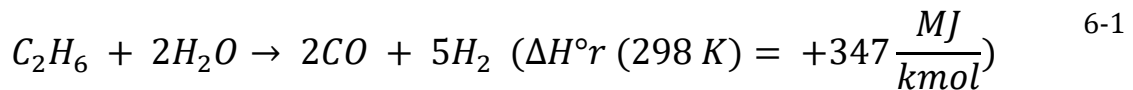
In order to maintain the high stability of the sorbent for the same number of cycles, we assume that we inject inert material with the sorbent. CaO-based

sorbent composition assumed in the simulation model is 40% wt. of CaO and 60% wt. of inert material with the same thermal properties of CaO, so from the energy point of view, this excess CaO is basically the support material.

Steam-to-carbon ratio, S/C, in the gas stream fed to the reformer-carbonator is 5 in all the cases to ensure a high $H_2$ yield.

After cooling and heat recovery, gas from the reformer is conditioned for compression by removing water in a condenser at 15 °C. After condensation, an $H_2$-rich gas stream is obtained.

For the reference case, solids leaving the reformer are sent to the calciner reactor that operates at a temperature the same as the reformer and a vacuum close to 15 kPa (in the reference case). these conditions are set by complying with several conflicting requirements that can be summarized as follows:

- the lower limit of the calciner operating temperature is the Equilibrium temperature of the carbonation reaction was calculated (75).
- Twenty degrees temperature margin over the previous limit must be kept providing enough driving force for regeneration reaction completion.
- On the other hand, a very high-temperature difference between carbonator and calciner influences fuel consumption in the calciner combustor to a large extent. Thus, the higher the temperature margin, the lower the process energy efficiency.
- Although commercial steam reforming catalysts can face temperatures up to 1273 K, Ca-based sorbent capacity is dramatically affected when going above 1223 K (134).

Energy for sorbent calcination is supplied by burning of around 28% of the total pyrolysis gas produced in the pyrolysis unit in the calciner burner. Inlet air injection was calculated such that in the combustor outlet, we have about 3% excess oxygen with respect to the stoichiometric amount to ensure complete fuel combustion. Produced heat in the calcination burner, after delivering enough heat for the calcination is recovered to first, generating superheated steam at 1 bar and 700°C for making the proper partial pressure of $CO_2$ in the calciner, then to generate superheated steam at 1 bar and 600°C to utilize in the reformer, then to preheat the combustion air to 400°C and finally to finish the evaporating and to superheat the steam which will be employed in the calciner to around 500°C and vent the flue gas at 110°C. Figure 6-2.

Gas from the calciner is cooled down to 105 °C and its heat is recycled before going to purification and compression. After further multi-stage cooling and compression, a seven-stage intercooled compression initially compresses the $CO_2$-

rich stream to 80 bars. Then, the $CO_2$-rich gas stream goes through a pump, and it is finally pumped to 100 bars.
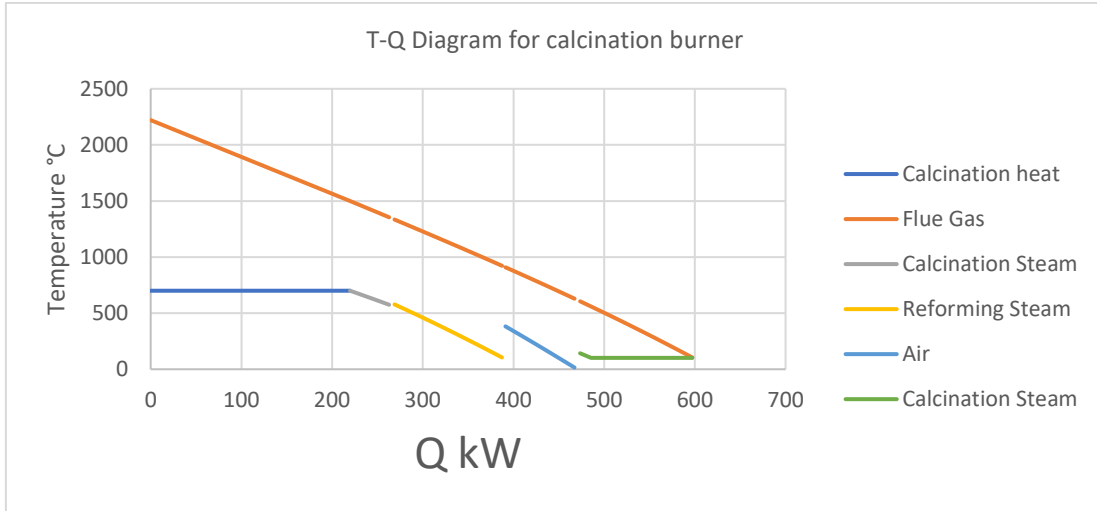


Figure 6-2 T-Q Diagram for calcination burner.

Energy for the plastic pyrolysis is provided by burning around 22% of the total pyrolysis gas produced in the pyrolysis unit in the pyrolysis burner. inlet air was calculated in the same way as for the calciner burner (COMBUST2 in flowsheet Figure 6-1). Produced heat in the pyrolysis burner, after delivering enough heat for the pyrolysis is recovered to heat the pyrolysis gas to 600°C, preheat the combustion air to 400°C, partial evaporation of the water required for calcination and vent the flue gas at 110.
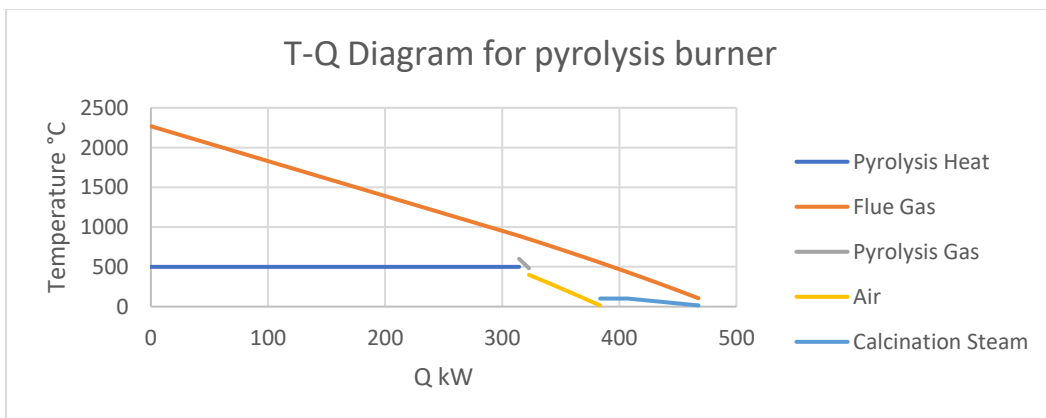


Figure 6-3 T-Q Diagram for pyrolysis burner.

In the Table 6-4 , the Main assumptions used for the modeling of the reference case have been presented.

Table 6-4 Main assumptions used for the modeling of the reference case .

| | | |
|---|---|---|
| NCG supply temperature | 15 | °C |
| NCG supply pressure | 1 | bar |
| Water supply temperature | 15 | °C |
| Water supply Pressure | 1 | bar |
| S/C molar ratio | 5 | - |
| Total NCG input | 160.20 | kg/hr |
| Air supply temperature | 15 | °C |
| Air supply pressure | 1 | bar |
| **Adiabatic Reformer (at equilibrium)** | | |
| Feed temperature | 600 | °C |
| Operating Temperature | 700 | °C |
| Operating Pressure | 20 | bars |
| **Inter-cooled $CO_2$ compressor** | | |
| Number of intercooled compression stages | 7 | - |
| Intercooling temperature | 15 | °C |
| Outlet pressure after compression stages | 80 | bars |
| Final $CO_2$ storage pressure | 100 | bars |
| Polytropic efficiency of compression stages | 80 | % |
| **Calciner** | | |
| Operating Temperature | 700 | °C |
| Operating Pressure | 15 | kPa |
| $CaCO_3$ conversion | 100 | % |

The following assumptions are also included in this model:

1. All the reactions in SESR reach chemical equilibrium when the entire process operates at a steady state. The chemical equilibrium is modeled using the RGibbs module in Aspen Plus, which minimizes the Gibbs free energy of the system.
2. The reaction in REG reaches 100% conversion of $CaCO_3$ when the entire process operates at a steady state. The 100% conversion is modeled using the RYield module in Aspen Plus.
3. The thermodynamic properties of all the components included in the process are determined using the Peng-Robinson equation of state.
4. Zero pressure drop across the unit operation blocks.
5. Gas and solid phases are instantaneously and perfectly mixed in both reactors. The separation efficiency of cyclones is 1, and perfect separation of solid and gas phases is assumed.
6. The CaO sorbent is fully regenerated.

## 6.2. Reference Case Results

Hydrogen Yield (H₂ Yield)

Hydrogen yield allows comparing the hydrogen produced in the process to the "equivalent hydrogen," which is defined as the maximum quantity of hydrogen that can be produced by complete conversion of the feed (according to steam reforming and water gas shift stoichiometry). To calculate the equivalent hydrogen entering the plant, the overall conversion reaction of a hydrocarbon CnHm must be written:

$$C_nH_m + 2n.H_2O \leftrightarrow \left(2n + \frac{m}{2}\right)H_2 + nCO_2 \tag{6-4}$$
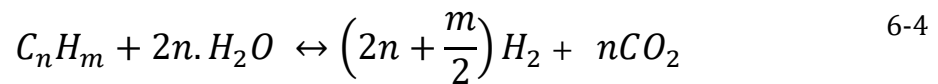
$$n_{H2,eq=}\left(2n + \frac{m}{2}\right)+n_{C_nH_m,in} \tag{6-5}$$

If, for example, methane is assumed and every mole of it is converted, a maximum of 4 moles of hydrogen could be produced.

The expression of the hydrogen yield (measured in kmolH₂/kmolH₂, eq) than results:

$$H_2\text{yield} = \frac{n_{H_2,out}}{n_{H_2,eq}} \tag{6-6}$$

Based on the amount of pyrolysis gas produced in the pyrolysis unit, the maximum quantity of hydrogen that can be produced by complete conversion of the feed is calculated as around 32 kmol/hr, whereas we are producing 14.87 kmol/hr of hydrogen, so in the reference case, we achieved up to 47% in hydrogen yield.

It is also worthy to note that here, we compare the hydrogen produced in this process with a case where the total pyrolysis gas is converted to hydrogen and the

energy for calcination and pyrolysis are provided externally so there is no surprise to have a low range of yields. for better comparison we have calculated the $H_2$ yield also for only the part going to the SER to have both numbers. The new index is $H_2$ yield 2nd kind which is 92%.

Hydrogen Molar Dry Concentration ($\boldsymbol{y_{H_2,dry}}$)

The hydrogen molar dry concentration is the concentration of hydrogen on a dry basis; it is assessed at the outlet of the reformer, and it is an index of hydrogen purity. The expression is:

$$\boldsymbol{y_{H_2,dry}} = \frac{\boldsymbol{y_{H_2}}}{\boldsymbol{1 - y_{H_2O}}} \qquad \text{6-7}$$

In the reference case, Hydrogen Molar Dry Concentration equal to 96.2% is achieved and since the composition of the NCG is constant, although we do the sensitivity analysis on temperature and pressure of calcination, the hydrogen molar dry concentration is the concentration is constant.

Reformer Carbon Capture Ratio (CCR1)

CCR1 is the ratio between the number of the $CaCO_3$ moles exiting the reformer and the molar flow rate (or equivalently the number of moles) of carbon atoms entering the reformer. This is the carbon capture efficiency related to the SER reactor. Presents how efficient our reformer Is working in $CO_2$ sorption, so this index does not account for calcination combustors since it simply assumes that we use green technology to regenerate the sorbent without burning carbon.

This index in the reference case is around: 91.53%

$$\boldsymbol{CCR_1} = \frac{\dot{\boldsymbol{n}}_{\boldsymbol{C,captured}}}{\dot{\boldsymbol{n}}_{\boldsymbol{C,reformer\ inlet}}} \qquad \text{6-8}$$

SER system carbon Capture Ratio (CCR2)

CCR2 is the ratio between the number of the $CaCO_3$ moles exiting the reformer and the molar flow rate (or equivalently the number of moles) of carbon atoms entering the reformer plus the carbon atoms emit by the calcination combustor as

CO₂. This is the carbon capture efficiency related to the SER system (reformer + calcination combustor); it presents how efficient our SER system is in terms of $CO_2$ emission.

This index in the reference case is around: 58.68%

$$CCR_2 = \frac{\dot{n}_{C,captured}}{\dot{n}_{C,reformer\ inlet} + \dot{n}_{C,emit\ by\ calcination\ combustor}} \qquad 6\text{-}9$$

Plant Carbon Capture Ratio 1st kind (CCR3)

CCR3 is the ratio between the $CaCO_3$ exiting the reformer and molar flow rate (or equivalently the number of moles) of carbon atoms entering the reformer and the number of plus the carbon atoms emitted by the calcination and pyrolysis combustor as $CO_2$. This is the carbon capture efficiency related to the plant; it presents our plant's efficiency in terms of $CO_2$ emission. This index takes that we will reserve the liquid fuel.

This index in the reference case is around: 45.77%

$$CCR_3 = \frac{\dot{n}_{C,captured}}{\dot{n}_{C,reformer\ inlet} + \dot{n}_{C,emit\ by\ combustors}} \qquad 6\text{-}10$$

Plant Carbon Capture Ratio 2nd kind (CCR4)

CCR3 is the ratio between the $CaCO_3$ exiting the reformer and molar flow rate (or equivalently the number of moles) of carbon atoms entering the reformer plus the carbon atoms emit by the calcination and pyrolysis combustor as $CO_2$ plus the carbon content in the liquid fuel. This is the carbon capture efficiency related to the whole plant; it presents our plant's efficiency in terms of $CO_2$ emission. This index takes we are going to burn the liquid.

This index in reference case is around: 11.86%

$$CCR_4 = \frac{\dot{n}_{C,captured}}{\dot{n}_{C,entring\ the\ system\ as\ plastic}} \qquad 6\text{-}11$$

Here, a table with all the results of the reference case is presented.

Table 6-5 the results of the reference case

| $H_2$yield | 47% |
|:---:|:---:|
| $H_2$yield 2nd | 92% |
| $y_{H_2,dry}$ | 96.2% |
| $CCR_1$ | 91.5% |
| $CCR_2$ | 58.6% |
| $CCR_3$ | 45.7% |
| $CCR_4$ | 11.8% |

# 7 Sensitivity Analysis & Discussion

This chapter is dedicated to evaluating the sensitivity of the obtained results to the various working conditions. This analysis has the scope of finding the more suitable calcination pressure and temperature for the plant in terms of $H_2$ production, Carbon capture rate, and required power to run the pump and compressors for $CO_2$ capture.

This sensitivity analysis is performed considering three different calcination pressures and temperature alternatives. In all the cases, after setting the calcination temperature, two options were compared for setting the $CO_2$ partial pressure in the calciner achieving a value sufficiently lower than the equilibrium partial pressure for the calcination reaction to have proper driving force towards the sorbent regeneration. The first option is to run the calciner in sub atmospheric condition and the second option evaluated is to dilute the reacting mixture by injecting superheated steam at a temperature equal to the calcination temperature.

## 7.1. Sensitivity Analysis of Calcination Temperature

as part of the NCG is combusted to deliver the heat required for calcination, the calcination temperature is expected to have a high impact on the process performance. On the one hand, high calcination temperature favors the $CaCO_3$ calcination reaction shifting the equilibrium partial pressure to a more elevated value that can reach more than 1 bar at 900 °C. on the other hand, from a technical point of view, swinging the reactor's temperature between the two steps of the process (reforming/regeneration) may guide to some difficulties and may lead to the specific requirement of material that would increase the cost of the plant.

### 7.1.1. Results & Discussion

$H_2$ Yield

In this section, a sensitivity analysis of calcination temperature has been performed. The calciner is operating at different temperatures and different vacuum pressures. In addition to vacuum, Steam in different quantities depends on the calcination temperature and the pressure was used to reduce the partial pressure of the $CO_2$ in the calciner to the equilibrium value.
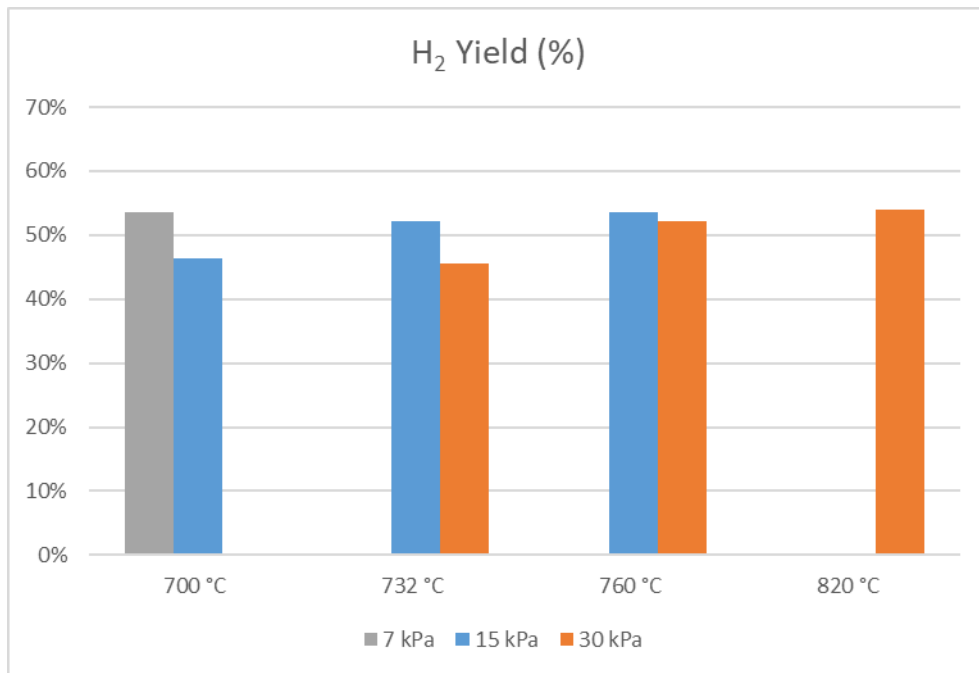
Figure 7-1 H2 yield sensitivity analysis on calcination temperature.

As we see in the graph, the higher the calcination temperature, the higher the index in terms of $H_2$ yield. The outcomes can be explained by describing the balance between two opposing reasons:

First, when the calcination is performed at a higher temperature, the required partial pressure of $CO_2$ at equilibrium will be higher at the same calcination pressure, so the amount of the steam needed to inject into the calciner at the same calcination pressure will be lower. Subsequently, the required fuel to provide the heat to bring the steam to the calcination temperature is lower, so the amount of feed available to deliver to the reforming unit will be higher. Second, when the calcination is performed at a higher temperature, the amount of fuel required to deliver the heat to complete the calcination at a higher temperature (temperature swing) will be higher, so the amount of feed available to deliver to the reforming unit will be lower. the benefit of having less steam overweights the detrimental effect of high temperature from an energy efficiency point of view. Subsequently, the hydrogen production yield will be higher at the same pressure, increasing the calcination temperature.

As result, $H_2$ yield, will be higher by increasing the temperature.

Carbon Capture efficiency

Since the configuration of the reformer reactor and the amount of the pyrolysis oil produced in the pyrolysis unit is the same in all the cases, performing the sensitivity analysis is only accomplished in the SER system carbon Capture Ratio (CCR2) and Plant Carbon Capture Ratio 1st kind (CCR3).
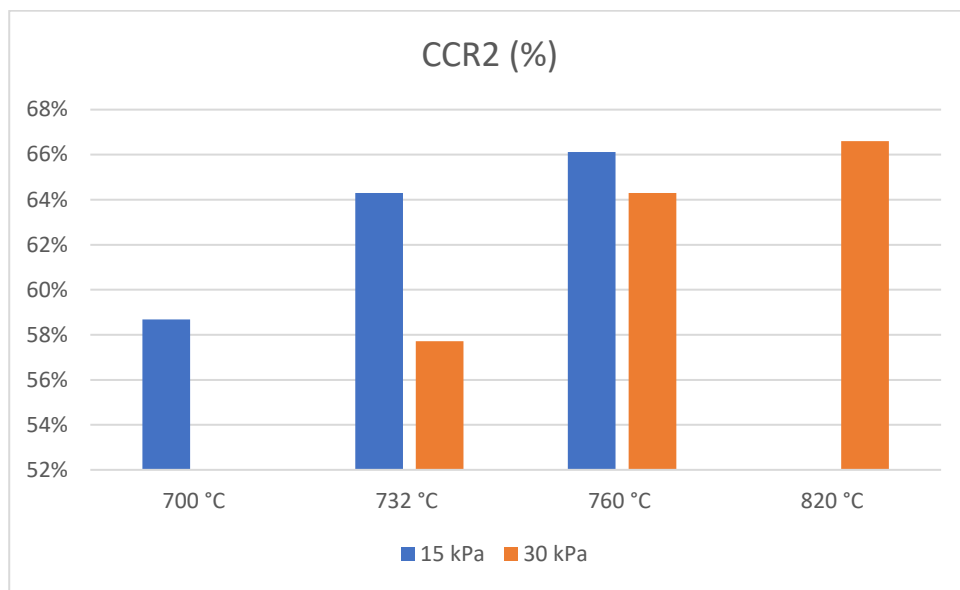


Figure 7-2 SER system carbon Capture Ratio sensitivity analysis on temperature.
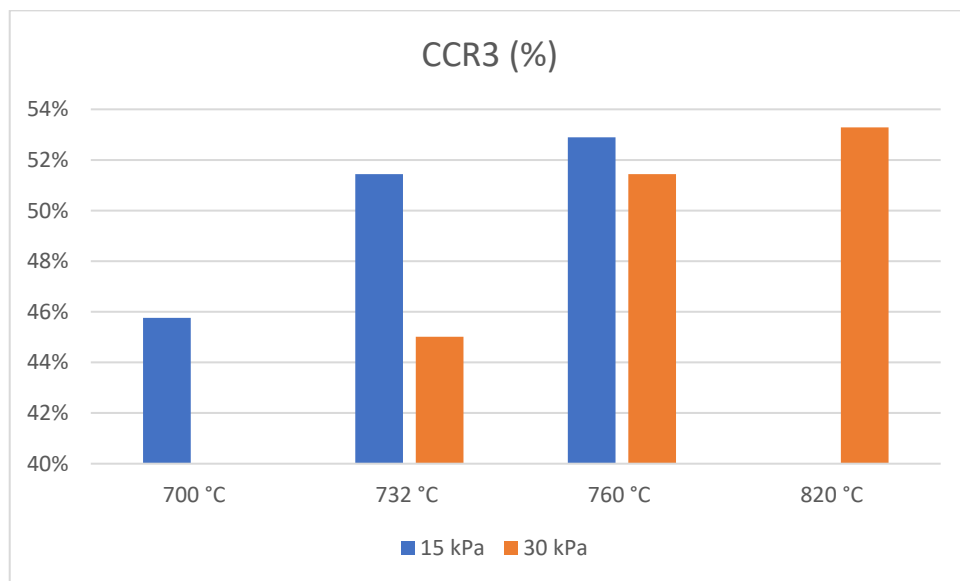


Figure 7-3 Plant Carbon Capture Ratio 1st kind analysis on temperature.

As the same reasons of $H_2$ yield which will be higher by increasing the temperature, both carbon capture efficiencies will be higher also since the more hydrogen produced in the reformer, the more CaO will turn to $CaCO_3$ and subsequently, the more $CO_2$ will be captured afterwards.

Compressors and pump specific power required
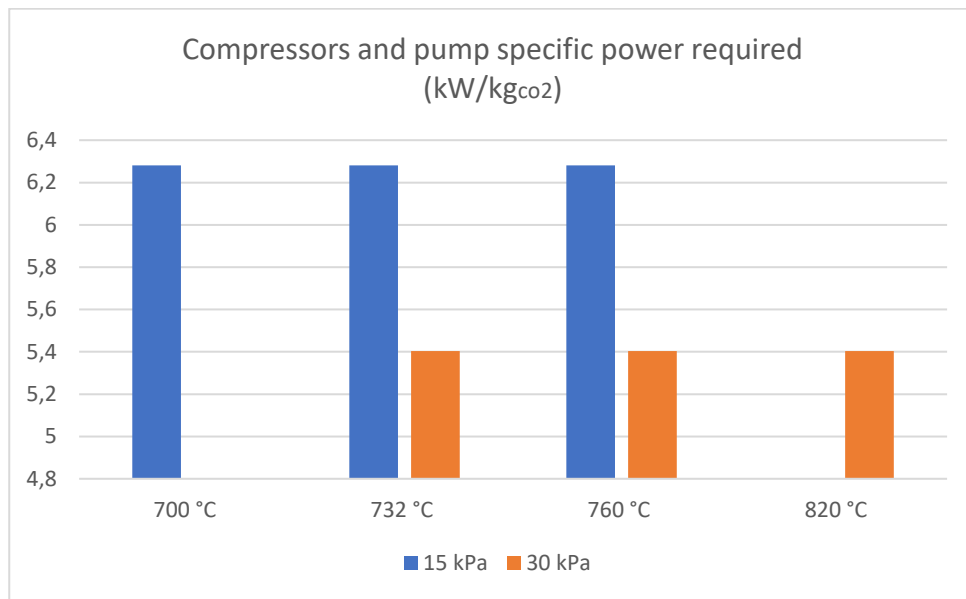


Figure 7-4 Compressors and pump total work required sensitivity analysis on temperature.

Regarding the required power to run the pump and compressors for $CO_2$ capture, the higher the calcination temperature, the higher the required power to run the pump and compressors for $CO_2$ capture because it is a result of burning less NCG so we are reforming more then we capture more. the compressors need to work more in order to bring more $CO_2$ from a certain pressure up to the same pressure (100 bars).

## 7.2.  Sensitivity Analysis on Calcination Pressure

Since the partial pressure of the $CO_2$ in the calciner should be set at equilibrium pressure at each specific temperature, we need to push the pressure down by injecting steam into the calciner, and due to the high specific heat capacity of the steam, the amount of the steam has a high impact on the process performance. So, the total pressure of the calciner is consequently expected to have a high effect on the process performance in energy point of view.

Furthermore, from a technical point of view, very low reactor's pressure may guide to some difficulties and may lead to the specific requirement of vacuum pumps that would increase the cost of the plant.

### 7.2.1.  Results & Discussion
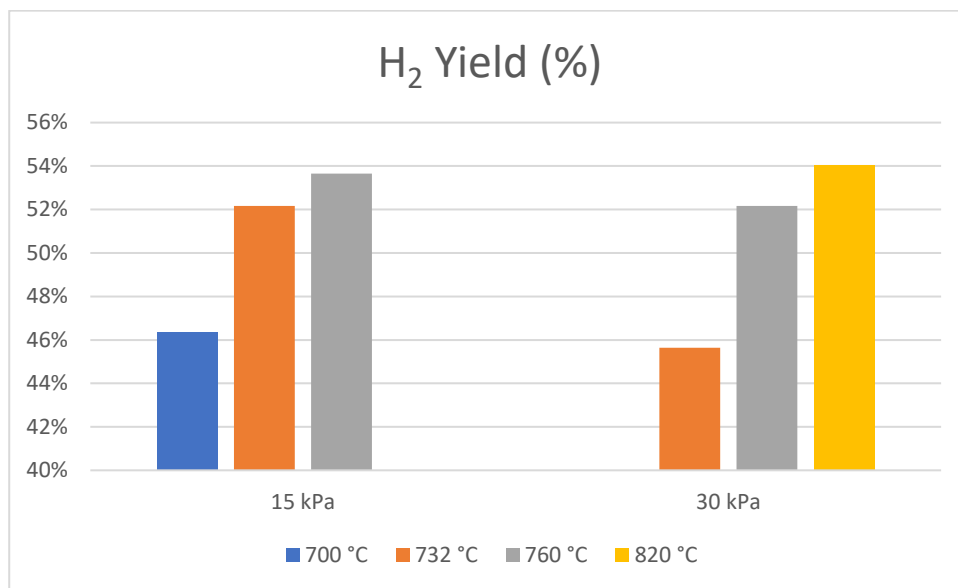
$H_2$ Yield



Figure 7-5 H2 yield sensitivity analysis on calcination pressure on pressure.

first by looking at the case of 30kPa (orange columns) we can see that the temperature increase has a positive effect on $H_2$ yield. the same behavior is predicted for the other evaluated pressures where the increase of the temperature improves the performances. additionally reducing the pressure may lead to technical difficulties on a large scale.

As we see in the graph, the lower the calcination pressure, the higher the index in terms of $H_2$ production at all the investigated temperatures. The outcomes can be explained as when the calcination is performed at a lower pressure, at the same

temperature with the same required partial pressure of $CO_2$ at equilibrium, the amount of the steam needed to inject into the calciner at the same temperature will be lower. Subsequently, the required fuel to provide the heat to bring the steam to the calcination temperature is lower, so the amount of feed available to deliver to the reforming unit will be higher. Subsequently, the hydrogen production yield will be higher at the temperature, decreasing the calcination pressure.

Carbon Capture efficiency
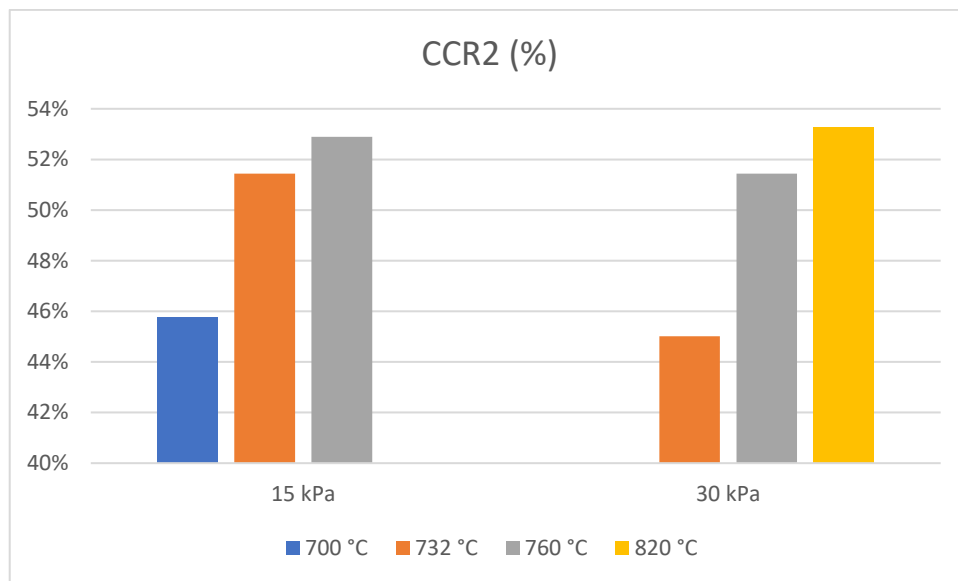


Figure 7-6 SER system carbon Capture Ratio sensitivity analysis on pressure.
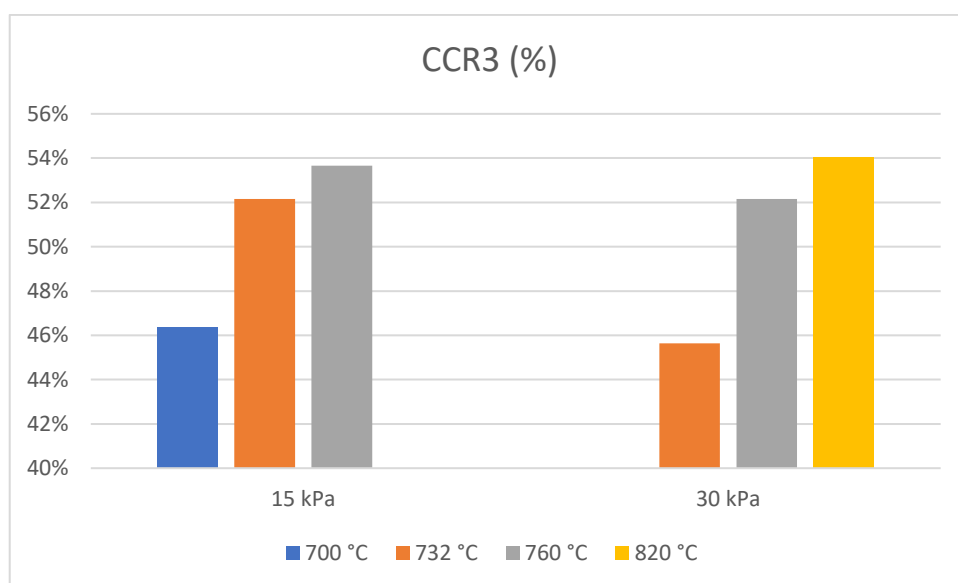


Figure 7-7 Plant Carbon Capture Ratio 1st kind sensitivity analysis on pressure.

Compressors and pump specific power required
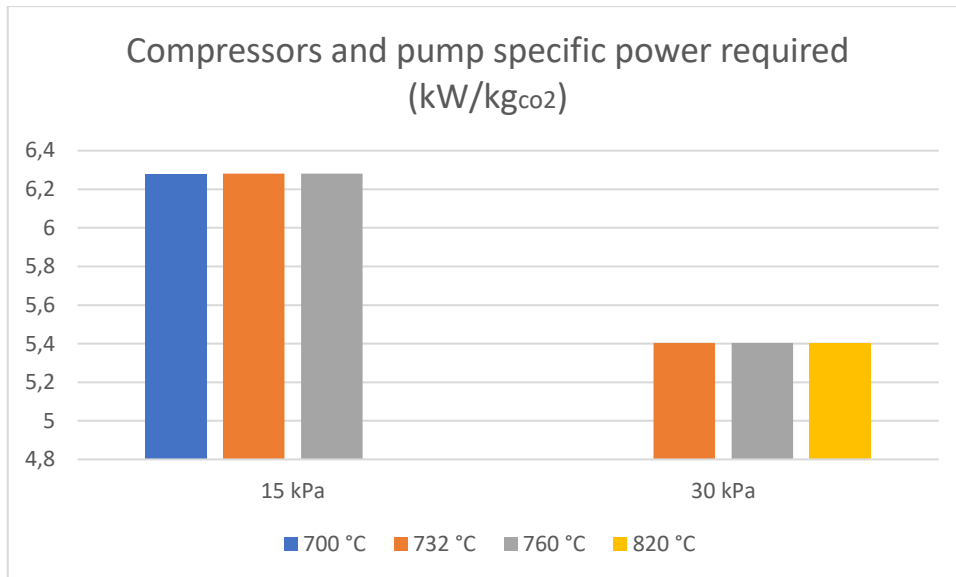


Figure 7-8 Compressors and pump total work required sensitivity analysis on pressure.

Regarding required power to run the pump and compressors for $CO_2$ capture, the lower the calcination pressure, the higher the required power to run the pump and compressors for $CO_2$ capture because the compressors need to work more in order to bring the $CO_2$ from a lower pressure up to certain pressure (100 bars).

# Conclusions

In this work the integration of the sorption enhanced steam reforming (SESR) process within a municipal plastic waste plant is studied with the aim of optimizing the plant configuration operate flexibly, performing pyrolysis of the municipal plastic waste and producing hydrogen with $CO_2$ capture. Comparing this technology with traditional hydrogen production plants has shown the potentiality of the system to provide a local source of hydrogen to cover the downstream upgrading processes.

The main energetic-environmental results that can be pointed out are the following ones:

- SESR of Non-Condensable Gas of Plastic Pyrolysis provides a hydrogen yield of around 47%, considering the energy required for pyrolysis of plastic and the sorbent regeneration is delivered by pyrolysis gas combustion. This value increases up to 92% considering that the plant's thermal demand is sustained externally.
- The carbon capturing ratio (CCR) of the SESR hydrogen production from the Non-Condensable Gas of Plastic Pyrolysis system exceeds 90% considering the SESR step alone and drops down to the range 58% to 67% (depending on the regeneration conditions) on considering the sorbent regeneration thermal demand.

The main design parameters which have been outlined can be summarized as follows:

- A pre-reformer might be helpful because pyrolysis gas contains hydrocarbons higher than methane.
- The sorbent regeneration pressure is quite crucial in the definition of plant performance; lower pressures increase the value of hydrogen production efficiency and raise the CCR of the plant but increases the power required to compress the $CO_2$ and the plant's capital cost.
- Vacuum calcination allows sustaining a low temperature sorbent regeneration limiting the temperature swings and improving the utilization of the energy for regeneration.

Further works will require experimental validations of the mathematical models used in this thesis to assess their validity.

# Bibliography

1. **Tan, Zhongchao.** Air Emissions. *Air Pollution and Greenhouse Gases.* s.l. : Springer, 2014, pp. 1--24.

2. **Houghton, Ed.** *Climate change 1995: The science of climate change: contribution of working group I to the second assessment report of the Intergovernmental Panel on Climate Change.* 1996.

3. *Gutowski, 10 WJ.* **Collins, M and Knutti, R and Arblaster, J and Dufresne, JL and Fichefet, T and Friedlingstein, P and Gao, X.** 2013, Johns, T., Krinner, G., Shongwe, M., Tebaldi, C., Weaver, AJ, and Wehner, M.: Long-term Climate Change: Projections, Commitments and Irreversibility. In: Climate Change.

4. **Irena, A.** Renewable capacity highlights. *Proc. Int. Renew. Energy Agency (IRENA).* 2020, pp. 1--8.

5. *Electricity Storage and Renewables: Costs and Markets to 2030.* **Renewable, I and IRENA, I Renewable and others.** 2017.

6. **Huggins, Robert A.** Hydrogen storage. *Energy Storage.* 2010, pp. 95--117.

7. *Global energy transformation: a roadmap to 2050.* **Gielen, Dolf and Gorini, Ricardo and Wagner, Nicholas and Leme, Rodrigo and Gutierrez, Laura and Prakash, Gayathri and Asmelash, Elisa and Janeiro, Luis and Gallina, Giacomo and Vale, Guilia and others.** 2019.

8. *Hydrogen scaling up: A sustainable pathway for the global energy transition.* **Council, Hydrogen.** 2017.

9. **CATALDO, Alessandro dE.** *Flexible system for electricity and hydrogen production from.* Energy Engineering, Politecnico di Milano. 2020.

10. *IPCC special report on carbon dioxide capture and storage.* **Rubin, E and De Coninck, H.** UK: Cambridge University Press. TNO (2004): Cost Curves for CO2 Storage, Part, p. 2005.

11. *A comparative overview of hydrogen production processes.* **Nikolaidis, Pavlos and Poullikkas, Andreas.** 2017, Renewable and sustainable energy reviews, pp. 597--611.

12. *Comparison of environmental and economic aspects of various hydrogen production methods.* **Kothari, Richa and Buddhi, D and Sawhney, RL.** 2008, Renewable and Sustainable Energy Reviews, Vol. 12, pp. 553--563.

13. *Reference data and supporting literature Review for SMR Based Hydrogen.* **s.l. : IEAGHG, 2017.**

14. *Review of plasma catalysis on hydrocarbon reforming for hydrogen production—interaction, integration, and prospects.* **Chen, Hsin Liang and Lee, How Ming and Chen, Shiaw Huei and Chao, Yu and Chang, Moo Been. 2008, Applied Catalysis B: Environmental, Vol. 85, pp. 1-9.**

15. *Investigation of hydrocarbon reforming processes for micro-cogeneration systems.* **Ers{\"o}z, Atilla. 2008, International journal of hydrogen energy, Vol. 33, pp. 7084--7094.**

16. *Natural gas to synthesis gas--Catalysts and catalytic processes.* **Aasberg-Petersen, K and Dybkj{\ae}r, I and Ovesen, CV and Schj{\o}dt, NC and Sehested, J and Thomsen, SG. 2011, Journal of Natural gas science and engineering, Vol. 3, pp. 423--459.**

17. *Modern and prospective technologies for hydrogen production from fossil fuels.* **Steinberg, Meyer and Cheng, Hsing C. International Journal of Hydrogen Energy, Vol. 14, pp. 797--820.**

18. *A comparison of electricity and hydrogen production systems with CO2 capture and storage. Part A: Review and selection of promising conversion and capture technologies.* **Damen, Kay and van Troost, Martijn and Faaij, Andre and Turkenburg, Wim. 2006, Progress in energy and combustion science, Vol. 32, pp. 215--246.**

19. *Hydrogen via methane decomposition: an application for decarbonization of fossil fuels.* **Muradov, Nazim. 2001, International Journal of Hydrogen Energy, Vol. 26, pp. 1165--1175.**

20. *Tubular reforming and autothermal reforming of natural gas — an overview of available processes.* **Dybkj{\ae}r, Ib. 1995, Fuel Processing Technology, Vol. 42, pp. 85--107.**

21. *Pd-Based Membrane Reactors for Syngas Preparation and WGS.* **Iaquaniello, Gaetano and Palo, Emma and Salladini, Annarita. 2016, Membrane Reactor Engineering: Applications for a Greener Process Industry, p. 184.**

22. *Idrogeno e gas di sintesi, Enciclopedia degli Idrocarburi.* **I. Dybkjær, T. Rostrup-Nielsen and K. Aasberg-Petersen.**

23. **Chiesa, P.** *Notes from Sistemi Energetici Avanzati course.* **2019.**

24. *Global carbon dioxide storage potential and costs.* Hendriks, Chris and Graus, Wina and van Bergen, Frank. 2004, Ecofys, Utrecht, Vol. 64.

25. *Hydrogen Production Technologies Overview.* El-Shafie, Mostafa Ibrahim and Kambara, Shinji and Hayakawa, Yukio. 2019, Journal of Power and Energy Engineering, Vol. 7, pp. 107-154.

26. *An economic survey of hydrogen production from conventional and alternative energy sources.* Bartels, Jeffrey R and Pate, Michael B and Olson, Norman K. 2010, Vol. 35, pp. 8371--8384.

27. *Modern and prospective technologies for hydrogen production from fossil fuels.* Steinberg, Meyer and Cheng, Hsing C. 1989, International Journal of Hydrogen Energy, Vol. 14, pp. 797--820.

28. *Hydrogen production and technology: today, tomorrow and beyond.* Balthasar, W. 1984, International Journal of Hydrogen Energy, Vol. 9, pp. 649--668.

29. *An overview of hydrogen production technologies.* Holladay, Jamie D and Hu, Jianli and King, David L and Wang, Yong. 2009, Catalysis today, Vol. 139, pp. 244--260.

30. *Persistent organic pollutants in the Great Lakes: an overview.* Hites, Ronald A. 2006, Persistent organic pollutants in the Great Lakes, pp. 1--12.

31. *Electrolysis of the Bunsen reaction and properties of the membrane in the sulfur--iodine thermochemical cycle.* Zhang, Yanwei and Ying, Zhi and Zhou, Junhu and Liu, Jianzhong and Wang, Zhihua and Cen, Kefa. 2014, Industrial \& Engineering Chemistry Research, Vol. 53, pp. 13581--13588.

32. *Hydrogen production from water by thermochemical cycles.* Bamberger, CE and Richardson, DM. 1976, Cryogenics, Vol. 16, pp. 197--208.

33. *Electrolysis of water on (oxidized) metal surfaces.* Rossmeisl, Jan and Logadottir, Ashildur and N{\o}rskov, Jens Kehlet. 2005, Chemical physics, Vol. 319, pp. 178--184.

34. *An analysis of hydrogen production from renewable electricity sources.* Levene, Johanna Ivy and Mann, Margaret K and Margolis, Robert M and Milbrandt, Anelia. 2007, Solar energy, Vol. 81, pp. 773--780.

35. *High-temperature electrolysis of water vapor—status of development and perspectives for application.* D{\"o}nitz, W and Erdle, E. 1985, International Journal of Hydrogen Energy, Vol. 10, pp. 291--295.

36. *Stand-alone PEM water electrolysis system for fail safe operation with a renewable energy source.* Clarke, RE and Giddey, Sarb and Badwal, SPS. 2010, International journal of hydrogen energy, Vol. 35, pp. 928--935.

37. *Environmental and exergetic evaluation of hydrogen production via lignocellulosic biomass gasification.* Iribarren, Diego and Susmozas, Ana and Petrakopoulou, Fontina and Dufour, Javier. 2014, Journal of cleaner production, Vol. 69, pp. 165--175.

38. *Comparative energy barriers for hydrogen activation by homogeneous and heterogeneous metal oxide catalyst.* Newsome, DS. 1980, Catal Rev Sci Eng, Vol. 21, pp. 275--318.

39. *Hydrogen production with CO2 capture.* Voldsund, Mari and Jordal, Kristin and Anantharaman, Rahul. 2016, International Journal of Hydrogen Energy, Vol. 41, pp. 4969--4992.

40. Commercial Scale Feasibility of Clean Hydrogen report. [Online] https://zeroemissionsplatform.eu/zep-launches-commercial-scale-feasibility-of-clean-hydrogen-report/.

41. *Tubular reforming and autothermal reforming of natural gas—an overview of available processes.* Dybkj{\ae}r, Ib. 1995, Fuel Processing Technology, Vol. 42, pp. 85--107.

42. *Hydrogen quality from decarbonized fossil fuels to fuel cells.* Besancon, Brian M and Hasanov, Vladimir and Imbault-Lastapis, Rapha{\"e}lle and Benesch, Robert and Barrio, Maria and M{\o}lnvik, Mona J. 2009, International Journal of Hydrogen Energy, Vol. 34, pp. 2350--2360.

43. *Pressure swing adsorption technology for hydrogen production.* Sircar, Shivaji and Golden, Timothy C. 2009, Hydrogen and syngas production and purification technologies, Vol. 10, pp. 414--450.

44. *Historical developments of pyrolysis reactors: a review.* Garcia-Nunez, JA and Pelaez-Samaniego, MR and Garcia-Perez, ME and Fonts, I and Abrego, J and Westerhof, RJM and Garcia-Perez, M. 2017, Energy \& fuels, Vol. 31, pp. 5751--5775.

45.                                                                                [Online] https://www.eeducation.psu.edu/egee439/node/537[Accessed:04.04.20].

46. *Hydrogen production via catalytic pyrolysis of biomass in a two-stage fixed bed reactor system.* Liu, Shaomin and Zhu, Jinglin and Chen, Mingqiang and

Xin, Wenping and Yang, Zhonglian and Kong, Lihong. 2014, International journal of hydrogen energy, Vol. 39, pp. 13128--13135.

47. *Gasification of biomass with oxygen-enriched air in a pilot scale two-stage gasifier.* Wang, Zhiqi and He, Tao and Qin, Jianguang and Wu, Jingli and Li, Jianqing and Zi, Zhongyue and Liu, Guangbo and Wu, Jinhu and Sun, Li. 2015, Fuel, Vol. 150, pp. 386--393.

48. *An experimental study on hydrogen-rich gas production via steam gasification of biomass in a research-scale fluidized bed.* Fremaux, Sylvain and Beheshti, Sayyed-Mohsen and Ghassemi, Hojat and Shahsavan-Markadeh, Rasoul. 2015, Energy Conversion and Management, Vol. 91, pp. 427--432.

49. *An overview of hydrogen production from biomass.* Ni, Meng and Leung, Dennis YC and Leung, Michael KH and Sumathy, KJFPT. 2006, Fuel processing technology, Vol. 87, pp. 461--472.

50. *Biomass resource facilities and biomass conversion processing for fuels and chemicals.* Demirba{\c{s}}, Ayhan. 2001, Energy conversion and Management, Vol. 42, pp. 1357--1378.

51. *Environmental and exergetic evaluation of hydrogen production via lignocellulosic biomass gasification.* Iribarren, Diego and Susmozas, Ana and Petrakopoulou, Fontina and Dufour, Javier. 2014, Journal of cleaner production, Vol. 69, pp. 165--175.

52. *Historical developments of pyrolysis reactors: a review.* Garcia-Nunez, JA and Pelaez-Samaniego, MR and Garcia-Perez, ME and Fonts, I and Abrego, J and Westerhof, RJM and Garcia-Perez, M. 2017, Energy \& fuels, Vol. 31, pp. 5751--5775.

53. Collard, F-X and Carrier, M and G{\"o}rgens, JF. *Fractionation of lignocellulosic material with pyrolysis processing.* 2016.

54. *Light olefins from HDPE cracking in a two-step thermal and catalytic process.* Artetxe, Maite and Lopez, Gartzen and Amutio, Maider and Elordi, G and Bilbao, J and Olazar, M. 2012, Chemical Engineering Journal, Vol. 207, pp. 27--34.

55. *Pyrolysis of a fraction of waste polypropylene and polyethylene for the recovery of BTX aromatics using a fluidized bed reactor.* Jung, Su-Hwa and Cho, Min-Hwan and Kang, Bo-Sung and Kim, Joo-Sik. 2010, Fuel processing technology, Vol. 91, pp. 277--284.

56. *Modelling of the pyrolysis of high density polyethylene: product distribution in a fluidized bed reactor.* Mastral, JF and Berrueco, C and Ceamanos, J. 2007, Journal of analytical and applied pyrolysis, Vol. 79, pp. 313--322.

57. *Feedstock recycling of polymers by pyrolysis in a fluidised bed.* Kaminsky, W and Predel, M and Sadiki, A. 2004, Polymer degradation and stability, Vol. 85, pp. 1045--1050.

58. *Pyrolysis of high-density polyethylene in a fluidised bed reactor. Influence of the temperature and residence time.* Mastral, FJ and Esperanza, E and Garc{\i}a, P and Juste, M. 2002, Journal of Analytical and Applied Pyrolysis, Vol. 63, pp. 1--15.

59. *Production of light olefins from polyethylene in a two-step process: pyrolysis in a conical spouted bed and downstream high-temperature thermal cracking.* Artetxe, Maite and Lopez, Gartzen and Elordi, Gorka and Amutio, Maider and Bilbao, Javier and Olazar, Martin. 2012, Industrial \& engineering chemistry research, Vol. 51, pp. 13915--13923.

60. *Defluidization modelling of pyrolysis of plastics in a conical spouted bed reactor.* Aguado, Roberto and Prieto, Rub{\'e}n and San Jos{\'e}, Mar{\i}a J and Alvarez, Sonia and Olazar, Mart{\i}n and Bilbao, Javier. 2005, Chemical Engineering and Processing: Process Intensification, Vol. 44, pp. 231--235.

61. *Pyrolysis of polyolefins in a conical spouted bed reactor: a way to obtain valuable products.* Arabiourrutia, Miriam and Elordi, Gorka and Olazar, Martin and Bilbao, Javier. 2017.

62. *Product yields and compositions in the continuous pyrolysis of high-density polyethylene in a conical spouted bed reactor.* Elordi, Gorka and Olazar, Martin and Lopez, Gartzen and Artetxe, Maite and Bilbao, Javier. 2011, Industrial \& engineering chemistry research, Vol. 50, pp. 6650--6659.

63. *Pyrolysis of polyolefins in a conical spouted bed reactor: a way to obtain valuable products.* Arabiourrutia, Miriam and Elordi, Gorka and Olazar, Martin and Bilbao, Javier. 2017.

64. Mahendra Rai, Avinash Ingle. *Sustainable Bioenergy.* 2019.

65. *Investigation of catalytic degradation of high-density polyethylene by hydrocarbon group type analysis.* Seo, Young-Hwa and Lee, Kyong-Hwan and Shin, Dae-Hyun. 2003, Journal of Analytical and Applied Pyrolysis, Vol. 70, pp. 383--398.

66. *Comparison of in-situ and ex-situ catalytic pyrolysis in a micro-reactor system.* Wang, Kaige and Johnston, Patrick A and Brown, Robert C. 2014, Bioresource technology, Vol. 173, pp. 124--131.

67. *Advances in upgrading lignin pyrolysis vapors by ex situ catalytic fast pyrolysis.* Xu, Lujiang and Zhang, Ying and Fu, Yao. 2017, Energy Technology, Vol. 5, pp. 30--51.

68. *Insights into the scalability of catalytic upgrading of biomass pyrolysis vapors using micro and bench-scale reactors.* Eschenbacher, Andreas and Saraeian, Alireza and Shanks, Brent H and Jensen, Peter Arendt and Henriksen, Ulrik Birk and Ahrenfeldt, Jesper and Jensen, Anker Degn. 2020, Sustainable Energy \& Fuels, Vol. 4, pp. 3780--3796.

69. K. V. Geem, Ed. *Thermochemical Process Engineering," in Advances in Chemical Engineering.* s.l. : Academic Press, 2016.

70. *Cracking of high density polyethylene pyrolysis waxes on HZSM-5 catalysts of different acidity.* Artetxe, Maite and Lopez, Gartzen and Amutio, Maider and Elordi, Gorka and Bilbao, Javier and Olazar, Martin. 2013, Industrial \& Engineering Chemistry Research, Vol. 52, pp. 10637--10645.

71. *Conceptual process design and techno-economic assessment of ex situ catalytic fast pyrolysis of biomass: A fixed bed reactor implementation scenario for future feasibility.* Dutta, Abhijit and Schaidle, Joshua A and Humbird, David and Baddour, Frederick G and Sahir, Asad. 2016, Topics in Catalysis, Vol. 59, pp. 2--18.

72. *Catalytic fixed-bed reactors.* Eigenberger, Gerhart and Ruppel, Wilhelm. 2000, Ullmann's Encyclopedia of Industrial Chemistry.

73. *Toward maximizing the recycling rate in a Sapporo waste plastics liquefaction plant.* Fukushima, Masaaki and Shioya, Misao and Wakai, Keiji and Ibe, Hidetoshi. 2009, Journal of material cycles and waste management, Vol. 11, pp. 11--18.

74. *A review on reforming bio-ethanol for hydrogen economy.* Ni, M and Leung, DYC and Leung, MKH. 2005, Int. J. Hydrogen Energy, Vol. 30, p. 225.

75. *Application of the sorption enhanced-steam reforming process in combined cycle-based power plants.* Romano, Matteo C and Cassotti, Eugenio N and Chiesa, Paolo and Meyer, Julien and Mastin, Johann. 2011, Energy Procedia, Vol. 4, pp. 1125--1132.

76. **Barin, Ihsan and Platzki, Gregor.** *Thermochemical data of pure substances.* **s.l. : Wiley Online Library, 1989.**

77. *Calcination of calcium-based sorbents at pressure in a broad range of CO2 concentrations.* **Garc{\i}a-Labiano, F and Abad, Alberto and De Diego, LF and Gay{\'a}n, P and Ad{\'a}nez, J. 2002, Chemical engineering science, Vol. 57, pp. 2381--2393.**

78. *The Dos and Don'ts of Adsorptive Reactors.* **Agar, David W. 2005, Integrated Chemical Processes: Synthesis, Operation, Analysis, and Control, pp. 203--232.**

79. *Hydrogen production via sorption enhanced steam methane reforming process using Ni/CaO multifunctional catalyst.* **Chanburanasiri, Naruewan and Ribeiro, Ana M and Rodrigues, Alirio E and Arpornwichanop, Amornchai and Laosiripojana, Navadol and Praserthdam, Piyasan and Assabumrungrat, Suttichai. 2011, Industrial \& engineering chemistry research, Vol. 50, pp. 13662--13671.**

80. *Hydrogen production from steam methane reforming coupled with in situ CO2 capture: Conceptual parametric study.* **Wang, Yi-Ning and Rodrigues, Alirio E. 2005, Fuel, Vol. 84, pp. 1778--1789.**

81. *Subsection-controlling strategy for improving sorption-enhanced reaction process.* **Xiu, GH and Li, P and Rodrigues, AE. 2004, Chemical Engineering Research and Design, Vol. 82, pp. 192--202.**

82. *Pre-combustion CO2 capture.* **Jansen, Daniel and Gazzani, Matteo and Manzolini, Giampaolo and van Dijk, Eric and Carbo, Michiel. 2015, International Journal of Greenhouse Gas Control, Vol. 40, pp. 167--187.**

83. *Adsorption-enhanced steam-methane reforming with intraparticle-diffusion limitations.* **Xiu, Guohua and Li, Ping and Rodrigues, Alirio E. 2003, Chemical Engineering Journal, Vol. 95, pp. 83--93.**

84. *Modelling of binary fluidized bed reactors for the sorption-enhanced steam methane reforming process.* **Chao, Zhongxi and Zhang, Yuanwei and Wang, Yuefa and Jakobsen, Jana P and Jakobsen, Hugo A. 2017, The Canadian Journal of Chemical Engineering, Vol. 95, pp. 157--169.**

85. *Sorption-enhanced steam methane reforming (SE-SMR)--A review: Reactor types, catalysts and sorbents characterization, process modelling.* **Cherba{\'n}ski, Robert and Molga, Eugeniusz. 2018, Chemical and Process Engineering, pp. 427--448.**

86. *The modeling of circulating fluidized bed reactors for SE-SMR process and sorbent regeneration.* **Wang, Jianfeng and Wang, Yuefa and Jakobsen, Hugo A. 2014, Chemical Engineering Science, Vol. 108, pp. 57--65.**

87. *—.***Wang, Jianfeng and Wang, Yuefa and Jakobsen, Hugo A. 2014, Chemical Engineering Science, Vol. 108, pp. 57--65.**

88. *A model for a countercurrent gas−solid−solid trickle flow reactor for equilibrium reactions. The methanol synthesis.* **Westerterp, KR and Kuczynski, M. 1987, Chemical engineering science, Vol. 42, pp. 1871--1885.**

89. *Methanol synthesis in a countercurrent gas−solid−solid trickle flow reactor. An experimental study.* **Kuczynski, M and Oyevaar, MH and Pieters, RT and Westerterp, KR. 1987, Chemical engineering science, Vol. 42, pp. 1887--1898.**

90. *A two dimensional steady-state model of the gas--solid--solid reactor: Example of the partial oxidation of methane to methanol.* **Dallos, Carlos Gregorio and Kafarov, Viatcheslav and Maciel Filho, Rubens. 2007, Chemical Engineering Journal, Vol. 134, pp. 209--217.**

91. *Sorption-enhanced methanol synthesis: Dynamic modeling and optimization.* **Dehghani, Z and Bayat, M and Rahimpour, MR. 2014, Journal of the Taiwan Institute of Chemical Engineers, pp. 1490--1500.**

92. *An appraisal of the heat transfer properties of metallic open-cell foams for strongly exo-/endo-thermic catalytic processes in tubular reactors.* **Bianchi, Enrico and Heidig, Tobias and Visconti, Carlo Giorgio and Groppi, Gianpiero and Freund, Hannsj{\"o}rg and Tronconi, Enrico. 2012, Chemical engineering journal, Vol. 198, pp. 512--528.**

93. *Methane reforming over Ni/Ce-ZrO2 catalysts: effect of nickel content.* **Dong, Wen-Sheng and Roh, Hyun-Seog and Jun, Ki-Won and Park, Sang-Eon and Oh, Young-Sam. 2002, Applied Catalysis A: General, Vol. 226, pp. 63--72.**

94. *日本セラミックス協会学術論文誌: Nippon Seramikkusu Kyokai gakujutsu ronbunshi= Journal of the Ceramic Society of Japan 113 (1322), 678-683, 2005-10-01.* **木村敏夫, 吉田登 and 安達成司 and 田付匡 and 田辺圭一 and 藤原忍 and. 1995, Physica C, Vol. 243, pp. 233--242.**

95. *Particle-resolved simulations of methane steam reforming in multilayered packed beds.* **GM, Karthik and Buwa, Vivek V. 2018, AIChE Journal, Vol. 64, pp. 4162--4176.**

96. *High temperature CO2 sorbents and their application for hydrogen production by sorption enhanced steam reforming process.* **Yancheshmeh, Marziehossadat**

Shokrollahi and Radfarnia, Hamid R and Iliuta, Maria C. 2016, Chemical Engineering Journal, Vol. 283, pp. 420--444.

97. *Hydrogen production by sorption-enhanced steam methane reforming using lithium oxides as CO2-acceptor.* Rusten, Hans Kristian and Ochoa-Fern{\'a}ndez, Esther and Lindborg, H{\aa}vard and Chen, De and Jakobsen, Hugo A. 2007, Industrial \& engineering chemistry research, pp. 8729--8737.

98. *Hydrogen production integrated with simultaneous CO2 sequestration on fly ashes from power plants.* Molga E., Cherbanski R., 2012. Hydrogen production integrated with simultaneous CO2 sequestration on fly. 2012, Chemical engineering \& technology, Vol. 35, pp. 539--546.

99. *Modeling and simulation for the methane steam reforming enhanced by in situ CO2 removal utilizing the CaO carbonation for H2 production.* Lee, Deuk Ki and Baek, Il Hyun and Yoon, Wang Lai. 2004, Chemical Engineering Science, Vol. 59, pp. 931--942.

100. *Solid sorbents for in-situ CO2 removal during sorption-enhanced steam reforming process: A review.* Dou, Binlin and Wang, Chao and Song, Yongchen and Chen, Haisheng and Jiang, Bo and Yang, Mingjun and Xu, Yujie. 2016, Renewable and Sustainable Energy Reviews, Vol. 53, pp. 536--546.

101. *Understanding the enhancement effect of high-temperature steam on the carbonation reaction of CaO with CO2.* Li, Zhenshan and Liu, Yang and Cai, Ningsheng. 2014, Fuel, Vol. 127, pp. 88--93.

102. *Effect of the product layer on the kinetics of the CO2-lime reaction.* Bhatia, SK and Perlmutter, DD. 1983, AIChE Journal, Vol. 29, pp. 79--86.

103. *Synthesis of mesoporous magnesium oxide: its application to CO2 chemisorption.* Bhagiyalakshmi, Margandan and Lee, Ji Yun and Jang, Hyun Tae. 2010, International Journal of Greenhouse Gas Control, Vol. 4, pp. 51--56.

104. *Thermodynamic equilibrium, kinetics, activation barriers, and reaction mechanisms for chemical reactions in karst terrains.* White, WB. Environmental Geology, Vol. 30, pp. 46--58.

105. *Regenerable MgO-based sorbent for high temperature CO2 removal from syngas: 3. CO2 capture and sorbent enhanced water gas shift reaction.* Abbasi, Emadoddin and Hassanzadeh, Armin and Zarghami, Shahin and Arastoopour, Hamid and Abbasian, Javad. 2014, Fuel, pp. 260--268.

106. *Adsorption of carbon dioxide onto hydrotalcite-like compounds (HTlcs) at high temperatures.* Yong, Zou and Mata, Vera and Rodrigues, Al{\'\i}rio E. 2001, Industrial \& Engineering Chemistry Research, Vol. 40, pp. 204--209.

107. *Chemisorption of carbon dioxide on potassium-carbonate-promoted hydrotalcite.* Lee, Ki Bong and Verdooren, A and Caram, HS and Sircar, S. 2007, Journal of colloid and interface science, Vol. 308, pp. 30--39.

108. *Equilibria and kinetics of CO2 adsorption on hydrotalcite adsorbent.* Ding, Y and Alpay, E. 2000, Chemical Engineering Science, Vol. 55, pp. 3461--3474.

109. *Sorption-enhanced reaction process for hydrogen production.* Hufton, JR and Mayorga, S and Sircar, S. 1999, AIChE Journal, Vol. 45, pp. 248--256.

110. *Nonequilibrium kinetic model that describes the reversible adsorption and desorption behavior of CO2 in a K-promoted hydrotalcite-like compound.* Ebner, Armin D and Reynolds, Steven P and Ritter, James A. 2007, Industrial \& engineering chemistry research, Vol. 46, pp. 1737--1744.

111. *CO2 sorption on hydrotalcite and alkali-modified (K and Cs) hydrotalcites at high temperatures.* Oliveira, Eduardo LG and Grande, Carlos A and Rodrigues, Al{\'\i}rio E. 2008, Separation and Purification Technology, Vol. 62, pp. 137--147.

112. *High-purity hydrogen production through sorption enhanced water gas shift reaction using K2CO3-promoted hydrotalcite.* Jang, Hyun Min and Lee, Ki Bong and Caram, Hugo S and Sircar, Shivaji. 2012, Chemical engineering science, Vol. 73, pp. 431--438.

113. *Adsorption of CO2 on hydrotalcite-derived mixed oxides: sorption mechanisms and consequences for adsorption irreversibility.* Le{\'o}n, Marta and Diaz, Eva and Bennici, Simona and Vega, Aurelio and Ord{\'o}nez, Salvador and Auroux, Aline. 2010, Industrial \& engineering chemistry research, Vol. 49, pp. 3663--3671.

114. *High temperature adsorption of CO2 on various hydrotalcite-like compounds.* Hutson, Nick D and Attwood, Brian C. 2008, Adsorption, Vol. 14, pp. 781--789.

115. *A novel method of CO 2 capture from high temperature gases.* Nakagawa, K and Ohashi, T. 1998, Journal of the Electrochemical Society, Vol. 145, p. 1344.

116. *A reversible change between lithium zirconate and zirconia in molten carbonate.* NAKAGAWA, Kazuaki and OHASHI, Toshiyuki. 1999, Electrochemistry, Vol. 67, pp. 618--621.

**117.** *Synthesis and CO2 sorption properties of pure and modified lithium zirconate.* **Ida, Jun-ichi and Xiong, Rentian and Lin, YS. 2004, Separation and Purification Technology, pp. 41--51.**

**118.** *Energy analysis on the effect of biogas composition in the sorption enhanced steam reforming (SESR) for green hydrogen production.* **Capa Tamargo, Alma and Garc{\'\i}a Fern{\'a}ndez, Roberto and Rubiera Gonz{\'a}lez, Fernando and Pevida Garc{\'\i. 2021.**

**119.** *Adsorption-Enhanced Steam-Methane Reforming.* **Ding, Yulong & Alpay, Esat. 2000, Chemical Engineering Science, Vol. 55, pp. 3929-3940.**

**120.** *Methane steam reforming, methanation and water-gas shift: I. Intrinsic kinetics.* **Xu, Jianguo and Froment, Gilbert F. 1989, AIChE journal, Vol. 35, pp. 88--96.**

**121.** *Hydrogen from methane in a single-step process.* **Balasubramanian, B and Ortiz, A Lopez and Kaytakoglu, S and Harrison, DP. 1999, Chemical Engineering Science, Vol. 54, pp. 3543--3552.**

**122.** *Hydrogen production using sorption-enhanced reaction.* **Lopez Ortiz, Alejandro and Harrison, Douglas P. 2001, Industrial \& engineering chemistry research, Vol. 40, pp. 5102--5109.**

**123.** *Continuous production of hydrogen from sorption-enhanced steam methane reforming in two parallel fixed-bed reactors operated in a cyclic manner.* **Li, Zhen-shan and Cai, Ning-sheng and Yang, Jing-biao. 2006, Industrial \& engineering chemistry research, Vol. 45, pp. 8788--8793.**

**124.** *Calcium enhanced hydrogen production with CO2 capture.* **Harrison, Douglas P. 2009, Energy Procedia, Vol. 1, pp. 675--681.**

**125.** *Sorbent enhanced steam reforming (SESR) of methane using dolomite as internal carbon dioxide absorbent: limitations due to Ca (OH) 2 formation.* **Hildenbrand, Nicolas and Readman, Jennifer and Dahl, Ivar M and Blom, Richard. 2006, Applied Catalysis A: General, Vol. 1, pp. 131--137.**

**126.** *Sorption-enhanced steam reforming of methane in a fluidized bed reactor with dolomite as CO2-acceptor.* **Johnsen, K and Ryu, HJ and Grace, JR and Lim, CJ. 2006, Chemical Engineering Science, Vol. 61, pp. 1195--1202.**

**127.** *Synthesis and CO2 capture properties of nanocrystalline lithium zirconate.* **Ochoa-Fern{\'a}ndez, Esther and R{\o}nning, Magnus and Grande, Tor and Chen, De. 2006, Chemistry of materials, Vol. 18, pp. 6037--6046.**

**128.** *Carbon dioxide absorption by lithium orthosilicate in a wide range of temperature and carbon dioxide concentrations.* Kato, M and Yoshikawa, S and Nakagawa, K. 2002, Journal of Materials Science Letters, Vol. 21, pp. 485--487.

**129.** *Development of new CaO based sorbent materials for CO2 removal at high temperature.* Martavaltzi, Christina S and Lemonidou, Angeliki A. 2008, Microporous and Mesoporous Materials, Vol. 110, pp. 119--127.

**130.** *Novel calcium-based regenerative sorbents for high temperature CO2-capture.* Mastin, J and Meyer, J. 2009, mastin2009novel, pp. 15--17.

**131.** *Modeling of sorption-enhanced steam reforming in a dual fluidized bubbling bed reactor.* Johnsen, Kim and Grace, John R and Elnashaie, Said SEH and Kolbeinsen, Leiv and Eriksen, Dag. 2006, Industrial \& engineering chemistry research, pp. 4133--4144.

**132.** Barin, Ihsan and Platzki, Gregor. *Thermochemical data of pure substances.* 1989.

**133.** McBride, Bonnie J. *Coefficients for calculating thermodynamic and transport properties of individual species.* 1993.

**134.** *CO2 capture capacity of CaO in long series of carbonation/calcination cycles.* Grasa, Gemma S and Abanades, J Carlos. 2006, Industrial \& Engineering Chemistry Research, Vol. 45, pp. 8846--8851.

**135.** *Natural gas to synthesis gas--Catalysts and catalytic processes.* Aasberg-Petersen, K and Dybkj{\ae}r, I and Ovesen, CV and Schj{\o}dt, NC and Sehested, J and Thomsen, SG. 2011, Journal of Natural gas science and engineering, Vol. 3, pp. 423--459.

**136.** *Technologies for large-scale gas conversion.* Aasberg-Petersen, K and Hansen, J-H Bak and Christensen, TS and Dybkjaer, I and Christensen, P Seier and Nielsen, C Stub and Madsen, SEL Winter and Rostrup-Nielsen, JR. 2001, Applied Catalysis A: General, Vol. 221, pp. 379--387.

**137.** *Hydrogen production via catalytic pyrolysis of biomass in a two-stage fixed bed reactor system.* Liu, Shaomin and Zhu, Jinglin and Chen, Mingqiang and Xin, Wenping and Yang, Zhonglian and Kong, Lihong. 2014, International journal of hydrogen energy, Vol. 39, pp. 13128--13135.

**138.** *Energy technology perspectives 2012: Pathways to a clean energy system.* IEA, Paris. 2012, International Energy Agency Paris.

**139.** *Calcination of calcium-based sorbents at pressure in a broad range of CO2 concentrations.* **Garc{\i}a-Labiano, F and Abad, Alberto and De Diego, LF and Gay{\'a}n, P and Ad{\'a}nez, J. 2002, Garc{\i}a-Labiano, F and Abad, Alberto and De Diego, LF and Gay{\'a}n, P and Ad{\'a}nez, J, pp. 2381--2393.**

# A  Appendix A
## Stream summary results reference case

| Stream Name | Units | 1.00 | 2.00 | 3.00 | 4.00 | 5.00 | 6.00 | 7.00 | 9.00 | 10.00 | 11.00 | 12.00 |
|---|---|---|---|---|---|---|---|---|---|---|---|---|
| Temperature | C | 500.00 | 400.00 | 120.00 | 20.00 | 482.61 | 482.62 | 600.00 | 600.00 | 700.00 | 700.00 | 700.00 |
| Pressure | bar | 1.00 | 1.00 | 1.00 | 1.00 | 1.00 | 1.00 | 1.00 | 1.00 | 20.00 | 20.00 | 0.15 |
| Mass Vapor Fraction | | 0.90 | 0.90 | 0.44 | 0.22 | 1.00 | 1.00 | 1.00 | 0.47 | 0.29 | 0.00 | 0.56 |
| Mass Liquid Fraction | | 0.00 | 0.00 | 0.46 | 0.68 | 0.00 | 0.00 | 0.00 | 0.00 | 0.00 | 0.00 | 0.00 |
| Mass Solid Fraction | | 0.10 | 0.10 | 0.10 | 0.10 | 0.00 | 0.00 | 0.00 | 0.53 | 0.71 | 1.00 | 0.44 |
| Mole Flows | kmol/hr | 7.85 | 7.85 | 7.85 | 7.85 | 4.67 | 2.34 | 2.34 | 37.36 | 41.28 | 10.44 | 45.94 |
| N2 | kmol/hr | 0.32 | 0.32 | 0.32 | 0.32 | 0.32 | 0.16 | 0.16 | 0.16 | 0.16 | 0.00 | 0.00 |
| CO2 | kmol/hr | 0.17 | 0.17 | 0.17 | 0.17 | 0.17 | 0.09 | 0.09 | 0.09 | 0.07 | 0.00 | 4.59 |
| O2 | kmol/hr | 0.00 | 0.00 | 0.00 | 0.00 | 0.00 | 0.00 | 0.00 | 0.00 | 0.00 | 0.00 | 0.00 |
| H2O | kmol/hr | 0.00 | 0.00 | 0.00 | 0.00 | 0.00 | 0.00 | 0.00 | 24.59 | 15.39 | 0.00 | 30.91 |
| H2 | kmol/hr | 0.23 | 0.23 | 0.23 | 0.23 | 0.23 | 0.12 | 0.12 | 0.12 | 14.87 | 0.00 | 0.00 |
| METHANE | kmol/hr | 0.93 | 0.93 | 0.93 | 0.93 | 0.93 | 0.46 | 0.46 | 0.46 | 0.31 | 0.00 | 0.00 |
| ETHANE | kmol/hr | 0.67 | 0.67 | 0.67 | 0.67 | 0.67 | 0.33 | 0.33 | 0.33 | 0.00 | 0.00 | 0.00 |
| ETHENE | kmol/hr | 0.75 | 0.75 | 0.75 | 0.75 | 0.75 | 0.38 | 0.38 | 0.38 | 0.00 | 0.00 | 0.00 |
| PROPANE | kmol/hr | 0.54 | 0.54 | 0.54 | 0.54 | 0.54 | 0.27 | 0.27 | 0.27 | 0.00 | 0.00 | 0.00 |
| PROPENE | kmol/hr | 0.54 | 0.54 | 0.54 | 0.54 | 0.54 | 0.27 | 0.27 | 0.27 | 0.00 | 0.00 | 0.00 |
| IBUTANE | kmol/hr | 0.01 | 0.01 | 0.01 | 0.01 | 0.01 | 0.00 | 0.00 | 0.00 | 0.00 | 0.00 | 0.00 |
| NBUTANE | kmol/hr | 0.10 | 0.10 | 0.10 | 0.10 | 0.10 | 0.05 | 0.05 | 0.05 | 0.00 | 0.00 | 0.00 |
| BUTENE | kmol/hr | 0.17 | 0.17 | 0.17 | 0.17 | 0.17 | 0.08 | 0.08 | 0.08 | 0.00 | 0.00 | 0.00 |
| IPENTANE | kmol/hr | 0.00 | 0.00 | 0.00 | 0.00 | 0.00 | 0.00 | 0.00 | 0.00 | 0.00 | 0.00 | 0.00 |
| NPENTANE | kmol/hr | 0.00 | 0.00 | 0.00 | 0.00 | 0.00 | 0.00 | 0.00 | 0.00 | 0.00 | 0.00 | 0.00 |
| HEPTANE | kmol/hr | 0.25 | 0.25 | 0.25 | 0.25 | 0.25 | 0.12 | 0.12 | 0.12 | 0.00 | 0.00 | 0.00 |
| C7 | kmol/hr | 0.31 | 0.31 | 0.31 | 0.31 | 0.00 | 0.00 | 0.00 | 0.00 | 0.00 | 0.00 | 0.00 |
| C8 | kmol/hr | 0.27 | 0.27 | 0.27 | 0.27 | 0.00 | 0.00 | 0.00 | 0.00 | 0.00 | 0.00 | 0.00 |
| C9 | kmol/hr | 0.24 | 0.24 | 0.24 | 0.24 | 0.00 | 0.00 | 0.00 | 0.00 | 0.00 | 0.00 | 0.00 |
| C10 | kmol/hr | 0.22 | 0.22 | 0.22 | 0.22 | 0.00 | 0.00 | 0.00 | 0.00 | 0.00 | 0.00 | 0.00 |
| C11 | kmol/hr | 0.09 | 0.09 | 0.09 | 0.09 | 0.00 | 0.00 | 0.00 | 0.00 | 0.00 | 0.00 | 0.00 |
| C12 | kmol/hr | 0.08 | 0.08 | 0.08 | 0.08 | 0.00 | 0.00 | 0.00 | 0.00 | 0.00 | 0.00 | 0.00 |
| C13 | kmol/hr | 0.07 | 0.07 | 0.07 | 0.07 | 0.00 | 0.00 | 0.00 | 0.00 | 0.00 | 0.00 | 0.00 |
| C14 | kmol/hr | 0.07 | 0.07 | 0.07 | 0.07 | 0.00 | 0.00 | 0.00 | 0.00 | 0.00 | 0.00 | 0.00 |
| C15 | kmol/hr | 0.06 | 0.06 | 0.06 | 0.06 | 0.00 | 0.00 | 0.00 | 0.00 | 0.00 | 0.00 | 0.00 |
| C16 | kmol/hr | 0.06 | 0.06 | 0.06 | 0.06 | 0.00 | 0.00 | 0.00 | 0.00 | 0.00 | 0.00 | 0.00 |
| C17 | kmol/hr | 0.06 | 0.06 | 0.06 | 0.06 | 0.00 | 0.00 | 0.00 | 0.00 | 0.00 | 0.00 | 0.00 |
| C18 | kmol/hr | 0.05 | 0.05 | 0.05 | 0.05 | 0.00 | 0.00 | 0.00 | 0.00 | 0.00 | 0.00 | 0.00 |
| C19 | kmol/hr | 0.05 | 0.05 | 0.05 | 0.05 | 0.00 | 0.00 | 0.00 | 0.00 | 0.00 | 0.00 | 0.00 |
| C20 | kmol/hr | 0.05 | 0.05 | 0.05 | 0.05 | 0.00 | 0.00 | 0.00 | 0.00 | 0.00 | 0.00 | 0.00 |
| C21 | kmol/hr | 0.04 | 0.04 | 0.04 | 0.04 | 0.00 | 0.00 | 0.00 | 0.00 | 0.00 | 0.00 | 0.00 |
| C22 | kmol/hr | 0.04 | 0.04 | 0.04 | 0.04 | 0.00 | 0.00 | 0.00 | 0.00 | 0.00 | 0.00 | 0.00 |
| C23 | kmol/hr | 0.02 | 0.02 | 0.02 | 0.02 | 0.00 | 0.00 | 0.00 | 0.00 | 0.00 | 0.00 | 0.00 |
| C24 | kmol/hr | 0.02 | 0.02 | 0.02 | 0.02 | 0.00 | 0.00 | 0.00 | 0.00 | 0.00 | 0.00 | 0.00 |
| C25 | kmol/hr | 0.02 | 0.02 | 0.02 | 0.02 | 0.00 | 0.00 | 0.00 | 0.00 | 0.00 | 0.00 | 0.00 |
| C26 | kmol/hr | 0.02 | 0.02 | 0.02 | 0.02 | 0.00 | 0.00 | 0.00 | 0.00 | 0.00 | 0.00 | 0.00 |
| C27 | kmol/hr | 0.02 | 0.02 | 0.02 | 0.02 | 0.00 | 0.00 | 0.00 | 0.00 | 0.00 | 0.00 | 0.00 |
| C28 | kmol/hr | 0.02 | 0.02 | 0.02 | 0.02 | 0.00 | 0.00 | 0.00 | 0.00 | 0.00 | 0.00 | 0.00 |
| C29 | kmol/hr | 0.02 | 0.02 | 0.02 | 0.02 | 0.00 | 0.00 | 0.00 | 0.00 | 0.00 | 0.00 | 0.00 |
| C30 | kmol/hr | 0.02 | 0.02 | 0.02 | 0.02 | 0.00 | 0.00 | 0.00 | 0.00 | 0.00 | 0.00 | 0.00 |
| C31 | kmol/hr | 0.08 | 0.08 | 0.08 | 0.08 | 0.00 | 0.00 | 0.00 | 0.00 | 0.00 | 0.00 | 0.00 |
| C35 | kmol/hr | 0.07 | 0.07 | 0.07 | 0.07 | 0.00 | 0.00 | 0.00 | 0.00 | 0.00 | 0.00 | 0.00 |
| CO | kmol/hr | 0.00 | 0.00 | 0.00 | 0.00 | 0.00 | 0.00 | 0.00 | 0.00 | 0.04 | 0.00 | 0.00 |
| CA(OH)2 | kmol/hr | 0.00 | 0.00 | 0.00 | 0.00 | 0.00 | 0.00 | 0.00 | 0.00 | 0.00 | 0.00 | 0.00 |
| CACO3 | kmol/hr | 0.00 | 0.00 | 0.00 | 0.00 | 0.00 | 0.00 | 0.00 | 0.00 | 4.59 | 4.59 | 0.00 |
| CAO | kmol/hr | 1.11 | 1.11 | 1.11 | 1.11 | 0.00 | 0.00 | 0.00 | 10.44 | 5.84 | 5.84 | 10.44 |

| Stream Name | Units | 13.00 | 14.00 | 15.00 | 16.00 | 17.00 | 18.00 | 19.00 | 20.00 | 21.00 | 22.00 | 23.00 | 24.00 |
|---|---|---|---|---|---|---|---|---|---|---|---|---|---|
| Temperature | C | 700.00 | 105.00 | 15.00 | 15.00 | 15.00 | 15.00 | 482.62 | 400.00 | 2268.84 | 889.51 | 849.89 | 553.27 |
| Pressure | bar | 0.15 | 0.15 | 0.15 | 0.15 | 80.00 | 80.00 | 1.00 | 1.00 | 1.00 | 1.00 | 1.00 | 1.00 |
| Mass Vapor Fraction | | 1.00 | 1.00 | 0.28 | 1.00 | 0.00 | 0.00 | 1.00 | 1.00 | 1.00 | 1.00 | 1.00 | 1.00 |
| Mass Liquid Fraction | | 0.00 | 0.00 | 0.72 | 0.00 | 1.00 | 1.00 | 0.00 | 0.00 | 0.00 | 0.00 | 0.00 | 0.00 |
| Mass Solid Fraction | | 0.00 | 0.00 | 0.00 | 0.00 | 0.00 | 0.00 | 0.00 | 0.00 | 0.00 | 0.00 | 0.00 | 0.00 |
| Mole Flows | kmol/hr | 35.50 | 35.50 | 35.50 | 5.05 | 4.62 | 4.62 | 1.03 | 19.00 | 20.49 | 20.49 | 20.49 | 20.49 |
| N2 | kmol/hr | 0.00 | 0.00 | 0.00 | 0.00 | 0.00 | 0.00 | 0.07 | 15.01 | 15.08 | 15.08 | 15.08 | 15.08 |
| CO2 | kmol/hr | 4.59 | 4.59 | 4.59 | 4.59 | 4.59 | 4.59 | 0.04 | 0.00 | 2.21 | 2.21 | 2.21 | 2.21 |
| O2 | kmol/hr | 0.00 | 0.00 | 0.00 | 0.00 | 0.00 | 0.00 | 0.00 | 3.99 | 0.44 | 0.44 | 0.44 | 0.44 |
| H2O | kmol/hr | 30.91 | 30.91 | 30.91 | 0.46 | 0.03 | 0.03 | 0.00 | 0.00 | 2.77 | 2.77 | 2.77 | 2.77 |
| H2 | kmol/hr | 0.00 | 0.00 | 0.00 | 0.00 | 0.00 | 0.00 | 0.05 | 0.00 | 0.00 | 0.00 | 0.00 | 0.00 |
| METHANE | kmol/hr | 0.00 | 0.00 | 0.00 | 0.00 | 0.00 | 0.00 | 0.20 | 0.00 | 0.00 | 0.00 | 0.00 | 0.00 |
| ETHANE | kmol/hr | 0.00 | 0.00 | 0.00 | 0.00 | 0.00 | 0.00 | 0.15 | 0.00 | 0.00 | 0.00 | 0.00 | 0.00 |
| ETHENE | kmol/hr | 0.00 | 0.00 | 0.00 | 0.00 | 0.00 | 0.00 | 0.17 | 0.00 | 0.00 | 0.00 | 0.00 | 0.00 |
| PROPANE | kmol/hr | 0.00 | 0.00 | 0.00 | 0.00 | 0.00 | 0.00 | 0.12 | 0.00 | 0.00 | 0.00 | 0.00 | 0.00 |
| PROPENE | kmol/hr | 0.00 | 0.00 | 0.00 | 0.00 | 0.00 | 0.00 | 0.12 | 0.00 | 0.00 | 0.00 | 0.00 | 0.00 |
| IBUTANE | kmol/hr | 0.00 | 0.00 | 0.00 | 0.00 | 0.00 | 0.00 | 0.00 | 0.00 | 0.00 | 0.00 | 0.00 | 0.00 |
| NBUTANE | kmol/hr | 0.00 | 0.00 | 0.00 | 0.00 | 0.00 | 0.00 | 0.02 | 0.00 | 0.00 | 0.00 | 0.00 | 0.00 |
| BUTENE | kmol/hr | 0.00 | 0.00 | 0.00 | 0.00 | 0.00 | 0.00 | 0.04 | 0.00 | 0.00 | 0.00 | 0.00 | 0.00 |
| IPENTANE | kmol/hr | 0.00 | 0.00 | 0.00 | 0.00 | 0.00 | 0.00 | 0.00 | 0.00 | 0.00 | 0.00 | 0.00 | 0.00 |
| NPENTANE | kmol/hr | 0.00 | 0.00 | 0.00 | 0.00 | 0.00 | 0.00 | 0.00 | 0.00 | 0.00 | 0.00 | 0.00 | 0.00 |
| HEPTANE | kmol/hr | 0.00 | 0.00 | 0.00 | 0.00 | 0.00 | 0.00 | 0.05 | 0.00 | 0.00 | 0.00 | 0.00 | 0.00 |
| C7 | kmol/hr | 0.00 | 0.00 | 0.00 | 0.00 | 0.00 | 0.00 | 0.00 | 0.00 | 0.00 | 0.00 | 0.00 | 0.00 |
| C8 | kmol/hr | 0.00 | 0.00 | 0.00 | 0.00 | 0.00 | 0.00 | 0.00 | 0.00 | 0.00 | 0.00 | 0.00 | 0.00 |
| C9 | kmol/hr | 0.00 | 0.00 | 0.00 | 0.00 | 0.00 | 0.00 | 0.00 | 0.00 | 0.00 | 0.00 | 0.00 | 0.00 |
| C10 | kmol/hr | 0.00 | 0.00 | 0.00 | 0.00 | 0.00 | 0.00 | 0.00 | 0.00 | 0.00 | 0.00 | 0.00 | 0.00 |
| C11 | kmol/hr | 0.00 | 0.00 | 0.00 | 0.00 | 0.00 | 0.00 | 0.00 | 0.00 | 0.00 | 0.00 | 0.00 | 0.00 |
| C12 | kmol/hr | 0.00 | 0.00 | 0.00 | 0.00 | 0.00 | 0.00 | 0.00 | 0.00 | 0.00 | 0.00 | 0.00 | 0.00 |
| C13 | kmol/hr | 0.00 | 0.00 | 0.00 | 0.00 | 0.00 | 0.00 | 0.00 | 0.00 | 0.00 | 0.00 | 0.00 | 0.00 |
| C14 | kmol/hr | 0.00 | 0.00 | 0.00 | 0.00 | 0.00 | 0.00 | 0.00 | 0.00 | 0.00 | 0.00 | 0.00 | 0.00 |
| C15 | kmol/hr | 0.00 | 0.00 | 0.00 | 0.00 | 0.00 | 0.00 | 0.00 | 0.00 | 0.00 | 0.00 | 0.00 | 0.00 |
| C16 | kmol/hr | 0.00 | 0.00 | 0.00 | 0.00 | 0.00 | 0.00 | 0.00 | 0.00 | 0.00 | 0.00 | 0.00 | 0.00 |
| C17 | kmol/hr | 0.00 | 0.00 | 0.00 | 0.00 | 0.00 | 0.00 | 0.00 | 0.00 | 0.00 | 0.00 | 0.00 | 0.00 |
| C18 | kmol/hr | 0.00 | 0.00 | 0.00 | 0.00 | 0.00 | 0.00 | 0.00 | 0.00 | 0.00 | 0.00 | 0.00 | 0.00 |
| C19 | kmol/hr | 0.00 | 0.00 | 0.00 | 0.00 | 0.00 | 0.00 | 0.00 | 0.00 | 0.00 | 0.00 | 0.00 | 0.00 |
| C20 | kmol/hr | 0.00 | 0.00 | 0.00 | 0.00 | 0.00 | 0.00 | 0.00 | 0.00 | 0.00 | 0.00 | 0.00 | 0.00 |
| C21 | kmol/hr | 0.00 | 0.00 | 0.00 | 0.00 | 0.00 | 0.00 | 0.00 | 0.00 | 0.00 | 0.00 | 0.00 | 0.00 |
| C22 | kmol/hr | 0.00 | 0.00 | 0.00 | 0.00 | 0.00 | 0.00 | 0.00 | 0.00 | 0.00 | 0.00 | 0.00 | 0.00 |
| C23 | kmol/hr | 0.00 | 0.00 | 0.00 | 0.00 | 0.00 | 0.00 | 0.00 | 0.00 | 0.00 | 0.00 | 0.00 | 0.00 |
| C24 | kmol/hr | 0.00 | 0.00 | 0.00 | 0.00 | 0.00 | 0.00 | 0.00 | 0.00 | 0.00 | 0.00 | 0.00 | 0.00 |
| C25 | kmol/hr | 0.00 | 0.00 | 0.00 | 0.00 | 0.00 | 0.00 | 0.00 | 0.00 | 0.00 | 0.00 | 0.00 | 0.00 |
| C26 | kmol/hr | 0.00 | 0.00 | 0.00 | 0.00 | 0.00 | 0.00 | 0.00 | 0.00 | 0.00 | 0.00 | 0.00 | 0.00 |
| C27 | kmol/hr | 0.00 | 0.00 | 0.00 | 0.00 | 0.00 | 0.00 | 0.00 | 0.00 | 0.00 | 0.00 | 0.00 | 0.00 |
| C28 | kmol/hr | 0.00 | 0.00 | 0.00 | 0.00 | 0.00 | 0.00 | 0.00 | 0.00 | 0.00 | 0.00 | 0.00 | 0.00 |
| C29 | kmol/hr | 0.00 | 0.00 | 0.00 | 0.00 | 0.00 | 0.00 | 0.00 | 0.00 | 0.00 | 0.00 | 0.00 | 0.00 |
| C30 | kmol/hr | 0.00 | 0.00 | 0.00 | 0.00 | 0.00 | 0.00 | 0.00 | 0.00 | 0.00 | 0.00 | 0.00 | 0.00 |
| C31 | kmol/hr | 0.00 | 0.00 | 0.00 | 0.00 | 0.00 | 0.00 | 0.00 | 0.00 | 0.00 | 0.00 | 0.00 | 0.00 |
| C35 | kmol/hr | 0.00 | 0.00 | 0.00 | 0.00 | 0.00 | 0.00 | 0.00 | 0.00 | 0.00 | 0.00 | 0.00 | 0.00 |
| CO | kmol/hr | 0.00 | 0.00 | 0.00 | 0.00 | 0.00 | 0.00 | 0.00 | 0.00 | 0.00 | 0.00 | 0.00 | 0.00 |
| CA(OH)2 | kmol/hr | 0.00 | 0.00 | 0.00 | 0.00 | 0.00 | 0.00 | 0.00 | 0.00 | 0.00 | 0.00 | 0.00 | 0.00 |
| CACO3 | kmol/hr | 0.00 | 0.00 | 0.00 | 0.00 | 0.00 | 0.00 | 0.00 | 0.00 | 0.00 | 0.00 | 0.00 | 0.00 |
| CAO | kmol/hr | 0.00 | 0.00 | 0.00 | 0.00 | 0.00 | 0.00 | 0.00 | 0.00 | 0.00 | 0.00 | 0.00 | 0.00 |

| Stream Name | Units | 25.00 | 26.00 | 27.00 | 28.00 | 29.00 | 30.00 | 31.00 | 32.00 | 33.00 | 34.00 | 35.00 | 37.00 |
|---|---|---|---|---|---|---|---|---|---|---|---|---|---|
| Temperature | C | 482.62 | 2220.92 | 1499.84 | ###### | 922.65 | 628.99 | 700.00 | 259.25 | 112.90 | 15.00 | 101.54 | 600.00 |
| Pressure | bar | 1.00 | 1.00 | 1.00 | 1.00 | 1.00 | 1.00 | 20.00 | 20.00 | 20.00 | 20.00 | 1.00 | 1.00 |
| Mass Vapor Fraction | | 1.00 | 1.00 | 1.00 | 1.00 | 1.00 | 1.00 | 1.00 | 1.00 | 0.21 | 0.14 | 0.30 | 1.00 |
| Mass Liquid Fraction | | 0.00 | 0.00 | 0.00 | 0.00 | 0.00 | 0.00 | 0.00 | 0.00 | 0.79 | 0.86 | 0.70 | 0.00 |
| Mass Solid Fraction | | 0.00 | 0.00 | 0.00 | 0.00 | 0.00 | 0.00 | 0.00 | 0.00 | 0.00 | 0.00 | 0.00 | 0.00 |
| Mole Flows | kmol/hr | 1.31 | 26.90 | 26.90 | 26.90 | 26.90 | 26.90 | 30.84 | 30.84 | 30.84 | 30.84 | 24.59 | 24.59 |
| N2 | kmol/hr | 0.09 | 19.84 | 19.84 | 19.84 | 19.84 | 19.84 | 0.16 | 0.16 | 0.16 | 0.16 | 0.00 | 0.00 |
| CO2 | kmol/hr | 0.05 | 2.81 | 2.81 | 2.81 | 2.81 | 2.81 | 0.07 | 0.07 | 0.07 | 0.07 | 0.00 | 0.00 |
| O2 | kmol/hr | 0.00 | 0.73 | 0.73 | 0.73 | 0.73 | 0.73 | 0.00 | 0.00 | 0.00 | 0.00 | 0.00 | 0.00 |
| H2O | kmol/hr | 0.00 | 3.52 | 3.52 | 3.52 | 3.52 | 3.52 | 15.39 | 15.39 | 15.39 | 15.39 | 24.59 | 24.59 |
| H2 | kmol/hr | 0.06 | 0.00 | 0.00 | 0.00 | 0.00 | 0.00 | 14.87 | 14.87 | 14.87 | 14.87 | 0.00 | 0.00 |
| METHANE | kmol/hr | 0.26 | 0.00 | 0.00 | 0.00 | 0.00 | 0.00 | 0.31 | 0.31 | 0.31 | 0.31 | 0.00 | 0.00 |
| ETHANE | kmol/hr | 0.19 | 0.00 | 0.00 | 0.00 | 0.00 | 0.00 | 0.00 | 0.00 | 0.00 | 0.00 | 0.00 | 0.00 |
| ETHENE | kmol/hr | 0.21 | 0.00 | 0.00 | 0.00 | 0.00 | 0.00 | 0.00 | 0.00 | 0.00 | 0.00 | 0.00 | 0.00 |
| PROPANE | kmol/hr | 0.15 | 0.00 | 0.00 | 0.00 | 0.00 | 0.00 | 0.00 | 0.00 | 0.00 | 0.00 | 0.00 | 0.00 |
| PROPENE | kmol/hr | 0.15 | 0.00 | 0.00 | 0.00 | 0.00 | 0.00 | 0.00 | 0.00 | 0.00 | 0.00 | 0.00 | 0.00 |
| IBUTANE | kmol/hr | 0.00 | 0.00 | 0.00 | 0.00 | 0.00 | 0.00 | 0.00 | 0.00 | 0.00 | 0.00 | 0.00 | 0.00 |
| NBUTANE | kmol/hr | 0.03 | 0.00 | 0.00 | 0.00 | 0.00 | 0.00 | 0.00 | 0.00 | 0.00 | 0.00 | 0.00 | 0.00 |
| BUTENE | kmol/hr | 0.05 | 0.00 | 0.00 | 0.00 | 0.00 | 0.00 | 0.00 | 0.00 | 0.00 | 0.00 | 0.00 | 0.00 |
| IPENTANE | kmol/hr | 0.00 | 0.00 | 0.00 | 0.00 | 0.00 | 0.00 | 0.00 | 0.00 | 0.00 | 0.00 | 0.00 | 0.00 |
| NPENTANE | kmol/hr | 0.00 | 0.00 | 0.00 | 0.00 | 0.00 | 0.00 | 0.00 | 0.00 | 0.00 | 0.00 | 0.00 | 0.00 |
| HEPTANE | kmol/hr | 0.07 | 0.00 | 0.00 | 0.00 | 0.00 | 0.00 | 0.00 | 0.00 | 0.00 | 0.00 | 0.00 | 0.00 |
| C7 | kmol/hr | 0.00 | 0.00 | 0.00 | 0.00 | 0.00 | 0.00 | 0.00 | 0.00 | 0.00 | 0.00 | 0.00 | 0.00 |
| C8 | kmol/hr | 0.00 | 0.00 | 0.00 | 0.00 | 0.00 | 0.00 | 0.00 | 0.00 | 0.00 | 0.00 | 0.00 | 0.00 |
| C9 | kmol/hr | 0.00 | 0.00 | 0.00 | 0.00 | 0.00 | 0.00 | 0.00 | 0.00 | 0.00 | 0.00 | 0.00 | 0.00 |
| C10 | kmol/hr | 0.00 | 0.00 | 0.00 | 0.00 | 0.00 | 0.00 | 0.00 | 0.00 | 0.00 | 0.00 | 0.00 | 0.00 |
| C11 | kmol/hr | 0.00 | 0.00 | 0.00 | 0.00 | 0.00 | 0.00 | 0.00 | 0.00 | 0.00 | 0.00 | 0.00 | 0.00 |
| C12 | kmol/hr | 0.00 | 0.00 | 0.00 | 0.00 | 0.00 | 0.00 | 0.00 | 0.00 | 0.00 | 0.00 | 0.00 | 0.00 |
| C13 | kmol/hr | 0.00 | 0.00 | 0.00 | 0.00 | 0.00 | 0.00 | 0.00 | 0.00 | 0.00 | 0.00 | 0.00 | 0.00 |
| C14 | kmol/hr | 0.00 | 0.00 | 0.00 | 0.00 | 0.00 | 0.00 | 0.00 | 0.00 | 0.00 | 0.00 | 0.00 | 0.00 |
| C15 | kmol/hr | 0.00 | 0.00 | 0.00 | 0.00 | 0.00 | 0.00 | 0.00 | 0.00 | 0.00 | 0.00 | 0.00 | 0.00 |
| C16 | kmol/hr | 0.00 | 0.00 | 0.00 | 0.00 | 0.00 | 0.00 | 0.00 | 0.00 | 0.00 | 0.00 | 0.00 | 0.00 |
| C17 | kmol/hr | 0.00 | 0.00 | 0.00 | 0.00 | 0.00 | 0.00 | 0.00 | 0.00 | 0.00 | 0.00 | 0.00 | 0.00 |
| C18 | kmol/hr | 0.00 | 0.00 | 0.00 | 0.00 | 0.00 | 0.00 | 0.00 | 0.00 | 0.00 | 0.00 | 0.00 | 0.00 |
| C19 | kmol/hr | 0.00 | 0.00 | 0.00 | 0.00 | 0.00 | 0.00 | 0.00 | 0.00 | 0.00 | 0.00 | 0.00 | 0.00 |
| C20 | kmol/hr | 0.00 | 0.00 | 0.00 | 0.00 | 0.00 | 0.00 | 0.00 | 0.00 | 0.00 | 0.00 | 0.00 | 0.00 |
| C21 | kmol/hr | 0.00 | 0.00 | 0.00 | 0.00 | 0.00 | 0.00 | 0.00 | 0.00 | 0.00 | 0.00 | 0.00 | 0.00 |
| C22 | kmol/hr | 0.00 | 0.00 | 0.00 | 0.00 | 0.00 | 0.00 | 0.00 | 0.00 | 0.00 | 0.00 | 0.00 | 0.00 |
| C23 | kmol/hr | 0.00 | 0.00 | 0.00 | 0.00 | 0.00 | 0.00 | 0.00 | 0.00 | 0.00 | 0.00 | 0.00 | 0.00 |
| C24 | kmol/hr | 0.00 | 0.00 | 0.00 | 0.00 | 0.00 | 0.00 | 0.00 | 0.00 | 0.00 | 0.00 | 0.00 | 0.00 |
| C25 | kmol/hr | 0.00 | 0.00 | 0.00 | 0.00 | 0.00 | 0.00 | 0.00 | 0.00 | 0.00 | 0.00 | 0.00 | 0.00 |
| C26 | kmol/hr | 0.00 | 0.00 | 0.00 | 0.00 | 0.00 | 0.00 | 0.00 | 0.00 | 0.00 | 0.00 | 0.00 | 0.00 |
| C27 | kmol/hr | 0.00 | 0.00 | 0.00 | 0.00 | 0.00 | 0.00 | 0.00 | 0.00 | 0.00 | 0.00 | 0.00 | 0.00 |
| C28 | kmol/hr | 0.00 | 0.00 | 0.00 | 0.00 | 0.00 | 0.00 | 0.00 | 0.00 | 0.00 | 0.00 | 0.00 | 0.00 |
| C29 | kmol/hr | 0.00 | 0.00 | 0.00 | 0.00 | 0.00 | 0.00 | 0.00 | 0.00 | 0.00 | 0.00 | 0.00 | 0.00 |
| C30 | kmol/hr | 0.00 | 0.00 | 0.00 | 0.00 | 0.00 | 0.00 | 0.00 | 0.00 | 0.00 | 0.00 | 0.00 | 0.00 |
| C31 | kmol/hr | 0.00 | 0.00 | 0.00 | 0.00 | 0.00 | 0.00 | 0.00 | 0.00 | 0.00 | 0.00 | 0.00 | 0.00 |
| C35 | kmol/hr | 0.00 | 0.00 | 0.00 | 0.00 | 0.00 | 0.00 | 0.00 | 0.00 | 0.00 | 0.00 | 0.00 | 0.00 |
| CO | kmol/hr | 0.00 | 0.00 | 0.00 | 0.00 | 0.00 | 0.00 | 0.04 | 0.04 | 0.04 | 0.04 | 0.00 | 0.00 |
| CA(OH)2 | kmol/hr | 0.00 | 0.00 | 0.00 | 0.00 | 0.00 | 0.00 | 0.00 | 0.00 | 0.00 | 0.00 | 0.00 | 0.00 |
| CACO3 | kmol/hr | 0.00 | 0.00 | 0.00 | 0.00 | 0.00 | 0.00 | 0.00 | 0.00 | 0.00 | 0.00 | 0.00 | 0.00 |
| CAO | kmol/hr | 0.00 | 0.00 | 0.00 | 0.00 | 0.00 | 0.00 | 0.00 | 0.00 | 0.00 | 0.00 | 0.00 | 0.00 |

| Stream Name | Units | 38.00 | 39.00 | 40.00 | 41.00 | 42.00 | 43.00 | 44.00 | 45.00 | 46.00 | 47.00 | 48.00 | 49.00 | 50.00 |
|---|---|---|---|---|---|---|---|---|---|---|---|---|---|---|
| Temperature | C | 101.54 | 101.54 | 15.00 | 163.08 | 575.00 | 15.00 | 15.00 | 15.00 | | | | 700.00 | 15.00 |
| Pressure | bar | 1.00 | 1.00 | 0.15 | 1.00 | 1.00 | 0.90 | 0.37 | 2.21 | | | | 1.00 | 0.15 |
| Mass Vapor Fraction | | 0.06 | 0.69 | 0.00 | 1.00 | 1.00 | 0.00 | 0.00 | 0.00 | | | | 1.00 | 0.00 |
| Mass Liquid Fraction | | 0.94 | 0.31 | 1.00 | 0.00 | 0.00 | 1.00 | 1.00 | 1.00 | | | | 0.00 | 1.00 |
| Mass Solid Fraction | | 0.00 | 0.00 | 0.00 | 0.00 | 0.00 | 0.00 | 0.00 | 0.00 | | | | 0.00 | 0.00 |
| Mole Flows | kmol/hr | 30.91 | 30.91 | 30.45 | 30.91 | 30.91 | 0.11 | 0.28 | 0.04 | 0.00 | 0.00 | 0.00 | 30.91 | 30.88 |
| N2 | kmol/hr | 0.00 | 0.00 | 0.00 | 0.00 | 0.00 | 0.00 | 0.00 | 0.00 | 0.00 | 0.00 | 0.00 | 0.00 | 0.00 |
| CO2 | kmol/hr | 0.00 | 0.00 | 0.00 | 0.00 | 0.00 | 0.00 | 0.00 | 0.00 | 0.00 | 0.00 | 0.00 | 0.00 | 0.00 |
| O2 | kmol/hr | 0.00 | 0.00 | 0.00 | 0.00 | 0.00 | 0.00 | 0.00 | 0.00 | 0.00 | 0.00 | 0.00 | 0.00 | 0.00 |
| H2O | kmol/hr | 30.91 | 30.91 | 30.45 | 30.91 | 30.91 | 0.11 | 0.28 | 0.04 | 0.00 | 0.00 | 0.00 | 30.91 | 30.88 |
| H2 | kmol/hr | 0.00 | 0.00 | 0.00 | 0.00 | 0.00 | 0.00 | 0.00 | 0.00 | 0.00 | 0.00 | 0.00 | 0.00 | 0.00 |
| METHANE | kmol/hr | 0.00 | 0.00 | 0.00 | 0.00 | 0.00 | 0.00 | 0.00 | 0.00 | 0.00 | 0.00 | 0.00 | 0.00 | 0.00 |
| ETHANE | kmol/hr | 0.00 | 0.00 | 0.00 | 0.00 | 0.00 | 0.00 | 0.00 | 0.00 | 0.00 | 0.00 | 0.00 | 0.00 | 0.00 |
| ETHENE | kmol/hr | 0.00 | 0.00 | 0.00 | 0.00 | 0.00 | 0.00 | 0.00 | 0.00 | 0.00 | 0.00 | 0.00 | 0.00 | 0.00 |
| PROPANE | kmol/hr | 0.00 | 0.00 | 0.00 | 0.00 | 0.00 | 0.00 | 0.00 | 0.00 | 0.00 | 0.00 | 0.00 | 0.00 | 0.00 |
| PROPENE | kmol/hr | 0.00 | 0.00 | 0.00 | 0.00 | 0.00 | 0.00 | 0.00 | 0.00 | 0.00 | 0.00 | 0.00 | 0.00 | 0.00 |
| IBUTANE | kmol/hr | 0.00 | 0.00 | 0.00 | 0.00 | 0.00 | 0.00 | 0.00 | 0.00 | 0.00 | 0.00 | 0.00 | 0.00 | 0.00 |
| NBUTANE | kmol/hr | 0.00 | 0.00 | 0.00 | 0.00 | 0.00 | 0.00 | 0.00 | 0.00 | 0.00 | 0.00 | 0.00 | 0.00 | 0.00 |
| BUTENE | kmol/hr | 0.00 | 0.00 | 0.00 | 0.00 | 0.00 | 0.00 | 0.00 | 0.00 | 0.00 | 0.00 | 0.00 | 0.00 | 0.00 |
| IPENTANE | kmol/hr | 0.00 | 0.00 | 0.00 | 0.00 | 0.00 | 0.00 | 0.00 | 0.00 | 0.00 | 0.00 | 0.00 | 0.00 | 0.00 |
| NPENTANE | kmol/hr | 0.00 | 0.00 | 0.00 | 0.00 | 0.00 | 0.00 | 0.00 | 0.00 | 0.00 | 0.00 | 0.00 | 0.00 | 0.00 |
| HEPTANE | kmol/hr | 0.00 | 0.00 | 0.00 | 0.00 | 0.00 | 0.00 | 0.00 | 0.00 | 0.00 | 0.00 | 0.00 | 0.00 | 0.00 |
| C7 | kmol/hr | 0.00 | 0.00 | 0.00 | 0.00 | 0.00 | 0.00 | 0.00 | 0.00 | 0.00 | 0.00 | 0.00 | 0.00 | 0.00 |
| C8 | kmol/hr | 0.00 | 0.00 | 0.00 | 0.00 | 0.00 | 0.00 | 0.00 | 0.00 | 0.00 | 0.00 | 0.00 | 0.00 | 0.00 |
| C9 | kmol/hr | 0.00 | 0.00 | 0.00 | 0.00 | 0.00 | 0.00 | 0.00 | 0.00 | 0.00 | 0.00 | 0.00 | 0.00 | 0.00 |
| C10 | kmol/hr | 0.00 | 0.00 | 0.00 | 0.00 | 0.00 | 0.00 | 0.00 | 0.00 | 0.00 | 0.00 | 0.00 | 0.00 | 0.00 |
| C11 | kmol/hr | 0.00 | 0.00 | 0.00 | 0.00 | 0.00 | 0.00 | 0.00 | 0.00 | 0.00 | 0.00 | 0.00 | 0.00 | 0.00 |
| C12 | kmol/hr | 0.00 | 0.00 | 0.00 | 0.00 | 0.00 | 0.00 | 0.00 | 0.00 | 0.00 | 0.00 | 0.00 | 0.00 | 0.00 |
| C13 | kmol/hr | 0.00 | 0.00 | 0.00 | 0.00 | 0.00 | 0.00 | 0.00 | 0.00 | 0.00 | 0.00 | 0.00 | 0.00 | 0.00 |
| C14 | kmol/hr | 0.00 | 0.00 | 0.00 | 0.00 | 0.00 | 0.00 | 0.00 | 0.00 | 0.00 | 0.00 | 0.00 | 0.00 | 0.00 |
| C15 | kmol/hr | 0.00 | 0.00 | 0.00 | 0.00 | 0.00 | 0.00 | 0.00 | 0.00 | 0.00 | 0.00 | 0.00 | 0.00 | 0.00 |
| C16 | kmol/hr | 0.00 | 0.00 | 0.00 | 0.00 | 0.00 | 0.00 | 0.00 | 0.00 | 0.00 | 0.00 | 0.00 | 0.00 | 0.00 |
| C17 | kmol/hr | 0.00 | 0.00 | 0.00 | 0.00 | 0.00 | 0.00 | 0.00 | 0.00 | 0.00 | 0.00 | 0.00 | 0.00 | 0.00 |
| C18 | kmol/hr | 0.00 | 0.00 | 0.00 | 0.00 | 0.00 | 0.00 | 0.00 | 0.00 | 0.00 | 0.00 | 0.00 | 0.00 | 0.00 |
| C19 | kmol/hr | 0.00 | 0.00 | 0.00 | 0.00 | 0.00 | 0.00 | 0.00 | 0.00 | 0.00 | 0.00 | 0.00 | 0.00 | 0.00 |
| C20 | kmol/hr | 0.00 | 0.00 | 0.00 | 0.00 | 0.00 | 0.00 | 0.00 | 0.00 | 0.00 | 0.00 | 0.00 | 0.00 | 0.00 |
| C21 | kmol/hr | 0.00 | 0.00 | 0.00 | 0.00 | 0.00 | 0.00 | 0.00 | 0.00 | 0.00 | 0.00 | 0.00 | 0.00 | 0.00 |
| C22 | kmol/hr | 0.00 | 0.00 | 0.00 | 0.00 | 0.00 | 0.00 | 0.00 | 0.00 | 0.00 | 0.00 | 0.00 | 0.00 | 0.00 |
| C23 | kmol/hr | 0.00 | 0.00 | 0.00 | 0.00 | 0.00 | 0.00 | 0.00 | 0.00 | 0.00 | 0.00 | 0.00 | 0.00 | 0.00 |
| C24 | kmol/hr | 0.00 | 0.00 | 0.00 | 0.00 | 0.00 | 0.00 | 0.00 | 0.00 | 0.00 | 0.00 | 0.00 | 0.00 | 0.00 |
| C25 | kmol/hr | 0.00 | 0.00 | 0.00 | 0.00 | 0.00 | 0.00 | 0.00 | 0.00 | 0.00 | 0.00 | 0.00 | 0.00 | 0.00 |
| C26 | kmol/hr | 0.00 | 0.00 | 0.00 | 0.00 | 0.00 | 0.00 | 0.00 | 0.00 | 0.00 | 0.00 | 0.00 | 0.00 | 0.00 |
| C27 | kmol/hr | 0.00 | 0.00 | 0.00 | 0.00 | 0.00 | 0.00 | 0.00 | 0.00 | 0.00 | 0.00 | 0.00 | 0.00 | 0.00 |
| C28 | kmol/hr | 0.00 | 0.00 | 0.00 | 0.00 | 0.00 | 0.00 | 0.00 | 0.00 | 0.00 | 0.00 | 0.00 | 0.00 | 0.00 |
| C29 | kmol/hr | 0.00 | 0.00 | 0.00 | 0.00 | 0.00 | 0.00 | 0.00 | 0.00 | 0.00 | 0.00 | 0.00 | 0.00 | 0.00 |
| C30 | kmol/hr | 0.00 | 0.00 | 0.00 | 0.00 | 0.00 | 0.00 | 0.00 | 0.00 | 0.00 | 0.00 | 0.00 | 0.00 | 0.00 |
| C31 | kmol/hr | 0.00 | 0.00 | 0.00 | 0.00 | 0.00 | 0.00 | 0.00 | 0.00 | 0.00 | 0.00 | 0.00 | 0.00 | 0.00 |
| C35 | kmol/hr | 0.00 | 0.00 | 0.00 | 0.00 | 0.00 | 0.00 | 0.00 | 0.00 | 0.00 | 0.00 | 0.00 | 0.00 | 0.00 |
| CO | kmol/hr | 0.00 | 0.00 | 0.00 | 0.00 | 0.00 | 0.00 | 0.00 | 0.00 | 0.00 | 0.00 | 0.00 | 0.00 | 0.00 |
| CA(OH)2 | kmol/hr | 0.00 | 0.00 | 0.00 | 0.00 | 0.00 | 0.00 | 0.00 | 0.00 | 0.00 | 0.00 | 0.00 | 0.00 | 0.00 |
| CACO3 | kmol/hr | 0.00 | 0.00 | 0.00 | 0.00 | 0.00 | 0.00 | 0.00 | 0.00 | 0.00 | 0.00 | 0.00 | 0.00 | 0.00 |
| CAO | kmol/hr | 0.00 | 0.00 | 0.00 | 0.00 | 0.00 | 0.00 | 0.00 | 0.00 | 0.00 | 0.00 | 0.00 | 0.00 | 0.00 |

# List of Figures

# List of Tables